ABSTRACT

Title of Document: SULFUR ISOTOPIC EVOLUTION ($\delta^{34}S$ AND $\Delta^{33}S$) OF PHANEROZOIC AND EDIACARAN SEAWATER SULFATE BASED ON THE ANALYSIS OF CARBONATE ASSOCIATED SULFATE

Nanping Wu, Doctor of Philosophy, 2013

Directed By: Dr. James Farquhar, Department of Geology, University of Maryland

Dynamics of $\delta^{34}S$ and $\Delta^{33}S$ of oceanic sulfate and sedimentary pyrite over geologic time has been used to understand and extract information about the marine sulfur cycle. My Ph.D project uses this approach to study the evolution of the marine sulfur cycle and focuses on:

- Providing temporal $\delta^{34}S$ and $\Delta^{33}S$ records for Phanerozoic and Ediacaran seawater sulfate based on the analysis of carbonate associated sulfate
- Reinterpreting previously documented variations of sulfur isotope fractionation ($\Delta^{34}S$) using new measurements of $\Delta^{33}S$ of oceanic sulfate. The sulfur isotope fractionation between sulfate and pyrite appears to have varied widely, between 25‰ to 40‰ over the course of Phanerozoic. For the earlier part of Phanerozoic, the values of sulfur isotope fractionation are approximately 35‰. The fractionation then decreases to 25‰ during the Carboniferous Period. Following this, the sulfur isotope fractionations progressively increase, reaching approximately 40‰ during the Cenozoic Period.

- Evaluating the connection between sulfate concentration, sulfide re-oxidation and sulfate exchange between water column and marine sediment systems using steady state and also non steady state models. The model results and the data presented here suggest the sulfur cycle in the Ediacaran Oman basin evolved from one that was similar to the global sulfur cycle to a sulfur cycle that was disconnected or partially was disconnected from the open ocean sulfur cycle. It also implies that the sulfate levels drop at this transition due to weakening of vertical bioturbation or weakening of other physical processes that involve in mixing of sulfate in pore water and overlying sulfate in marine settings.

The significance of these three directions is the new information that they provide about the evolution of the sulfur cycle. It is relevant to understanding the environmental changes and their connections to sulfur ecosystem evolution for the geological time interval extending from present until latest Precambrian.

Sulfur isotopic evolution ($\delta^{34}S$ and $\Delta^{33}S$) of Phanerozoic and Ediacaran seawater sulfate based on the analysis of carbonate associated sulfate

Nanping Wu

Dissertation submitted to the Faculty of the Graduate School of the

University of Maryland, College Park, in partial fulfillment

of the requirements for the degree of

Doctor of Philosophy

2013

Advisory Committee:

Dr. James Farquhar (Department of Geology, University of Maryland, Chair)

Dr. Alan Jay Kaufman (Department of Geology, University of Maryland)

Dr. Michael Evans (Department of Geology, University of Maryland)

Dr. Sarah Penniston-Dorland (Department of Geology, University of Maryland)

Dr. Neil Blough (Department of Chemistry, University of Maryland)

DEDICATION

I dedicate my dissertation work to Dr. John Morse and Dr. Ethan Grossman. A special feeling of gratitude to Ethan who brings me back to science and gives me tremendous support, and special thanks to John whose words of encouragements always sustain me throughout these years.

ACKNOWLEDGEMENTS

I would like to acknowledge and thank my advisor, Dr. James Farquhar, for his great patience and enormous help throughout this project. Without him, this thesis work would not have been possible. I could not use any words to fully express how I appreciate what James gave me. I also must thank my committee members (Dr. Jay Kaufman, Dr. Mike Evans and Dr. Sarah Penniston-Dorland) for their providing constructive comments in revising this dissertation. A special thanks to Dr. William McDonough for his magic support in this project.

Dr. Neil Blough is thanked for serving as a Dean's representative on my dissertation committee. Dr. Harald Strauss and Dr. David Fike are thanked for their help and providing samples in this project. I would like to thank Andrew Masterson and Dr. SangTae Kim for their teaching me a lot on the analytical measurements when I arrived in Maryland.

I am also very thankful and grateful to my friends: Clark Kung, Edith Bai, Daozheng Chen, Amanda Wang, and Jaya Koo for smiles, inside jokes, and memories. I would like to thank staff and faculty members and fellow students, including Jeanne Martin, Sandy Romeo, Dorothy Brown, Todd Karwoski, Michelle Montero, Dr. Rich Walker and Dr. Igor Puchte, Brian Harms for your support.

Table of Contents

List of Tables

List of Figures

Chapter 1: Introduction

Abstract: This chapter gives a general view of sulfur biogeochemistry and the role of microbial sulfate reduction in cycling of sulfur. The sedimentary sulfur cycle is also briefly described by its important sulfur reserviors, including seawater sulfate, sedimentary pyrite and evaporites, and sulfur fluxes into and out of the oceans. The proxies (evaporites, barite and carbonate associated sulfate) used to reconstruct the sulfur isotopic records of oceanic sulfate over geologic time is introduced, and questions about the marine sulfur cycle addressed in the following chapters are also introduced in the end of this chapter.

1.1 Overview of sulfur biogeochemistry

The element sulfur has four stable isotopes, ^{32}S, ^{33}S, ^{34}S and ^{36}S with natural abundances of approximately 95.04%, 0.75%, 4.20% and 0.015%, respectively (Coplen et al., 2002). Sulfur is a reactive element and occurs naturally in various forms, such as sulfate (SO_4^{2-}) with oxidized valence of (+6), sulfide (S^{2-}) of reduced valence of (-2), and thiosulfate ($S_2O_3^{2-}$) and elemental sulfur (S^0) with intermediate valences of (+2) and (0), respectively. Dissolved sulfate (SO_4^{2-}) in oceans plays a central role in marine chemistry, mostly due to its high concentration in modern seawater of ~28mM. For instance, microbial sulfate reduction accounts for ~50% of organic matter mineralization in marine settings (Jorgensen and Kasten, 2006).

Seawater sulfate-sulfur is one of the major sulfur pools on the Earth's surface and it plays a critical role in the sedimentary sulfur cycle. The sulfur isotope geochemistry of oceanic sulfate is controlled by various chemical and biochemical reactions in the biogeochemical cycling of sulfur. Knowledge of the behavior of sulfur isotopes in those reactions that involve oxidation and reduction of sulfur species (Figure 1) is critical for a better understanding of the variations in sulfur isotopic compositions of oceanic sulfate and sedimentary pyrite over geologic time (Canfield, 1999, 2001).

Special attention is paid to the process of dissimilatory sulfate reduction, a microbial process that couples the oxidation of organic matter and/or hydrogen and the reduction of dissolved

sulfate under anaerobic conditions. This process releases energy used by the sulfate-reducing bacteria for their metabolism. It is estimated that most of microbial sulfate reduction occurs in the continental shelf and slope where organic matter is sufficiently abundant and metabolized by sulfate reducers (Jorgensen, 2006).

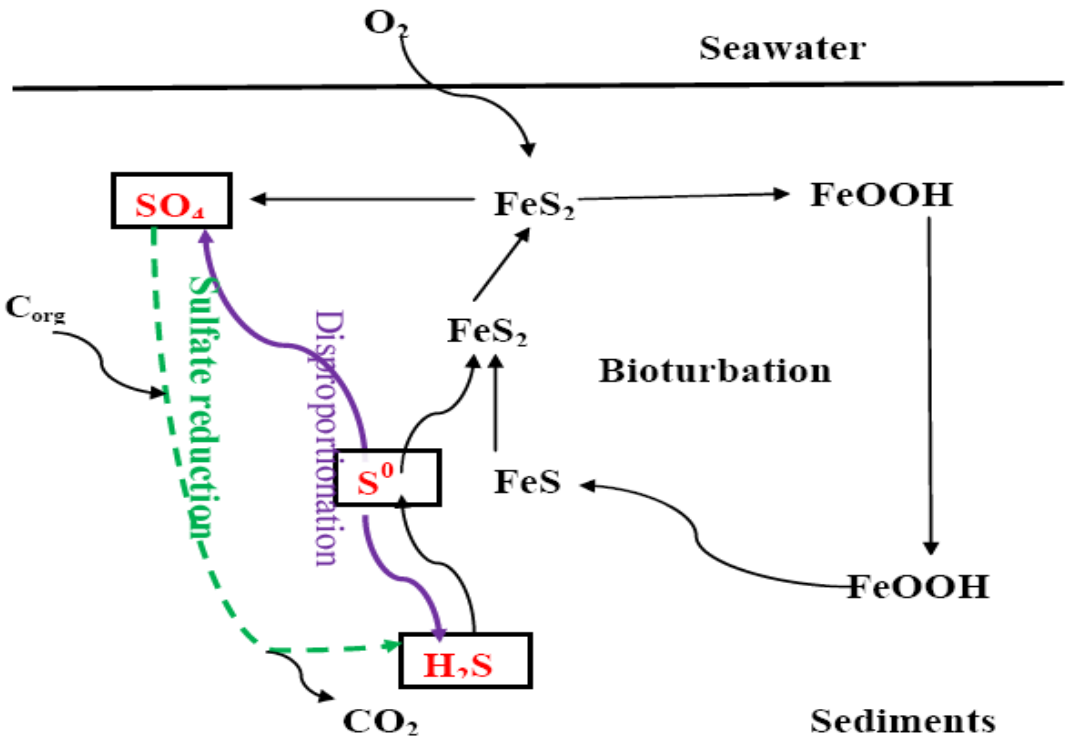

Figure 1.1. Diagram of the sulfur cycle in marine sediments. C_{org} represents the organic matter that is available for sulfate reducers. Sulfate reducing bacteria oxidize the organic substrates using dissolved sulfate to obtain energy for metabolic activities. The biogenic product, H_2S, reacts with iron oxides to form FeS and subsequently to form FeS_2. Part of this H_2S is oxidized to intermediate sulfur compounds (e.g., elemental sulfur, S^0). The fate of the intermediate sulfur species is disproportionation into dissolved sulfate and H_2S, or oxidation to other intermediate sulfur compounds and/or dissolved sulfate. Bioturbation by the burrowing macrofauna mixes the sulfur and iron compounds within the sediments contributing to the rate of sulfur cycling. Modified from Jorgensen (2006).

The role of this anaerobic process on the sulfur isotope geochemistry of oceanic sulfate is twofold. First, microbial sulfate reduction drives the consumption of sulfate-sulfur at a global scale (Schidlowski, 1989). An estimate of the rate of global bacterial sulfate reduction is ~

7.5×10^{13} mol SO_4^{2-} yr^{-1}, and the turnover time of modern oceanic sulfate-sulfur is estimated at ~ 0.5 million years (Jorgensen, 2006). Second, bacterial sulfate reduction produces large sulfur isotopic fractionations in nature and forms ^{32}S-enriched product of hydrogen sulfide. The hydrogen sulfide subsequently reacts with iron minerals and/or is incorporated into organic matter to form syn-sedimentary pyrite and organic sulfur. Both sinks contribute to the depletion of ^{32}S in the sedimentary sulfide pool (Thode et al., 1961), leaving the residual sulfate enriched in ^{34}S.

1.2 Overview of the sulfur cycle

The sedimentary sulfur cycle can be viewed as the microbial and abiotic transfer of sulfur between various pools, which can be simplified into seawater sulfate, sedimentary pyrite and evaporite sulfate minerals. A simple box model thus provides a baseline to 1) understand the long term variations of sulfur isotopic compositions of oceanic sulfate, 2) estimate sulfur fluxes or pools that are inaccessible and unknown over geologic time, and 3) achieve a better understanding of the relations between the sulfur cycle and other elemental cycles.

Sulfur on Earth's surface is originally derived from the mantle. The three sulfur reservoirs listed above are several orders of magnitude larger than other sulfur pools in the sedimentary sulfur cycle, such as sulfur in standing biomass (Schidlowski, 1989) and atmospheric sulfate aerosols (Brimblecombe et al., 1989). The major flux of sulfur to the oceans is transported by rivers, which is produced from sulfide (primarily sedimentary pyrite) and evaporite weathering (Meybeck, 1979; Walker, 1986). The magnitude of this flux has varied throughout the Phanerozoic in response to changes in the area of emergent land, continental runoff rates, oxygen levels, and sea level fluctuations (Garrels and Mackenzie, 1971; Garrels and Lerman, 1984;

Berner, 1987, 1991; Canfield, 2004). Other sources of sulfur to the oceans include contributions from volcanoes and mid ocean ridges eruption (Canfield, 2004) and through atmospheric deposition (Walker and Brimblecombe, 1983). These fluxes are also thought to have varied over the course of the Phanerozoic in response to the changes in volcanic outgasing and rates of seafloor production and subduction (Canfield, 2004; Lein and Ivanov, 1989; Walker, 1986).

The removal of sulfur from the oceans is through burial of oxidized sulfur (deposition of evaporites and lattice-bound sulfate in carbonate) and burial of reduced sulfur (sedimentary pyrite and organic sulfur). Evaporites occur in a variety of geographic environments, including lagoons, sabhka shorelines and deep basins. The formation of evaporites was highly episodic during the Phanerozoic (Holser et al., 1989; Halevy et al., 2012). Burial of reduced sulfur is also thought to have varied over Phanerozoic time (Strauss, 1999; Berner, 2004).

Constraints on the fluxes of sulfur introduced to and removed from the oceans have been provided by various isotopic and geological records. Important records are provided by buried pyrite, evaporite abundance (Holser, 1988, Halevy et al. 2012) and isotopic composition (e.g., Claypool et al., 1980) and by carbonate associated sulfate (CAS) (Burdett et al, 1989). Carbonate associated sulfate is a trace constituent that is incorporated into the lattice of carbonate minerals (Takano et al., 1985; Pingitore et al., 1995). In natural samples, the concentration of CAS in carbonates ranges from a few to several thousand ppm (Staudt et al., 1995; Kampschulte et al., 2001; Kampschulte and Strauss, 2004).

1.3 Records of seawater sulfate-sulfur isotopic compositions

Due to a minor kinetic sulfur fractionation (in terms of ^{34}S /^{32}S ~0-2.4‰, Raab and Spiro, 1991) associated with the precipitation of seawater sulfate, evaporite sulfate minerals have been

assumed to record the sulfur isotopic compositions of oceanic sulfate at the time of deposition (e.g., Claypool et al., 1980; Strauss, 1999). While these records are not perfect, they contain both global signals and local effects and provide important information about the isotopic composition of global oceanic sulfate in discrete time intervals. Another complication arises from the episodic nature of the evaporite record (Hosler et al., 1988), which makes these seawater proxies difficult to correlate across basins, and thus limits the resolution of evaporite-based sulfur isotope age curves (Bottrell and Newton, 2006).

Carbonate associated sulfate was introduced as an alternative to evaporites and thought to have potential advantages over evaporite-based isotopic records because of the wide temporal and spatial distribution of carbonate throughout the Phanerozoic (Bottrell and Newton, 2006). The extraction of carbonate-associated sulfate (CAS) has been developed into a routine practice (Kampschulte et al., 2001; Kampschulte and Strauss, 2004; Gill et al., 2007; this study); studies to assess the effect of diagenesis on the preservation of $^{34}S/^{32}S$ signals have shown that this proxy can be used in many cases to obtain information about sulfate at the time carbonates were deposited (Gill et al., 2008).

Studies of modern biogenic and non-biogenic carbonates have indicated that the $^{34}S/^{32}S$ of CAS is broadly consistent with that of seawater sulfate. The CAS-based $^{34}S/^{32}S$ records match those derived from coeval evaporites. Carbonate associate sulfate has also been proven to be a reliable way to reconstruct high-resolution sulfur isotopic records of Phanerozoic seawater (Burdett et al., 1989; Strauss, 1999; Kampschulte et al., 2001; Kampschulte and Strauss, 2004). This proxy will be used in this study to reconstruct a record of $^{33}S/^{32}S$ from the latest Neoproterozoic to the Triassic Period.

1.4 Contributions of this work

In this study, I examine several questions about the marine sulfur cycle and the controls on the isotopic compositions of oceanic sulfate through time, including:

Chapter 2, where I describe the basic notations and review the dynamics of multiple sulfur isotopes afforded by the isotope mass balance equations. This context provides the foundation that is used in later parts of this thesis;

Chapter 3, where I revisit what is known about the sedimentary sulfur cycle and explore the records of Phanerozoic seawater sulfate concentration, sulfur isotopic records of oceanic sulfate, and fluxes into and out of the oceans. I also discuss the use of $\Delta^{33}S$ as a way to better understand the evolution of the sulfur cycle throughout geologic time, and as a way to test and/or simulate ideas about the internal mechanisms in the sulfur cycle;

Chapter 4, where I describe the analytical approaches that have been used in the case studies. I also evaluate the uncertainty associated with these chemical procedures and isotopic measurements using a mass spectrometer;

Chapter 5, where I provide new sulfur isotope measurements ($\delta^{34}S$ and $\Delta^{33}S$) of carbonate associate sulfate (CAS) and sedimentary pyrite for previously studied samples from the Huqf Supergroup, in Oman (Fike et al., 2006, Fike and Grotzinger, 2008). These multiple sulfur isotope records are examined to understand the connections between sulfur isotope fractionation, sulfate concentrations and sulfide reoxidation;

Chapter 6, where I present a previously published study evaluating the sulfur isotope fractionation associated with Phanerozoic pyrite burial (Wu, et al., 2010). This case study

provides two approaches to constrain the sulfur isotope fractionation throughout the Phanerozoic, yielding similar results shwoing that the sulfur isotope fractionation changed from slightly lower values in the early Phanerozoic to higher values starting in the Triassic. This chapter also presents a reanalysis of the Phanerozoic record that draws on samples collected from the archive of the Bochum-Ottawa carbonate samples (Veizer et al., 1999). These carbonate samples have been used in prior studies to establish high-resolution records of Phanerozic seawater $^{87}Sr/^{86}Sr$, $^{13}C/^{12}C$, and $^{18}O/^{16}O$. I have focused on well-preserved biogenic calcite (e.g. brachiopods and belemnites) and limestones samples from the Cambrian to the Triassic to begin building a long-term trend for $\delta^{34}S$ and $\Delta^{33}S$ of oceanic sulfate and to understand their implications;

And chapter 7, wehere I present an overview of the future direction and emerging questions about the sulfur cycle over geological time.

Chapter 2: Systematics of sulfur isotopes, fractionation and mass balance

Abstract: The fundamental concenpts and systematics of sulfur isotopes are introduced in this chapter, and the pertinent isotope mass balance in the cycling of sulfur in biogeochemical systems under various conditions (open system, closed system, steady state, and non steady state) is examined and expressed in $\Delta^{33}S$-$\delta^{34}S$. Dynamics of $\Delta^{33}S$ provide another way to test existing hypotheses inferred from $\delta^{34}S$ records, and provide additional information about temporal changes in the sulfur cycle.

2.1 Mass dependent fractionation (MDF) and isotope fractionation factor (α)

The substitution of different sulfur isotopes into chemical compounds results in subtle but measurable differences in chemical and physical properties (known as isotope effects) and these are the root cause of sulfur isotope redistribution in chemical, physical, and biochemical processes. The magnitude of isotope discrimination is expressed as the fractionation factor (α) and is defined as:

$$^{3x}a_{ij} = \frac{^{3x}R_i}{^{3x}R_j},$$

$$^{3x}R = \frac{^{3x}S}{^{32}S},$$

$$x = 3, 4, 6,$$

where ^{3x}R is the sulfur isotopic ratio in sulfur chemical species *i* or *j*; $^{3x}\alpha$ is the fractionation factor for sulfur chemical species *i* and *j*.

The relative mass difference between ^{32}S and ^{34}S is two atomic mass units, while that between ^{32}S and ^{33}S is one atomic mass unit. Mass dependent isotope effects are so called because they strongly rely on the mass differences associated with isotopic substitution. Since mass-dependent fractionation scales with relative mass differences, the mass-dependent fractionations for $^{33}S/^{32}S$

are typically one-half of those for $^{34}S/^{32}S$. A power law is used to describe the relationship between fractionation for the minor sulfur isotopes:

$$^{33}\alpha = {}^{34}\alpha^{\,^{33}\theta}$$

$$^{36}\alpha = {}^{34}\alpha^{\,^{36}\theta}$$

where $^{33}\theta$ ($^{36}\theta$) is an exponent and its values are around 0.515 (1.90 for $^{36}\theta$) for equilibrium isotopic exchange.

The major processes which are the ultimate source of the variations in the sulfur isotopic compositions of seawater sulfate, include bacterial sulfate reduction, sulfide oxidation, and sulfur disproportionation, which are all associated with mass-dependent fractionations. Those sulfur isotope fractionations are impartedto oceanic sulfate-sulfur via sulfur isotope mass transfers among sulfur pools.

2.2 δ and Δ Notations

The sulfur isotopic abundances of individual samples are described using delta notation (δ) (mostly due to the technical reasons of mass spectrometric measurements of isotope abundances):

$$\delta^{3x}S = \frac{^{3x}R_{sample}}{^{3x}R_{\text{standard}}} - 1$$

$$x = 3, 4, 6$$

The $\delta^{3x}S$ notation expresses the deviation of the sulfur isotopic abundance in samples relative to the isotopic abundance in the reference material. The reference material used to report $\delta^{3x}S$ is

the V-CDT , which is calibrated via the IAEA standards, and the deviations are reported in parts per thousand (per mil, ‰). The fractionation factor (α) between sulfur compounds i and j can be expressed in terms of the (δ) notations as:

$$^{3x}\alpha_{ij} = \frac{^{3x}\delta_i + 1}{^{3x}\delta_j + 1}$$

The capital delta (Δ) notation is defined as:

$$\Delta^{33}S = \frac{^{33}R_{sample}}{^{33}R_{\text{standard}}} - \left\{ \frac{^{34}R_{sample}}{^{34}R_{\text{standard}}} \right\}^{0.515}$$

$$\Delta^{36}S = \frac{^{36}R_{sample}}{^{33}R_{\text{standard}}} - \left\{ \frac{^{34}R_{sample}}{^{34}R_{\text{standard}}} \right\}^{1.90}$$

Where the exponent of 0.515 (1.90) is chosen as a reference that approximates the exponent value relating to the low-temperature mass-dependent sulfur isotope exchange reactions (Hulston and Thode, 1965). $\Delta^{33}S$ and $\Delta^{36}S$ values describe deviations of sulfur isotopic abundances expressed in parts per thousand (per mil, ‰) in a sample relative to those isotopic abundances predicted by the mass-dependent isotope fractionation array.

Measurements of $\Delta^{33}S$ and $\Delta^{36}S$ values for reference materials reveal deviations from $\Delta^{33}S = \Delta^{36}S = 0$ that are significantly larger than analytical uncertainties (internal precision of mass spectrometric measurements). These subtle but measurable variations for $\Delta^{33}S$ and $\Delta^{36}S$ are derived from mass-dependent isotope fractionation processes other than equilibrium isotope exchange and mixing, as well as mass-independent isotope fractionation processes (Thiemens, 1999; Farquhar et al., 2000; Ono et al., 2006; Farquhar et al., 2007). The sulfur isotope

fractionations associated with microbial sulfate reduction, sulfur oxidation, and sulfur disproportionation, and their propagation via the mass transfer among sulfur pools in the sulfur cycle have the potential to generate non-zero and long term changes in $\Delta^{33}S$ and $\Delta^{36}S$ of oceanic sulfate-sulfur.

2.3 Dynamics of $\Delta^{33}S$-$\delta^{34}S$

In this section, emphasis is focused on the basic principles of isotope mass conservation. Evolutionary trajectories are plotted in $\Delta^{33}S$-$\delta^{34}S$ space for reversible/irreversible reactions in closed systems (two limiting cases), open systems at steady state, and open systems at non-steady state. These principles can also be applied to the study of dynamics of $\Delta^{36}S$-$\delta^{34}S$ relationships, which are not examined in this study, insofar as these can be inferred from $\Delta^{33}S$-$\delta^{34}S$ dynamics.

In systems where sulfur isotopes are concerned, sulfur isotopic compositions of products and reactants are dependent on their degree of openness. Closed systems are those where there is no mass exchange between the studied system and its surroundings. Open systems are those where mass transfer occurs between the studied system and its surroundings.

There are geochemical analogs of closed systems at various spatial and temporal scales. For instance, the behavior of porewater sulfate (variations in concentrations and sulfur isotopic compositions) in rapidly accumulated sediments can be described as a closed system. The Phanerozoic sedimentary sulfur cycle is thought tobehave approximately like a closed system where sulfur exchange between the mantle and surface sulfur pools is minor (Holser, et al., 1988).

Open systems occur naturally and ubiquitously. For instance, levels of oceanic sulfate are balanced by the transfer of sulfur into and out of the oceans. Geological evidence from fluid inclusion studies have shown that the concentration of seawater sulfate has varied over time (Horita et al., 2002), imposing a effect on mixing and homogenizing the sulfur isotopes of oceanic sulfate.

The sulfur isotopic compositions of studied sulfur species are also dependent on whether the system is at steady-state or at non-steady-state. The steady-state systems are those where the characterized property is balanced by factors that influence this property (e.g. concentration). The non- steady-state systems are those where the characterized property varies with time. An efficient way to deal with the non-steady-state system to view such a system as a continuous, but transient, steady state.

2.3.1 Dynamics of $\Delta^{33}S$-$\delta^{34}S$ for reversible reaction in closed systems

A reversible reaction is a process that occurs in both the forward and reverse directions between reactants and products. The evolution of sulfur isotopes for products and reactants can be illustrated graphically in geometric terms in two dimensional $\Delta^{33}S$-$\delta^{34}S$ space. The magnitude of isotope exchange for reversible reactions can be described in terms of a fractionation factor, which is assumed to be constant.

The isotope mass balance is conserved in closed systems, and the exact isotope mass balance requirements are followed in my study: the specific isotopes in precursor reactants equal the sum of the specific isotopes in products. This fundamental concept can be expressed in mathematical terms as:

$$m_{\Sigma} \times f_{\Sigma} = \sum_{i} m_i \times f_i$$

where *m* is the molar quantity of the element of interest, and *f* is the fractional isotope abundance of the species of interest. The subscript Σ represents the total sample: the combination of sub samples of *i*.

This rudimentary equation is also the root of the mixing/un-mixing effects on variation in $\Delta^{33}S$ and $\delta^{34}S$. $\delta^{34}S$ and $\Delta^{33}S$ values can be expressed in terms of any reference scale of isotope abundances, but the same reference scale must be used for products and reactants. Table 2.1 lists the starting isotopic values and fractionation factors that are used in calculations in sections of 2.3.1 to 2.3.4.

Table 2.1values used in calculations

Table 2.1	Values used in calculations
$\delta^{34}S$ (‰)	0
$\Delta^{33}S$(‰)	0
$^{34}\alpha$	0.975
$^{33}\alpha$	0.987

Figure 2.1 shows the calculated results under the condition of a reversible reaction in a closed system. The residual reactant (red line) is progressively enriched in ^{34}S as the product is accumulated. The product (blue line) will reach the starting isotopic values of the initial reactant when 100% of the reactant is converted to product. To a first-order approximation, there are few geochemical systems on Earth's surface that behave as a closed system. However, these calculated results place a limit on how reactants and products could evolve.

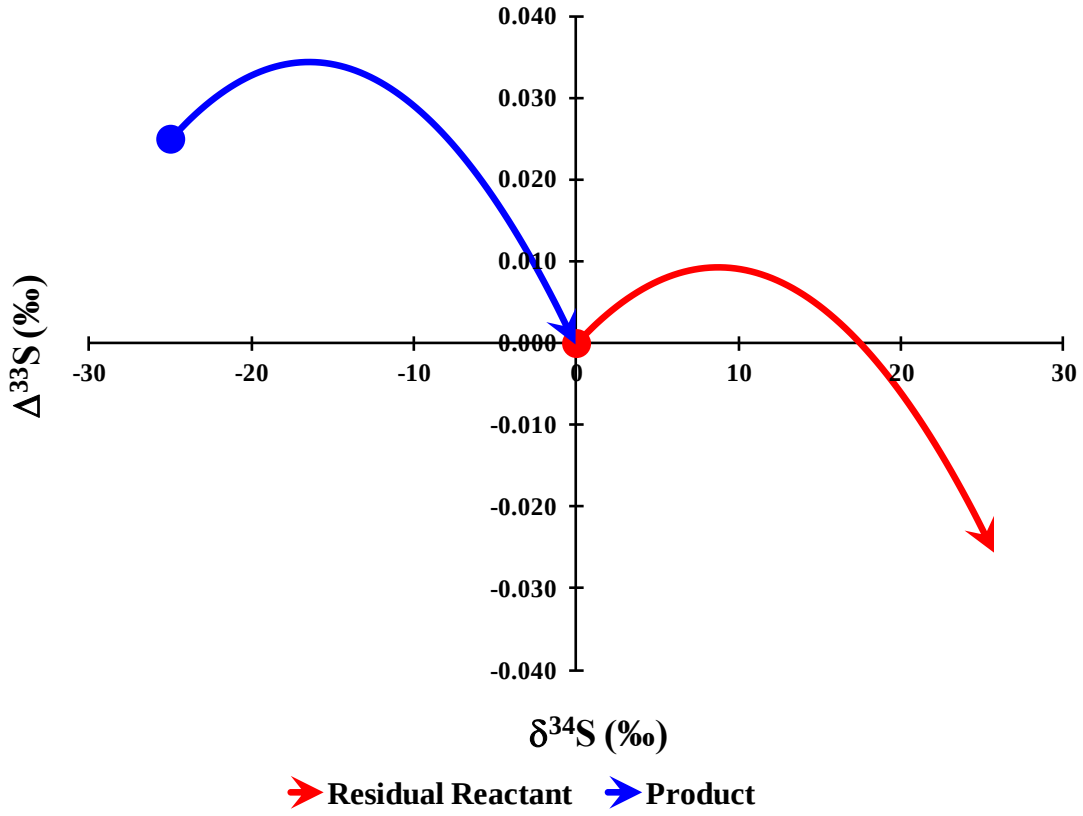

Figure 2.1. Isotopic trajectories for reactant and product sulfur pools under conditions of a reversible reaction in a closed system. The origin is the assumed starting compositions of the reactant. The red line shows the isotopic evolution path of the reactant, indicating an increase in both $\Delta^{33}S$ and $\delta^{34}S$ at early stage, and then a decrease in $\Delta^{33}S$, but with continuously increasing $\delta^{34}S$ at later stage. The blue curve shows the isotopic evolution path of the product, which tracks the path of the reactant, but with constant differences in both $\Delta^{33}S$ and $\delta^{34}S$.

2.3.2 Dynamics of $\Delta^{33}S$-$\delta^{34}S$ for irreversible reaction in closed systems

An irreversible reaction is a process that proceeds to completion in one direction. A limiting case for irreversible reactions can be described as Rayleigh distillation. In such a system, isotope fractionation occurs between the reactant and the instant product, and the product is lost from the system. The basic equation for the isotopes of the residual reactant is expressed as:

$$^{3x}R_{residual} = {}^{3x}R_{initial} \times f^{(^{3x}\alpha - 1)}$$

Where the x=3, 4, 6, and R represents the isotopic ratios of residual reactant and initial reactant. The parameter of f is the molar fraction of the residual reactant in the closed system, and the parameter of α is the fractionation factor associated with the irreversible reaction. The calculated results are shown in Figure 2.2.

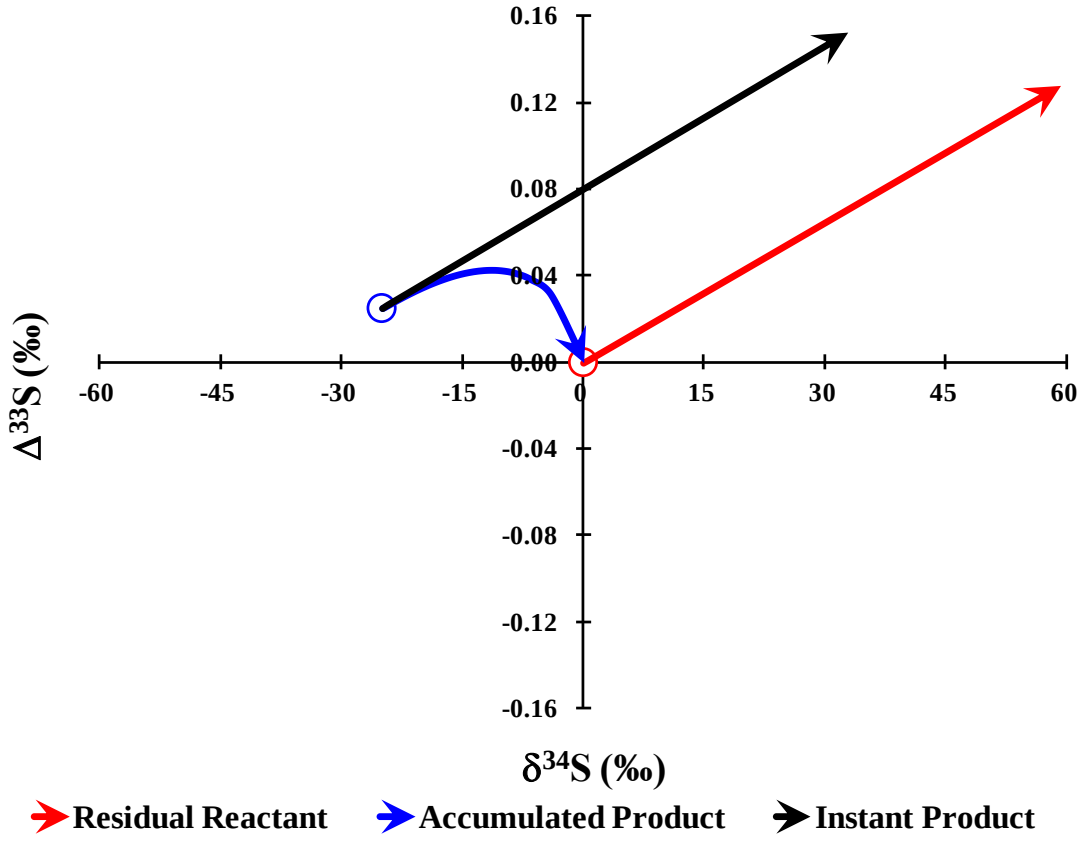

Figure 2.2. Isotopic trajectories for reactant, instant product, and accumulated product for an irreversible reaction in a closed system. The origin is the assumed starting compositions of the reactant. The red line shows the isotopic evolution of residual reactant, the blue line indicates the isotopic evolution of the accumulated product, and the black line expresses the isotopic evolution of the instant product. With the reaction proceeding, the residual reactant becomes progressively enriched in ^{34}S and $\Delta^{33}S$. The instant product tracks the trajectory of the residual reactant, but with lower values in $\delta^{34}S$ and higher values in $\Delta^{33}S$. The isotopic values of the accumulated product will eventually evolve to those values of the initial reactant.

A geochemical system of a hypothetical closed ocean basin can be approximated as an irreversible reactions. The instant product may be represented by sedimentary pyrite formed in

local basins while the residual reactant represents seawater sulfate. In such a system, the formation of evaporate sulfate minerals is negligible compared to the continuous removal of sulfur via pyrite burial. However, the formation of evaporite sulfate minerals may influence the levels of seawater sulfate on shorter time scales, resulting in a reservoir effect, which may be detected on high resolution sulfur isotopic records of oceanic sulfate. The uncertainty regarding the time intervals when ocean basins approximate closed systems limits such signals of geochemical parameters to be fully identified and/or expressed in natural samples. The calculated results place another type of limit on how the isotopic compositions of reactant and product could evolve.

2.3.3 Dynamics of $\Delta^{33}S$-$\delta^{34}S$ for open systems at steady state

The mathematical treatment of open systems at steady state is illustrated by a reaction box with one flow into the box and two flows out of the box. This model approximates the isotopic fractionation at an enzymatic reaction site. This view is also applicable to the cycling of oceanic sulfate-sulfur at global/basinal scales where the inflow describes the sulfur flux to the oceans, and the outflows are the burial of pyrite-sulfur and the formation of evaporite sulfate minerals.

The underlying assumption for traditional interpretations of variations in sulfur isotope compositions of seawater sulfate over geological time is that the oceanic sulfate-sulfur system is in a continuous but transient steady state. This assumption is justified when studying the sulfur cycle at a low-resolution of sampling (e.g., evaporite sulfate mineral samples) with large age uncertainties that would be of the same order of the response times needed for the oceanic sulfate to reach a new steady state.

The common steady-state equation relating ^{34}S to ^{32}S for the sulfur cycle is expressed as:

$$\delta^{34}S_{SW} = \delta^{34}S_{\text{in}} + f_{PY} \times \Delta^{34}S_{SW-PY}$$

Where $\delta^{34}S_{SW}$ is the sulfur isotopic composition of seawater sulfate, and $\delta^{34}S_{in}$ is the isotopic composition of influx sulfur. The f_{PY} is the fraction of sulfur buried as sedimentary pyrite, and $\Delta^{34}S_{SW\text{-}PY}$ is the isotopic difference between the isotopic compositions of marine sulfate and coeval sedimentary pyrite.

In addition, the equation above implies the continuous sulfate-sulfur removal by evaporite sulfate minerals or hydrothermal sulfate reduction and no sulfur isotope fractionation is associated with these two pathways. These assumptions can be relaxed for non steady state systems.

The inferred parameter of f_{PY} is usually interpreted from the observed sulfur isotopic variations of seawater sulfate (Figure 2.3A). The positive sulfur isotope shifts may represent more removal of ^{32}S from the oceanic sulfate by increasing f_{PY}, whereas negative sulfur isotope shifts may indicate a smaller f_{PY}. However, the interpretations for changes in f_{PY} are not unique. For instance, the increase of f_{PY} may result from either enhanced preservation or enhanced pyrite formation, or both. Changes in f_{PY} over time are also thought to be linked with the oxidation state of the water column and processes that occurred in marine sediments where the sedimentary pyrite is formed .

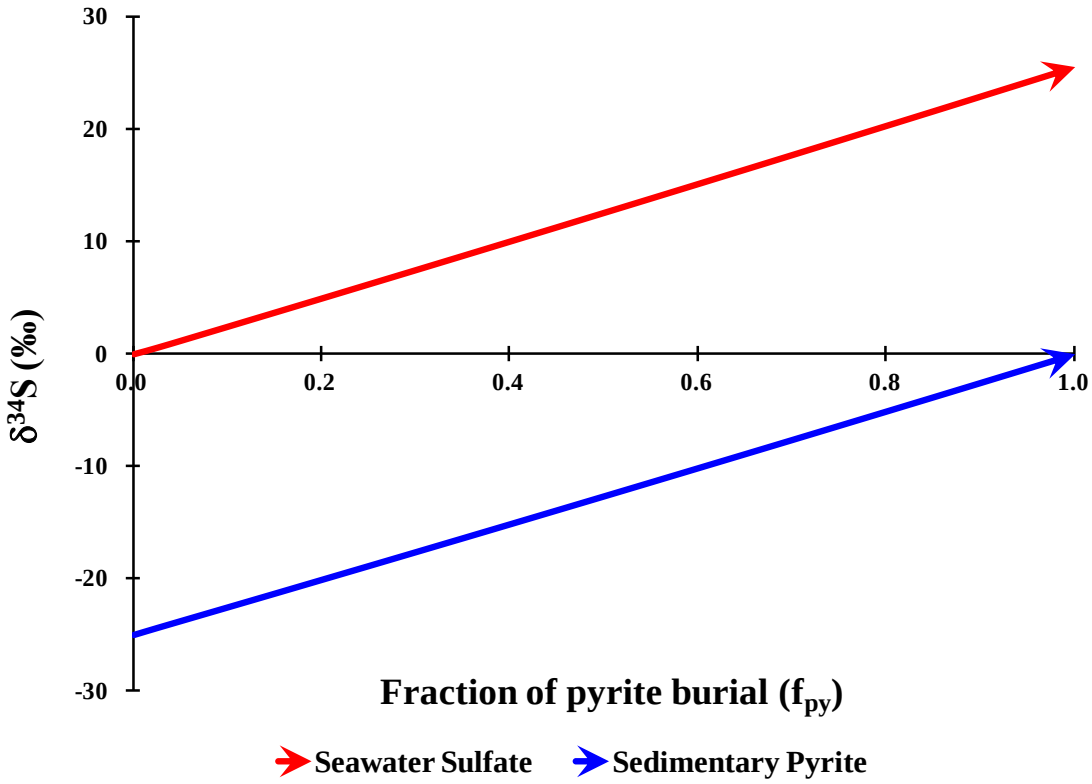

Figure 2.3A. Relationship between the isotopic composition of seawater sulfate (red line) and pyrite (blue line) fraction of pyrite burial.

A coupled steady-state equation relating ^{33}S to ^{32}S for the sulfur cycle is expressed as:

$$\delta^{33}S_{SW} = \delta^{33}S_{\text{in}} + f_{PY} \times \Delta^{33}S_{SW-PY}$$

Where $\delta^{33}S_{SW}$ is the sulfur isotopic composition of seawater sulfate, and $\delta^{33}S_{in}$ is the isotopic composition of influx sulfur. The f_{PY} is the fraction of sulfur buried as sedimentary pyrite, and $\Delta^{33}S_{SW\text{-}PY}$ is the isotopic difference between the isotopic compositions of oceanic sulfate and coeval sedimentary pyrite.

These two steady state equations can be used to derive the dynamics of $\Delta^{33}S\text{-}\delta^{34}S$ for reactants, and the dynamics of $\Delta^{33}S\text{-}\delta^{34}S$ for products by taking advantage of isotope mass balance

requirements. The calculated results are shown in Figure 2.3B. The evolutionary line of seawater sulfate provides a way to test ideas about changes in the sulfur cycle, and the projected line of sedimentary pyrite also provide a way to differentiate local signal imposed on the global signal.

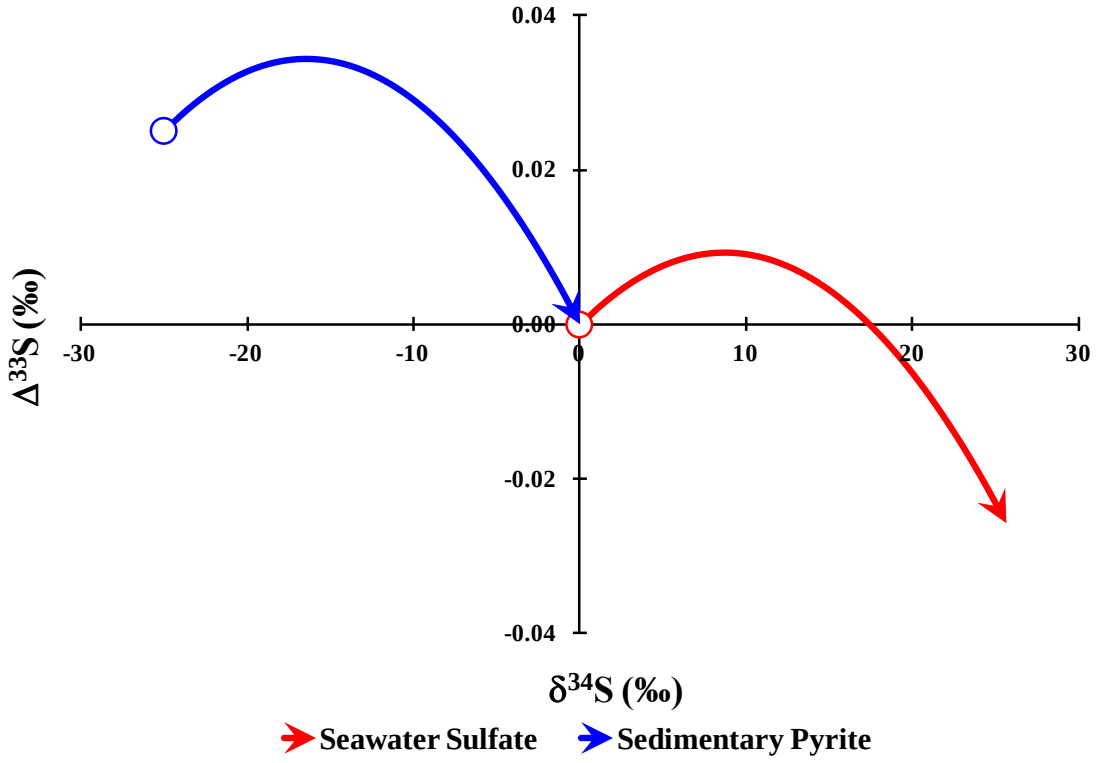

Figure 2.3B. Isotopic trajectories for seawater sulfate (red line) and buried pyrite (blue line). The origin is the assumed isotopic compositions of influx sulfur to oceans. The pyrite-sulfur isotopes track that of oceanic sulfate, with constant differences in both $\Delta^{33}S$ and $\delta^{34}S$.

2.3.4 Dynamics of $\Delta^{33}S$-$\delta^{34}S$ for open systems at non-steady state

The isotope mass balance among the sulfur pools at non-steady state conditions can be expressed in two basic equations, in terms of the size of the sulfur pool, and sulfur fluxes into and/or out of thisreservoir:

$$\frac{d^{3x}R_{SS}}{dt} = \frac{\sum({}^{3x}R_{\text{in}} - {}^{3x}R_{SS}) \times \varphi_{in} + \sum({}^{3x}R_{\text{out}} - {}^{3x}R_{SS}) \times \varphi_{out}}{M}$$

$$\frac{dM}{dt} = \sum \varphi_{in} - \sum \varphi_{out}$$

Where x=3, 4, 6, R_{SS} is the sulfur isotopic ratio of the studied sulfur pool, R_{in} and R_{out} are the isotopic ratios of the sulfur flux into and/or out of the sulfur pool, and φ represents the sulfur transfer into and/or out the reactive chamber. M represents the size of the sulfur pool.

One reaction chamber with a single influx and single out-flux is constructed to illustrate how the sulfur isotopes respond to changes in sulfur fluxes. The magnitude of the outflow from the reaction chamber is proportional to the size of the sulfur pool. The calculated results are shown in Figure 2.4.

Modern oceanic sulfate is out of balance with respect to the sulfur influxes and outfluxes, and this is also likely to be the case during the Phanerozoic. The isotopic evolution of oceanic sulfate in this calculation is also controlled by the sulfur isotope fractionation factor and the possible fluxes out of the oceanic sulfate system (e.g., the deposition of evaporite sulfate minerals). The comparisons between the simulation results and time-series observations may provide hints to the complexities of the sulfur cycle. However, the simulation results can only allow the exclusion of some scenarios combining factors that control the sulfur isotope mass balance. The simulation results can also reflect high frequency variations in both $\delta^{34}S$ and $\Delta^{33}S$ of oceanic sulfate that may not be recorded in samples due to practical reasons (for example, the uncertainty in age constraints on samples and sampling frequency).

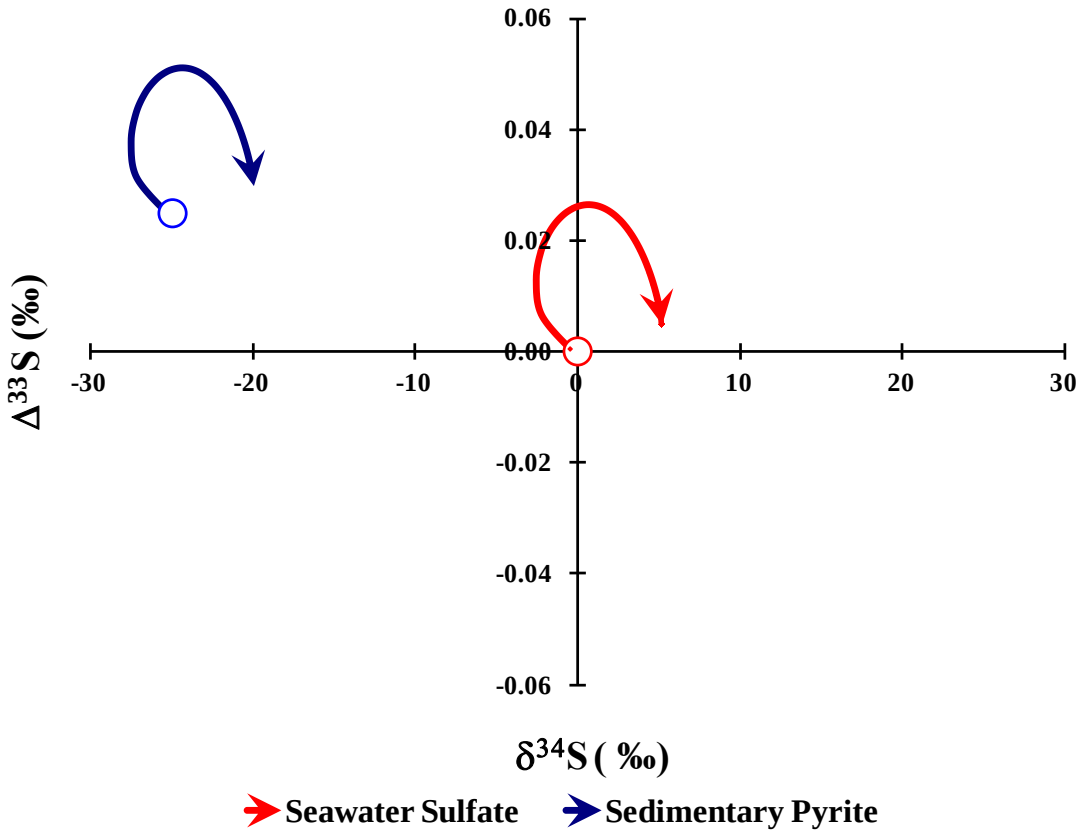

Figure 2.4. Isotopic trajectories for seawater sulfate (red line) and sedimentary pyrite (blue line). The origin is the starting composition of oceanic sulfate. The influx sulfur fractionations are set to be $\delta^{34}S$=-20‰ and $\Delta^{33}S$=0.030 relative to the starting oceanic sulfate. The change in sulfur flux to the oceans is set at an initial value of 50% to 100% the modern sulfur influx into the oceans within 0.03 million years. The pyrite burial rate is also assumed to follow first order kinetics, which are dependent on the concentrations of seawater sulfate. The oceanic sulfate-sulfur system reaches steady state within 5 Ma. The $\delta^{34}S$ of oceanic sulfate firstly decreases, associated with the increase in $\Delta^{33}S$, because the influx sulfur has a lower value of $\delta^{34}S$, and higher values of $\Delta^{33}S$ cannot be compensated by the burial of pyrite with positive values of $\Delta^{33}S$. Secondly, the $\delta^{34}S$ and $\Delta^{33}S$ of seawater sulfate increase at the same pace. At some turning point, the $\delta^{34}S$ continues increasing while the $\Delta^{33}S$ begins to decrease. The values of both $\delta^{34}S$ and $\Delta^{33}S$ in pyrite track the path of oceanic sulfate-sulfur.

2.3.5 Dynamics of $\Delta^{33}S$-$\delta^{34}S$ in network mixing at various scales

Non-zero $\Delta^{33}S$ values can be produced by primary processes (physical and/or chemical processes) , which have θ values different from the reference value (0.515). However, non-zero $\Delta^{33}S$ can also be produced by mixing of several sulfur pools with different sulfur isotopic

compositions. This basic concept can be illustrated using binary mixing in $\Delta^{33}S$-$\delta^{34}S$ space (Figure 2.5). Non-zero $\Delta^{33}S$ can be produced by mixing two end members with zero $\Delta^{33}S$ that fall on the reference fractionation line, which is horizontal in $\Delta^{33}S$-$\delta^{34}S$ space. The mixing line in this case is a curve (blue line), showing a non-linear relationship between $\Delta^{33}S$ and $\delta^{34}S$. The non-zero values of $\Delta^{33}S$ due to mixing are larger than the analytical uncertainties associated with the mass spectrometric isotopic measurements (1σ: 0.011‰, see chapter 4 for more details).

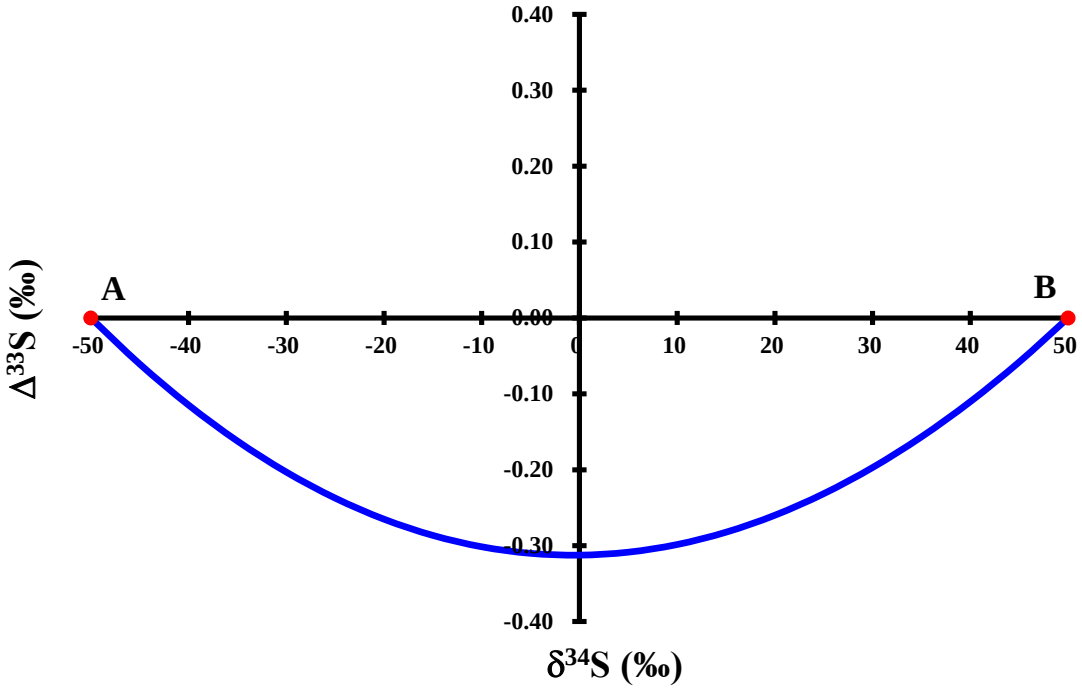

Figure 2.5. Mixing line for two end memberss A and B. A andB have zero values of $\Delta^{33}S$. However, mixtures from different proportional mixing of A and B have non-zero values of $\Delta^{33}S$.

Regarding the measurable $\Delta^{33}S$ in sulfur species, two cases are used to demonstrate the application of $\Delta^{33}S$ to obtaining new information about the evolution of the sulfur cycle at different temporal and spatial scales. The first case is applied to the conceptual sulfur network

model for microbial sulfate reduction proposed by Rees (1973) to understand the internal mechanism of the sulfur isotope fractionation. The second case for the application of measurable non zero $\Delta^{33}S$ variations applies to the study of the evolution of the sulfur cycle over geologic time.

Under the assumption of steady state for internal sulfur pools, there should be a continuous backwards sulfur flux of intermediate sulfur compounds or reaction sites in order to preserve isotope mass balance. Therefore, the presence of non-zero $\Delta^{33}S$ can be used to constrain the proportion of forward and backwards sulfur reactions, and to test assumptions used in the Rees model (1973).

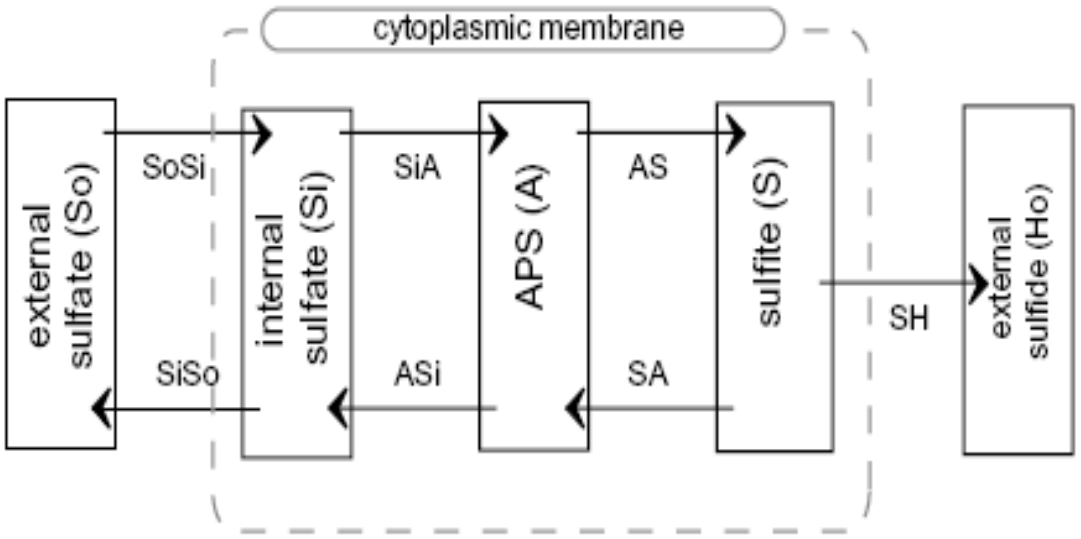

Figure2.6. APS represents the Adenosine-5'-phosphosulfate pool. The sulfur fluxes are: SoSi, SiSo, SiA, ASi, AS, SA, and SH. The associated $^{34}\alpha$ values are: 1.003, 0.975, and 0.975 for SoSi, AS and SH pathways, respectively. Associated $^{34}\alpha$ values are set to be 1.000 for the remaining pathways. (from Farquhar et al., 2007).

The mathematical treatment of sulfur networks defines the fractions of outflow to the upstream sulfur pools in terms of the total influx to the studied sulfur pool. In the Rees model (1973), the controlling backflows are named SiSo and SA. The changes in SiSo and SA may link to changes

in environmental conditions for bacterial sulfate reduction. The graph below is constructed in terms of these two parameters and the resulting field provides the basic framework for data interpretation.

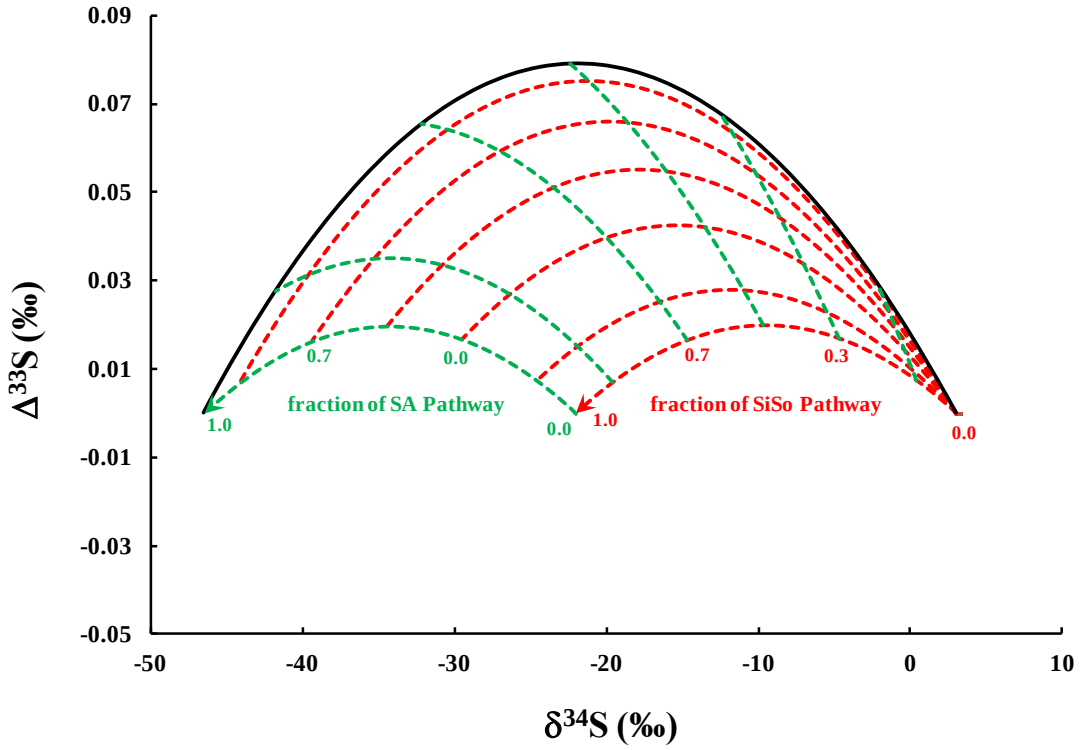

Figure 2.7. Calculated field for the Rees model (1973). The field defines the possible sulfur isotope fractionations between the starting sulfate and final product H_2S. The $\delta^{34}S$ and $\Delta^{33}S$ values are normalized to the starting values of sulfate. The red lines show the trajectories for the constant backflow fraction of the SA pathway and various backflow fractions of the SiSo pathway. The green lines show the trajectories for a constant fraction of backflow in the SiSo pathway, and various backflow fractions of SA. With the increasing fraction of SA and SiSo, the $\delta^{34}S$ values consistently increase, while the $\Delta^{33}S$ values show various paths.

The biogeochemical tracer of $\Delta^{33}S$ has been used in studies that provide insights into the internal mechanism of the sulfur cycling (Johnston et al., 2005, Ono et al., 2006, Wu et al., 2010). The working networks for sulfur cycling that are used to track the isotopic evolution of oceanic sulfate-sulfur are constructed in terms of sulfur transformations in the marine sulfur cycle (Wu et

al., 2010). A calculated case is illustrated in Figure 2.8 showing how sulfur reoxidation may influence the isotopic evolution of oceanic sulfate at steady state. The field for pyrite-sulfur (green grid in Figure 2.8) is interpreted to represent basin-scale averages. The measured sulfur isotope data from sedimentary pyrite may embed information about local geochemical or biogeochemical factors controlling its sulfur isotopoic compositions. The imprint of such processes at global scale may be recorded in the sulfur isotopes of oceanic sulfate-sulfur (red grid in Figure 2.8), which can be tested using coeval samples from different oceanic basins.

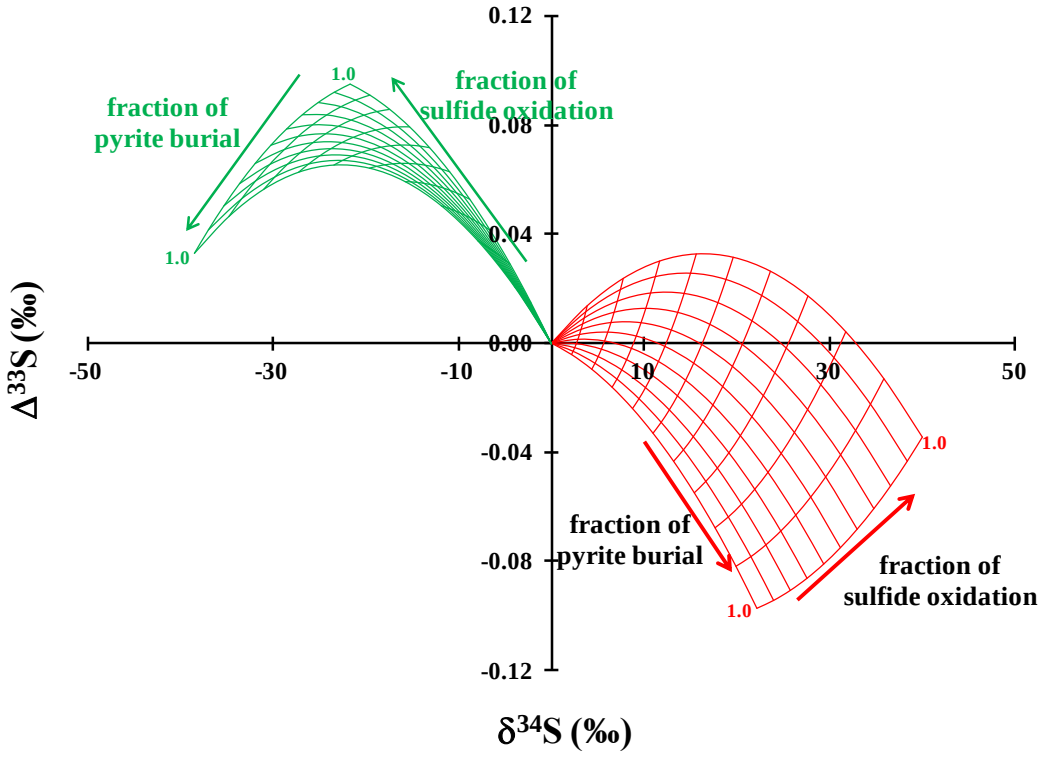

Figure 2.8. Trajectories for seawater sulfate (red field) and pyrite (green field) at steady state for the marine sulfur cycle. The origin is the isotopic composition of influx sulfate-sulfur to the oceans. In this model, no fractionation is associated with sulfide reoxidation or sulfur intermediates transformed via sulfur disproportionation. With an increasing fraction of pyrite burial, $\delta^{34}S$ values also increase while the $\Delta^{33}S$ values decrease. The values of both $\delta^{34}S$ and $\Delta^{33}S$ increase with an increasing fraction of sulfur intermediate reoxidation. The values for pyrite track the ones for oceanic sulfate. The mixing line for oceanic sulfate and the corresponding predicted pyrite go through the origin in this graph.

The basic principles described in this chapter are applied to my current study on the evolution of the sulfur cycle since the latest Neoproterzoic Era. Carbonate associated sulfate (CAS) has potential advantages over other proxies for reconstructing seawater sulfate-sulfur isotopes because of the wide distribution of carbonates, global correlations among ocean basins, and temporally continuous coverage throughout the Phanerozoic (Bottrell and Newton, 2006). The variations in sulfur isotopic compositions of ancient oceans may indicate the influence on the sulfur cycle by large-scale biogeochemical processes.

My project focuses on using the systematics of $^{33}S/^{32}S$ ($\Delta^{33}S$) as a biogeochemical indicator in order to evaluate inferences from $\delta^{34}S$ records of oceanic sulfate, and more importantly gain new insight on the sulfur cycle. The following chapters will present the un-resolved questions about sulfur cycling on geologic time scales, present the scientific questions to be addressed in my study, evaluate the uncertainty associated with chemical extraction and isotopic measurements, and finally interpret the data and point to future directions for the research.

Chapter 3: The Sedimentary sulfur cycle

Abstract: This chapter presents an overview and summary of what is known about the sedimentary sulfur cycle: estimates of size of pyrite-sulfur, evaporite sulfate-sulfur, and oceanic sulfuate-sulfur over the course of Phanerozoic, and estimates of sulfur flux into and out of modern oceans. This chapter also discusses the time scales (on order of 50,000 years, smaller than the time resolution of sampling) for homogenizing sulfur isotopes of oceanic sulfate between water masses. A broad review of what is new (with emphasis on minor sulfur isotope measurments over the past decade) in sulfur geochemistry research is presented. The newly $\delta^{34}S$ record derived from the proxy of carbonate associated sulfate confirms the long term features of the evolution of the sulfur cycle observed from $\delta^{34}S$ record of evaporite through the Phanerozoic. The $\Delta^{33}S$ records over the Phanerozoic is a combination of sulfur tranfer and sulfur isotope effect associated sulfur transformation between sulfur pools and their implications will be examined in following chapters.

3.1 Sulfur isotopic compositions of modern seawater sulfate

The sulfur isotopic compositions of oceanic sulfate in Modern marginal marine and open ocean environments have been determined from seawater samples collected from various locations and depths. These results give values ($\delta^{34}S$) that range from 18‰ to 22‰ (Bottcher et al., 2007). The range of $\delta^{34}S$ values can be due to several factors, including: 1) mixing with fresh water sulfate; 2) oxidation of reduced sulfur compounds introduced from the marine sediments; 3) mixing with porewater sulfate across the sediment-water surface; 4) production of organic-sulfur by sulfate assimilation; and 5) decomposition and recycling of organic-sulfur in water columns. These processes play different roles in regulating the variations in sulfur isotopic composition of oceanic sulfate.

The $\delta^{34}S$ composition of dissolved sulfate in open oceans have been constrained from several water column profiles in the Atlantic and Pacific oceans. Rees et al (1978) reported the sulfur isotopic compositions of oceanic sulfate with an average of 21.00‰ ($\delta^{34}S$, CDT scale, see Figure 3.1) using the SF_6 analytical method. In my study, the multiple sulfur isotopic compositions of modern seawater sulfate have been characterized using the NBS-127 standard (barite). NBS-127

samples were prepared by ion exchange of seawater sulfate from Monterey Bay, California (Pacific Ocean). Results from thirteen analysis of NBS-127 show that the value of $\delta^{34}S$ is 21.15±0.12‰ (2σ, n=13, 95% confidence level) and the value of $\Delta^{33}S$ is 0.038±0.007‰ (2σ, n=13, 95% confidence level). I suggest that the slightly higher value of NBS-127 is a more robust estimate of modern oceanic sulfate, and that the $\Delta^{33}S$ of present day sulfate has a value of 0.038‰±0.007‰. The $\Delta^{33}S$ of modern seawater sulfate also has been constrained from forty-six analyse of IAEA-S2 in this study. The IAEA-S2 samples were prepared from gypsum that naturally precipitated from modern seawater collected from the Pacific Ocean near New Zealand. The data show that the IAEA-S2 has a $\delta^{34}S$ value of 22.16±0.05‰ (2σ, n=46, 95% confidence level) and the value of $\Delta^{33}S$ is 0.041±0.004‰ (2σ, n=46, 95% confidence level). The $\Delta^{33}S$ values of NBS-127 and IAEA-S2 are statistically indistinguishable. However, the average $\delta^{34}S$ values of NBS-127 and IAEA-S2 are statistically distinguishable even considering the uncertainty associated with fluorination and isotopic analysis (0.40‰, 2σ), whereas the $\delta^{34}S$ of NBS-127 in this study is statistically indistinguishable from those by Rees et al. (1978).

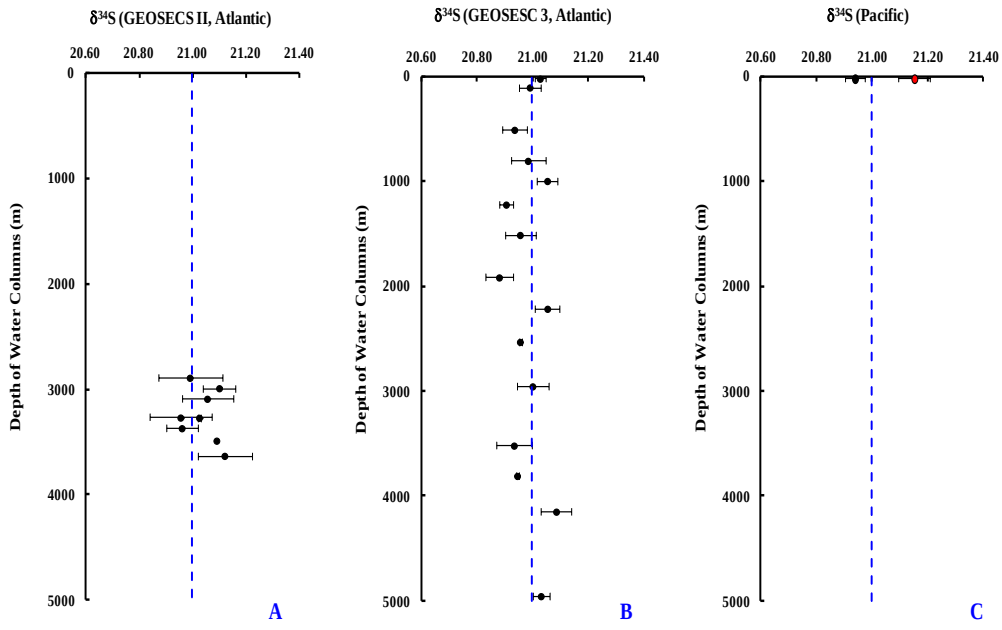

Figure 3.1. Depth profiles of $\delta^{34}S$ values of seawater sulfate determined in this study. The error bars represent $\pm 1\sigma$ uncertainty (the standard deviation of the mean). The blue dashed lines represent the average of the Rees et al. (1978) data. The red dot is the $\delta^{34}S$ value of NBS-127 samples in this study (Modified from Rees et al. (1978)).

3.2 Sedimentary sulfur pools

The sulfur in Earth's surface is ultimately derived from the mantle. The exchange rate of sulfur between the Earth's surface and deep mantle is thought to be controlled by tectonic processes. The size of the Earth's surface sulfur pool is not thought to have been constant throughout geologic time, and some studies (Canfield, 2004) have proposed that this sulfur pool shrank during the Proterozoic, reaching a minimum in the late Neoproterozic as a result of a high fraction of pyrite burial and subduction of sulfide associated with widespread euxinia.

There are three pools that account for most of the sulfur in the sedimentary sulfur cycle: oceanic sulfate, sedimentary pyrite and evaporite-sulfate minerals. Other sulfur reservoirs (e.g., standing biomass, porewater sulfate and sulfide, and species with oxidation states intermediate between sulfate and sulfide) are negligible in terms of isotope mass balance on geological time scales. The estimate of sedimentary pyrite-sulfur and evaporite-mineral-sulfur pools over geologic time are listed in Figure 3.2.

The size of the present-day pyrite-sulfur pool is estimated to be $\sim 4.869 \times 10^9$ Tg S ($\sim 1.518 \times 10^{20}$ mole), and the mass of sulfur in evaporite minerals is estimated at $\sim 2.596 \times 10^9$ Tg S ($\sim 8.096 \times 10^{19}$ mole). These values are minimum estimates for the current sedimentary sulfur pools, and each comes with large uncertainty. These estimates are made by the accessible existence of sedimentary rocks (Holser et al., 1988).

Modern oceanic sulfate levels have been estimated at ~28.2 mM and the total mass of sulfate-sulfur in the world oceans amounts to $\sim 1.277 \times 109$ Tg S ($\sim 3.827 \times 10^{19}$ mole) (Horn, 1969). The levels of oceanic sulfate have been thought to vary with time. These have been estimated

through modeling of rates of change of oceanic sulfate-sulfur isotopes, and the analyses of fluid inclusion in halite minerals(Kah et al., 2004; Horita et al., 2002). Estimates of sulfate levels during the Phanerozoic are presented in Figure 3.3

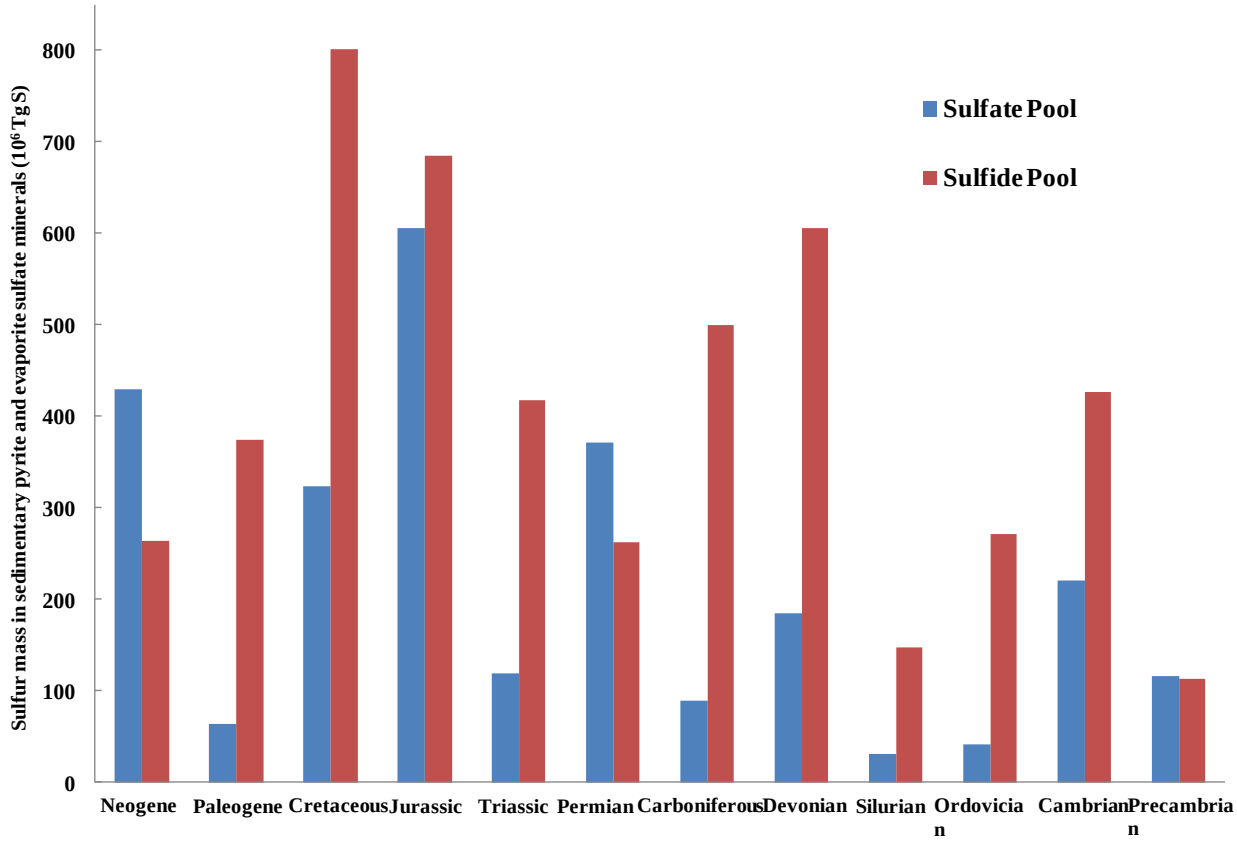

Figure 3.2. Estimate of the sulfur mass in sedimentary pyrite and evaporite-mineral pools (10^6 Tg S)(Modified from Holser et al., 1998)

Oceanic sulfate levels are thought to have fluctuated between 5 mM and 29 mM since the latest Neoproterozoic (Figure 3.3). At these levels, sulfate concentrations are high enough that the average residence time for oceanic sulfate in water columns will be long (2 to 10 million years) and the oceanic sulfate will be isotopically well mixed in water mass of open oceans at the global scale (see section 3.4 for details).

Variations in past oceanic sulfate levels are thought to reflect changes in the balance between the flux into and out of the ocean. The sulfate levels during earliest Cambrian, the Permian, and the latest Cenozoic are higher than those of the Paleozoic and the late Mesozoic. These higher levels of sulfate concentration are roughly coincident with the higher depositional rate of evaporites (Railsback, 1992), but coincident with lower sea levels (Miller et al., 2005).

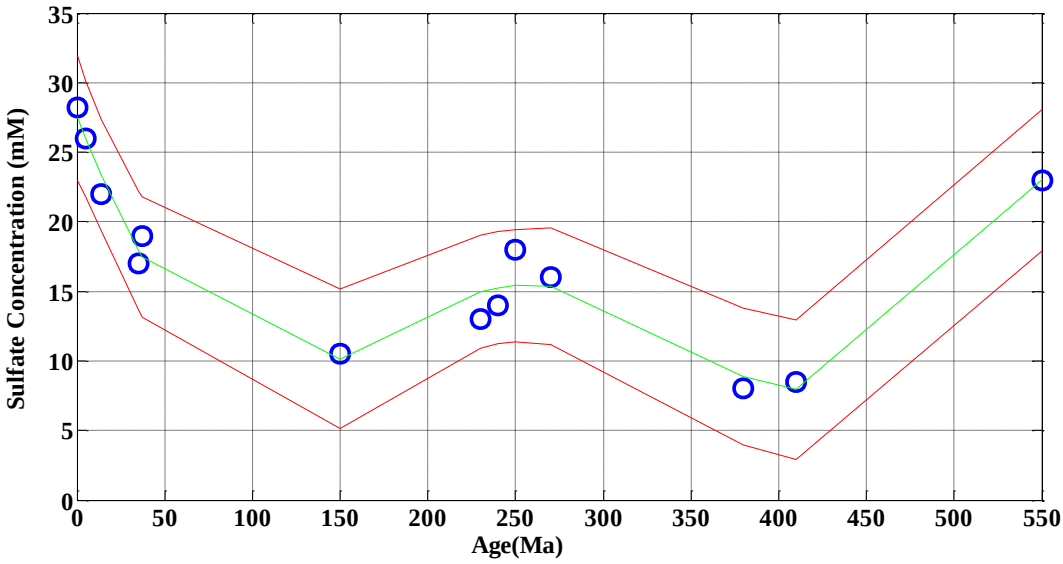

Figure 3.3. Oceanic sulfate concentrations with time. The blue dots represent the individual estimates for different geologic times(Modified from Horita et al., 2002). The uncertainties associated with these esimates are subject to those assumption used in the calculation (e.g. stoichiometric constant of calicum sulfate). The green fitting age-curve is curvilinear regression for a polynomial of degree 6 and the red lines are the 2σ error bounds.

3.3 Sulfur fluxes between sulfur pools

The present sulfur fluxes into the world's ocean are primarily due to the weathering of sedimentary sulfur since the early Proterozoic. During the Phanerozoic, most of the sulfur to the oceans was introduced in the form of dissolved sulfate transported in rivers. The burden of dissolved sulfate in rivers originates as a product of the combination of weathering of sedimentary pyrite and evaporite sulfate minerals. The magnitude of the sulfate influx to the world's oceans today is estimate to be ~1.148×102 Tg S (~3.580×10^{12} mole) per year.

Contributions of sulfur from mantle sources also make up the balance of the source flux via three channels: 1) volcanic outgassing; 2) hydrothermal input; and 3) ocean crust weathering.

Sulfur is removed from the world's ocean mainly through two channels: 1) the formation of sedimentary pyrite and 2) the formation of evaporite sulfate minerals. Most pyrite is formed in the marginal marine shelf and slope environment where most organic carbon accumulates. The key step for pyrite formation in marine sediments is the production of hydrogen sulfide by microbial sulfate reduction under anoxic conditions. Most of the sulfide produced by microbial sulfate reduction is reoxidized to oceanic sulfate, but the 10-20% that is ultimately converted to iron sulfides yields a net deposition rate of pyrite-sulfur of ~ 7.5×10^{13} mole per year (Jørgensen, 2006). The formation of sulfate evaporites throughout geologic time is much more difficult to constrain. Evaporite formation occurs episodically in locations including: sabkha shorelines, lagoons, and deep basins. There appears to be no significant amount of sulfate evaporite minerals forming at present.

Other minor (or transient) sinks for oceanic sulfate-sulfur include: 1) hydrothermal sulfate reduction, 2) sulfate incorporation into carbonate, 3) sulfate in clay sediments, 4) barite formation, and 5) organic-sulfur in marine sediments. The sulfate in carbonate minerals are thought to be lattice bound (Staudt and Schoonen, 1995), and the removal of sulfate by carbonate precipitation is estimated to be ~4.81 Tg S/yr (1.50×10^{11} mole/yr), or ~ 4% of the modern riverine sulfate flux into the world oceans. For the marine biomass, ~ 3.60×10^{2} Tg S (1.123×10^{13} mole) are annually involved in the biogenic sulfur cycling, and ~ 1.80TgS (5.614×10^{10} mole) is estimated to be buried in marine sediments. The sulfur flux into and out of the world oceans are summarized in Table 3.1.

Table 3.1 Sulfur flux into and out of the world ocean at present day

Flux	Magnitude (mole/Year)	Reference
Riverin dissovled Sulfate	3.58×10^{12}	Volkov and Rozanvo, 1983
Volcanic outgassing	1.0 to 3.0 $\times10^{12}$	Holser et al., 1988
Hyrothermal input	0.9 to 9.6 $\times10^{11}$	Elderfield and Schultz, 1996
Weathering of oceanic crust	0.2 $\times10^{11}$	Alt et al., 1994 1995
Pyrite-sulfur	7.5×10^{12}	Jorgensen, 2006
Hyrothermal sulfate reduction	0.4 to 0.9×10^{11}	Alt et al., 1994 1995
Sulfate in Carbonate	1.5×10^{11}	Staut and Schoonen, 1995
Sulfate in clay minerals	4.2×10^{11}	Volkov and Rozanvo, 1983
sulfur in organic matter	0.6×10^{11}	Volkov and Rozanvo, 1983
Barite-sulfur	1.5×10^{11}	Volkov and Rozanvo, 1983
Evaporite-sulfur	0	Holser et al., 1988

3.4 Homogeneity of the oceanic sulfate for different water masses

The cycling of oceanic sulfate-sulfur can be characterized by three basic parameters: the concentration, sulfur isotopic composition, and residence time. The concentration of sulfate in the oceans is related to the total amount of sulfate (the burden) and the residence time, which is defined as the average retention time of an individual sulfate ion in the water column. The residence time is equal to the turnover time of oceanic sulfate under steady state, where the turnover time is defined as the ratio of sulfate levels to the flux of incoming sulfur.

The residence time for sulfate in modern oceans is estimated to be ~ 10Ma, but during past geological time intervals when sulfate levels were lower, the residence time would have been shorter. This is because levels of oceanic sulfate change with time and also because the sulfur flux into and out of the oceans may change over geologic time (Canfield, 2004; Canfield and Farquahr, 2009). For instance, if estimates of sulfate levels for Paleozoic oceans are inferred from fluid inclusion chemistry (Horita et al., 2002), the residence time of oceanic sulfate is

estimated to be ~2 Ma with an assumed influx of sulfur to oceans the same as that of present day. Given this residence time, sulfate would still be well mixed (see Figure 3.4).

The exchange of sulfate between a larger deep ocean sulfate pool and a smaller surface ocean sulfate pool is examined using this two layer model that evaluates mixing times, which are dependent on the exchange rate of sulfur between pools. The results are shown in Figure 3.4. If the exchange rate is same as today's (Figure 3.4A and Figure 3.4C), sulfate concentration will be homogenous within 50,000 years (0.05 Ma) given sulfate concentration in deep oceans of 29 mM (approximate of modern ocean's sulfate levels) or 1 mM (the most conservative estimate of sulfate levels for the Ediacaran Period). If we assume that the exchange rate is one order of magnitude lower than today's exchange rate (Figure 3.4B and Figure 3.4D), the time required to homogenize the oceanic sulfate is on the order of 500,000 years (0.5 Ma).

My study focuses on the analysis of carbonate associated sulfate. If sulfate is extracted from unaltered samples without fractionation, the data for each sample will capture a snapshot of the sulfur isotopic composition of depositional sulfate. Several issues arise related to such a data. First, the issue of homogeneity of oceanic sulfate is important to connect the data to models of oceanic sulfate cycling. Second, the issue of continuity of a sulfur isotope record in time is important when considering high resolution record (on the order of ~0.1 to 1 Ma) of carbonate associated sulfate.

These factors can be confounded if the carbonate platforms from which the samples are extracted are formed in a marginal oceanic setting where the water mass of the open ocean is connected with the water mass of the coastal ocean, and if sulfate is at low enough abundance to have a residence time approaching that of the water mass in ocean basins

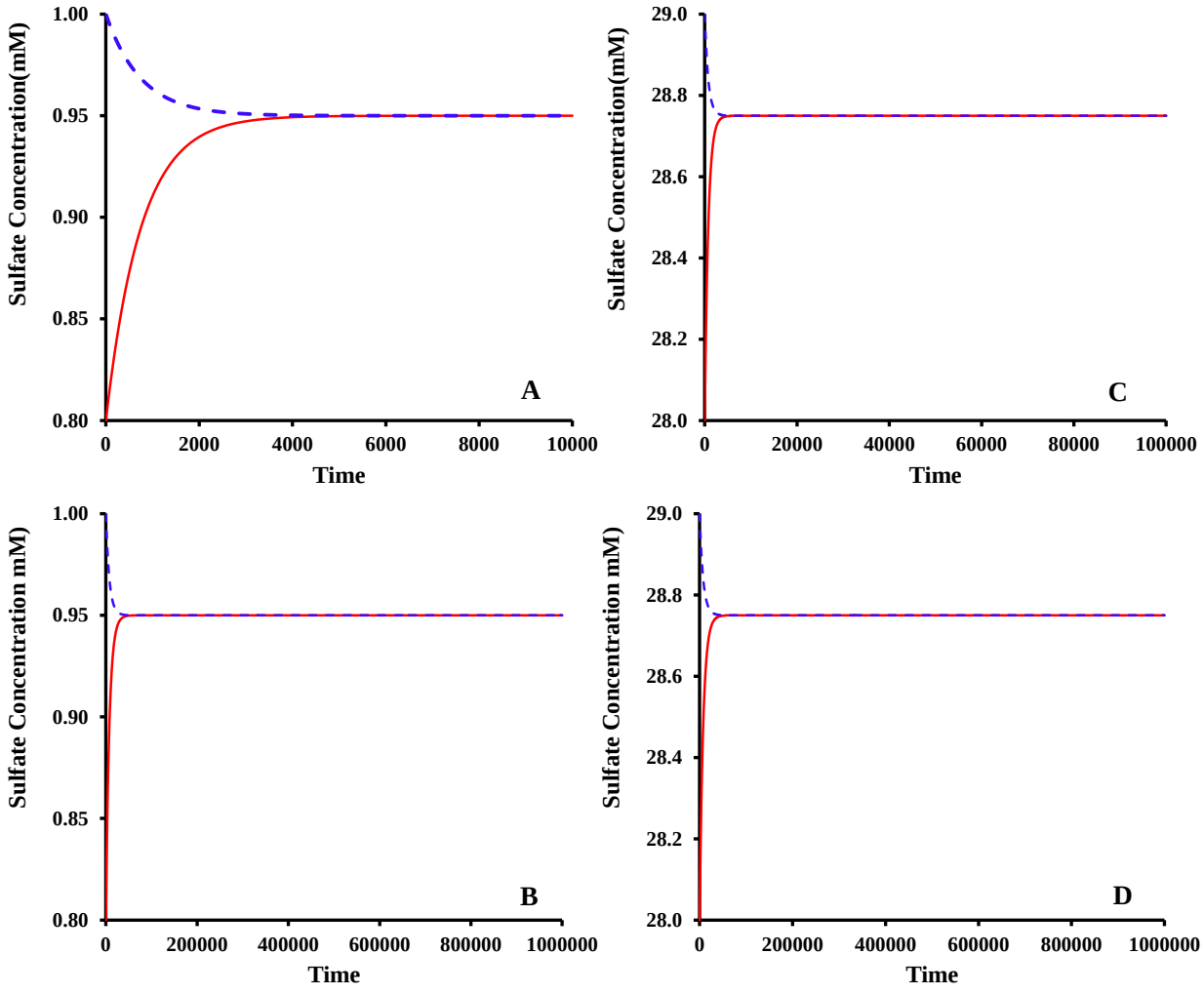

Figure 3.4. Simulation results of the time scale for homogeneity between a larger deep ocean sulfate pool and a smaller surface ocean sulfate poolat various exchange rates. The sulfate exchange rates are set to be as today's in Panel A and panel C, and the exchange rates are set to be 10% of today's in Panel B and Panel D.

A model with two water masses with distinct sulfur isotopic compositions is explored to determine the time scale of mixing and/or homoginization of sulfur isotopes within these two water masses (see Figure 3.5). This sensitivity test is designed to evaluate the influences of sulfate concentrations on the mixing of sulfur isotopes for two discrete sulfate pools. The results show that the mixing time for sulfur isotopes is within 0.1 Ma at the present day exchange rate of water columns within open ocean basins. This simulation suggests that short term heterogeneity

may be due to sluggish mixing rate or persistant sulfur isotope fractionation processes (e.g asssimilation of sulfate in surface oceans).

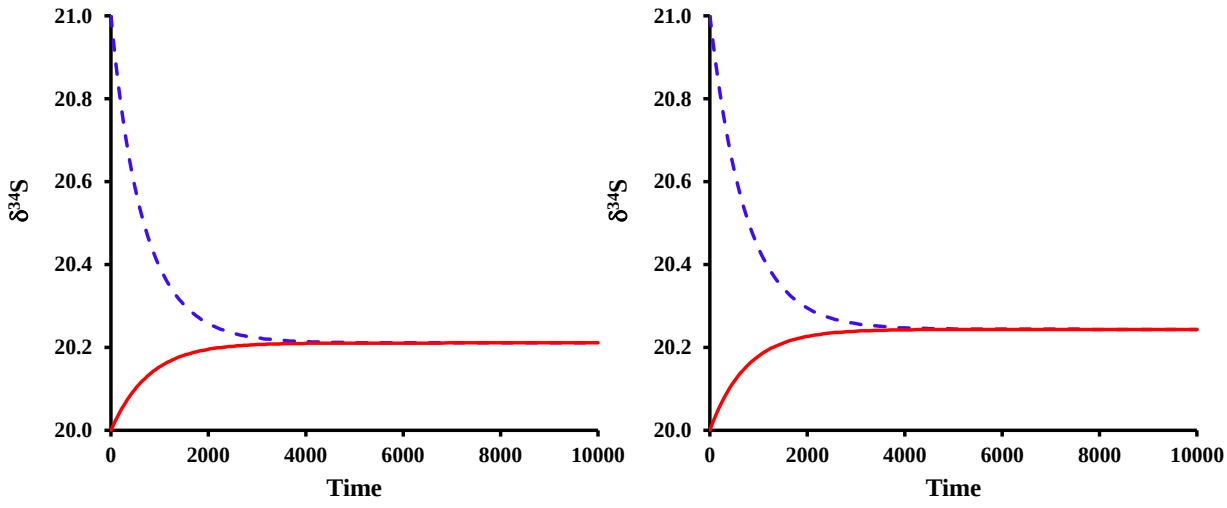

Figure 3.5. Mixing time scale for sulfur isotope between two sulfate pools at present day exchange rates of water masses (3 meter per year). The left panel show the results for two sulfate pool with 1.0 mM ($\delta^{34}S$= 21.0‰) and 0.8mM sulfate ($\delta^{34}S$= 20.0‰), and the right panel shows the results for two sulfate pool with 29.0 mM ($\delta^{34}S$= 21.0‰) and 28.0mM sulfate ($\delta^{34}S$= 20.0‰).

3.5 $\delta^{34}S$ Age Curve of Oceanic-Sulfate

The $\delta^{34}S$ compositinos of seawater sulfate have been reconstructed over the Phanerozoic by using a variety of proxies - evaporite-sulfate, water column barite, and sulfate in carbonate minerals (Claypool et al., 1980, Paytan et al., 1998, 2004; Gill et al., 2007, Fike et al., 2008). During the past decade, data from carbonate associated sulfate (CAS) and water column barite have begun to provide a higher resolution $\delta^{34}S$ record for Mesozoic, Paleozoic and Precambrian seawater sulfate (Kampschulte and Strauss, 2004, Newton et al., 2004, Goldberg et al., 2005, Fike et al. 2006, 2008, Gill et al. 2007, Hurtgen et al., 2009). The $\delta^{34}S$ record provided by CAS has shown to be comparable to the one established by evaporite minerals. An advantage of CAS is that carbonate minerals can be used to construct a much more continuous record than evaporite

minerals. It was also hoped that CAS might not be subject to diagenetic or post diagenetic alteration, but this has not proven to be the case, and interpretation of CAS data as a proxy for oceanic sulfate requires careful consideration of factors (e.g.post diagensis of carbonate minerals and contamination by pyrite oxidation in in CAS extraction) that can confound the primary oceanic signal. Figure 3.6 presents the present dataset along with reanalysis of samples examined in this dissertation.

The factors that influence seawater $\delta^{34}S$ include: 1) the process of microbial sulfate reduction and sedimentary pyrite formation which represents a ^{32}S-enriched sulfur sink, 2) the proportion of sulfate that is lost to sulfate minerals (gypsum or anhydrite) compared to that lost to pyrite, and 3) the balance of sulfate produced by weathering of ^{32}S-enriched sulfide minerals relative to that of ^{32}S-depleted evaporites in the riverine sulfate flux to the oceans. The sulfur isotopic record of oceanic sulfate has thus been interpreted in the context of these factors, most commonly by making assumption about the isotopic composition of buried pyrite (factor 1), and then making inference from mass balance about the relative burial fluxes and source contributions (factors 2 and 3).

The sulfur isotope fractionations (factor 1) between seawater sulfate and pyrite have been calibrated by several approaches, including laboratory culture experiments, core top calibration of marine sediments and pore water sulfate, and direct measurement of the sulfur isotopic composition of coeval sulfide and sulfate minerals. For instance, Garrels and Lerhman (1981) assumed a constant value of 35‰ in their mass balance model, which is a compromise of results from various laboratory culture experiments. On the other hand, Strauss (1997) assigned a constant value (~50‰) for the Phanerozoic sulfur cycle based on the sulfur isotopic differences between oceanic sulfate and coeval sedimentary pyrite.

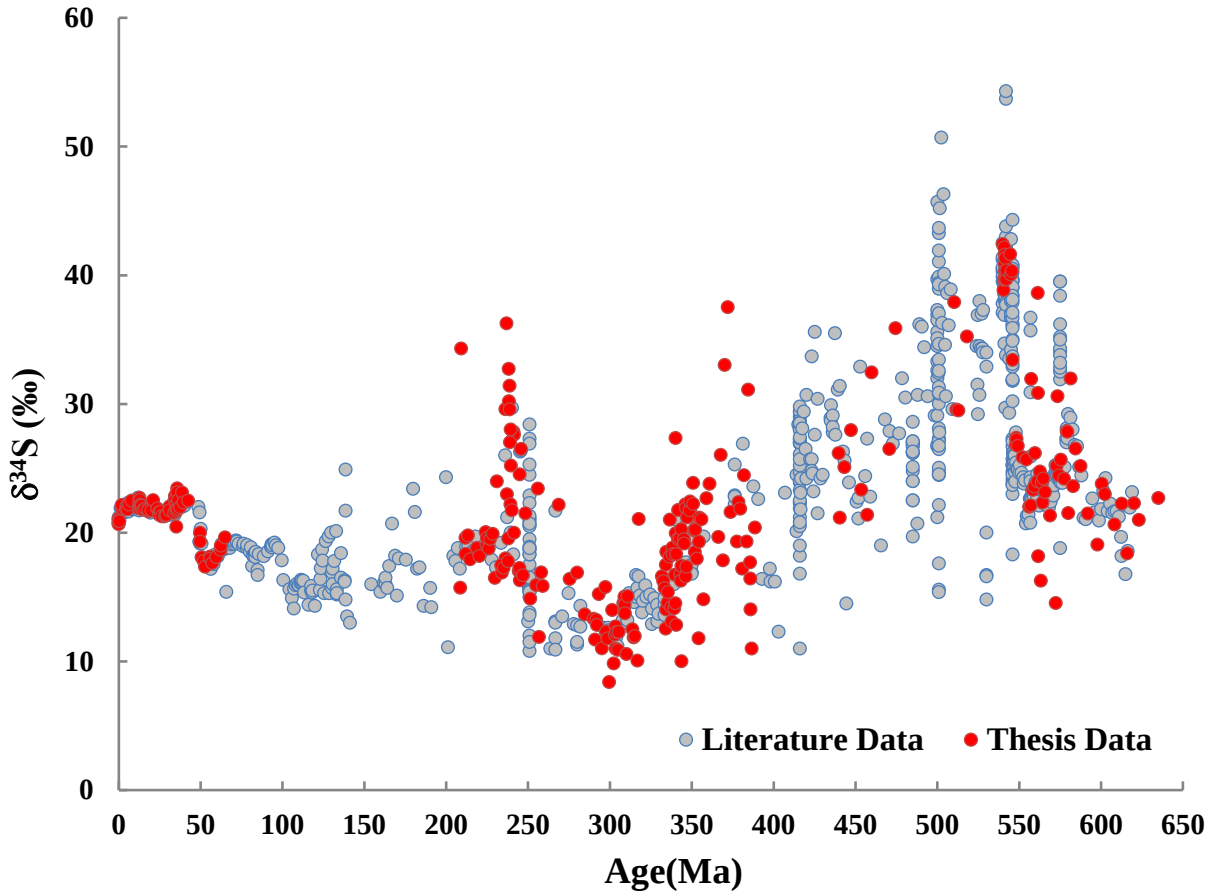

Figure 3.6. $\delta^{34}S$ of oceanic sulfate with time. The gray dots are literature data and the red dot are data in my study. Age has been updated to GST 2004. Reference are follows: Paytan et al., 1998, 2004, Newton et al., 2004, Kampschulte and Strauss, 2004, Goldberg et al., 2005, Fike et al. 2006, 2008, Gill et al. 2007, Hurtgen et al., 2009.

Wu et al. (2010) (Chapter 6) also used inferences obtained from the dataset of isotopic measurements of Phanerozoic sedimentary pyrite, but instead of using a constant fractionation, explored the possibility that the mean of pyrite-sulfur isotopes might be more representative of the time-dependent composition of buried pyrite. Wu et al. (2010) argue that the isotopic fractionation between sulfate and buried pyrite appeared to vary between two stable values depending on the time interval of interest. These authors suggest that the Paleozoic Era was characterized by a fractionation of ~30‰ while the Mesozoic and Cenozoic eras were characterized by a fractionation of ~ 42‰. Wu et al.(2010) developed a model based on multiple sulfur isotope age curves of oceanic sulfate to check for consistency with their approach using

average values of sulfate and pyrite, assuming a well-mixed oceanic sulfate pool with a long residence time. The model calibrated values are comparable to values derived from the direct measurements of sulfide and sulfate minerals, with the assumption that sulfur inputs (factor 2 and factor 3 listed above) to the ocean are known or can be calibrated using information from present-day determinations of flux into oceans and information about geological factors that may have modified these in the past such as sea floor spreading rates or sea leve rise and fall.

3.6 $\Delta^{33}S$ Age Curve

Over the past fifteen years, it has become apparent that additional environmental information may be preserved in the time-series records of minor sulfur isotopes (^{33}S and ^{36}S). This includes the discovery of anomalous ^{33}S and ^{36}S abundances in Archean sulfate and sulfide minerals (Farquhar et al., 2000) (Figure 3.7). The earliest Proterozoic marks the transition from mass-independent fractionation (MIF) to mass-dependent fractionation (MDF) in sedimentary reservoirs. The early MIF signals have been interpreted to reflect the influence of atmospheric sulfur chemistry under anoxic surface environmental conditions. The production of MIF-S is attributed to some aspect of the chemistry of atmospheric sulfur dioxide photolysis that includes, but is not limited to, primary photochemical effects, shielding, and absorption (Farquhar et al., 2000, 2001; Lynos, 2007; Danielache et al., 2008; Ueno et al., 2009).

This Archean $\Delta^{33}S$ record is complex and various proposals have been made to explain its structure. The formation of an organic haze has been invoked to interpret the $\Delta^{33}S$ values for the Mesoarchean (Farquhar et al., 2007, Domagal-Goldman et al., 2008). Alternatively, the changes in ratios of SO_2:H_2S by volcanic emissions were argued to be the main factor that controls the temporal structure (Halevy et al., 2010). While these hypotheses may contribute to the long-term $\Delta^{33}S$ structure in the Archean record, high frequency variations in $\Delta^{33}S$ have been measured at

the scale of thin sections and hand samples (Kamber and Whitehouse, 2007; Farquhar et al., 2007; Kaufman et al., 2007). Searching and indentifying the sulfur isotope compositions of individual pyrite (sedimentary-origin) and sulfate minerals using the SIMS techiques may help understand the origin of the high frequency variations in $\Delta^{33}S$ records.

The evident asymmetry in $\Delta^{33}S$ (negative values *vs.* positive values) for Archean is not well understood. If the ultraviolet photolysis of atmospheric SO_2 is the main contribution to sedimentary sulfur budget, the sulfate minerals would expect to carry a more negative $\Delta^{33}S$ signal than that of pyrite. Specially, there is an isotope mass balance issue for the Neoarchean $\Delta^{33}S$ record. The resolution of this issue lies on the searching for sulfate minerals that carry the large negative $\Delta^{33}S$ signals, as well as estimate of the sizes of reduced sulfur and oxidized sulfur pools in the Archean oceans.

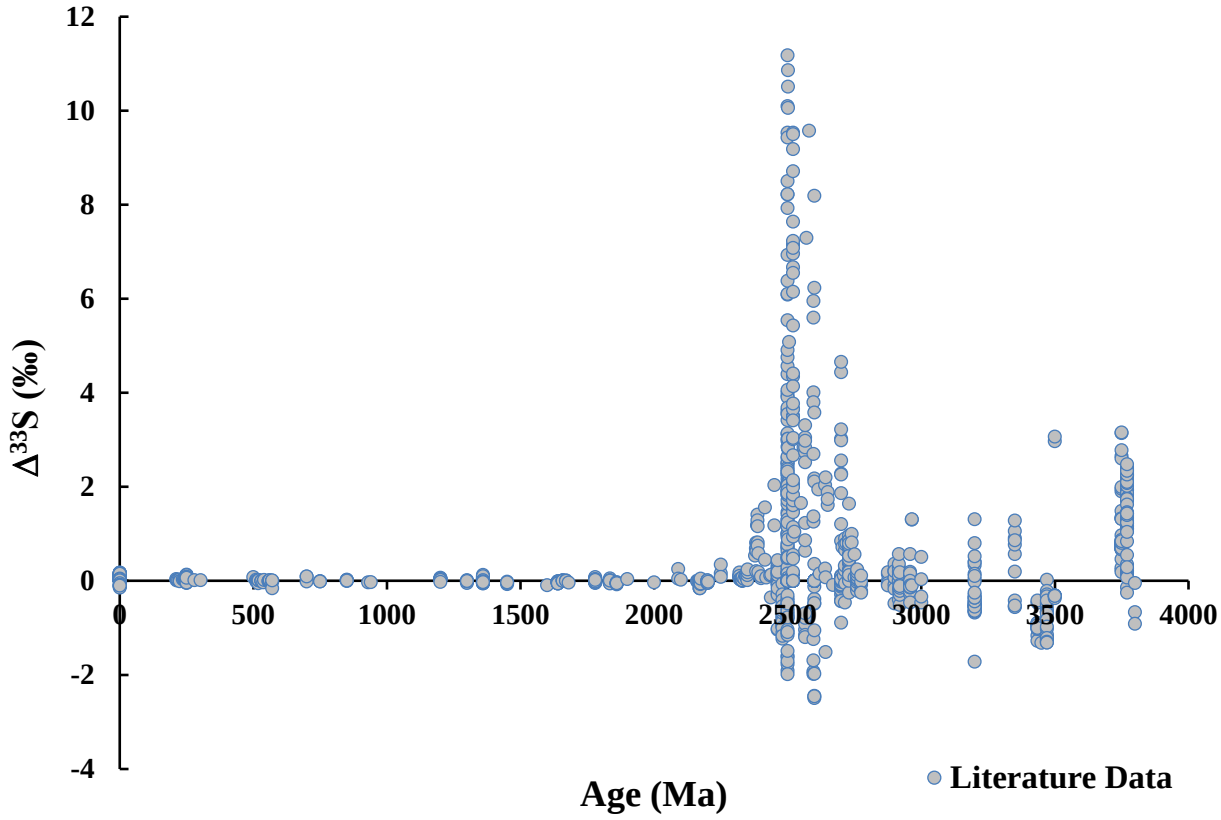

Figure 3.7. Plot of $\Delta^{33}S$ versus sample age. The samples older than ~2.4 Ga preserve MIF signal associated with mass-independent fractionation processes; the samples younger than ~2.4 Ga carry MDF signals associated with mass-dependent fractionation by microbial sulfate reduction and other sulfur cycle processes. The Archean $\Delta^{33}S$ record shows a temporal structure that includes: 1) moderate $\Delta^{33}S$ values for Eoarchean and Paleoarchean; 2) near zero $\Delta^{33}S$ values for Mesoarchean; and 3) highest amplitude in $\Delta^{33}S$ variations for the Neoarchean. These changes may be associated with UV optical depth or other changes in atmospheric composition (Farquhar et al., 2007; Domagal-Goldman et al., 2008; Halevy et al., 2010; Zerkle et al., 2012).

The $\Delta^{33}S$ record since ~2450 Ma is marked by a mass-dependent signal that reflects cycling of sulfur by sulfate reducers and sulfide oxidation, as well as a combination of other biological and abiological processes. The $\Delta^{33}S$ record is thought to provide additional information about mixing at global/basin scales, about sulfur transformations (sulfur disproportion and sulfide re-oxidation), and about sulfur transportation (ocean circulation and exchange between seawater and marine sediments systems). The principles of this approach have been described in three studies to date (Johnston et al., 2005; Ono et al. 2006; Wu et al., 2010). Figure 3.8 is the new

compilation of data for the samples that are younger than 2000 Ma. The variations of $\Delta^{33}S$ are larger than the uncertainty associated with the analytical error (0.022‰, 2σ), which is derived from threeyears of monitoring the isotopic measurement of IAEA-S2.

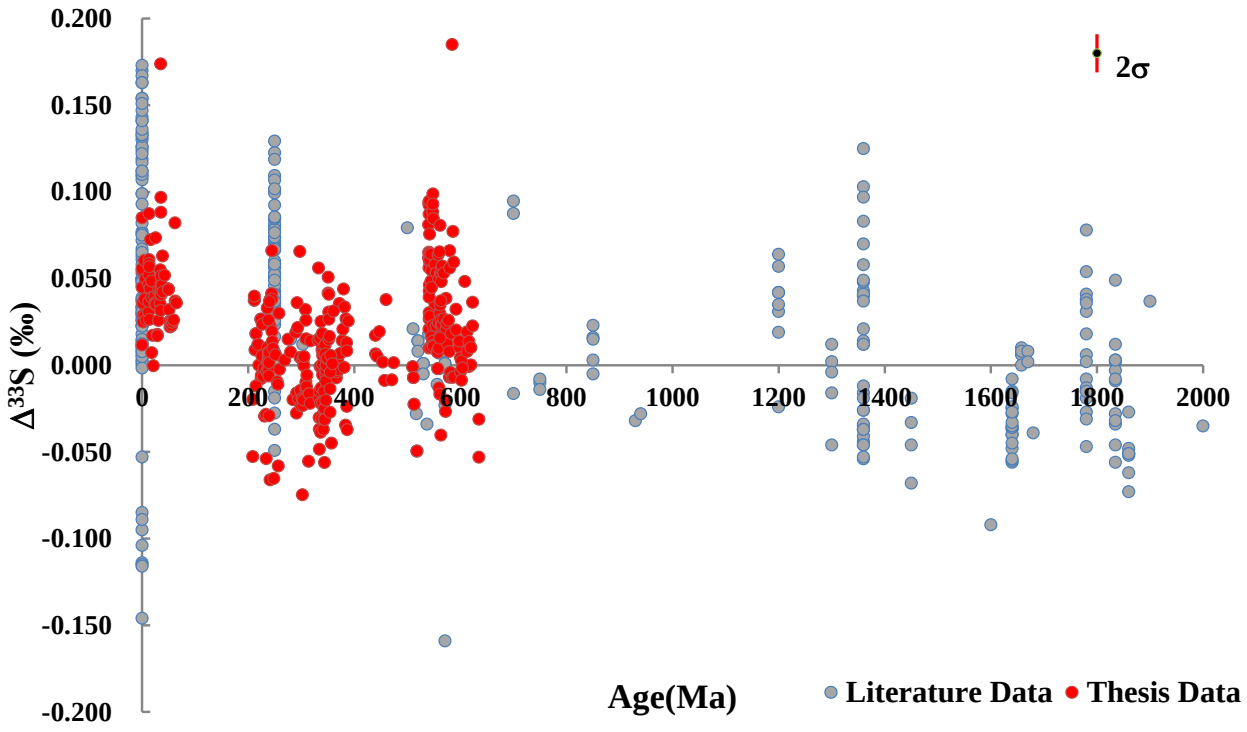

Figure 3.8. Plot of $\Delta^{33}S$ values versus sample age. The samples (sulfate and sulfide, gray dots) are from literature compilations and samples (sulfate and sulfide, red dots) from this study.

In the application of the $\Delta^{33}S$-age record, several assumptions have to be made in order to narrow the number of free parameters, and other geochemical proxies need to be used to test or to provide independent evidence to support or eliminate possible scenarios for interpreting observed sulfur isotopic records. For this reason, the work presented in the next three chapters should be considered with caution. Conclusion may change as the sulfide-sulfur dataset is updated, as constraints are improved for the mass and isotopic composition of influx sulfur to the oceans with time, as the laboratory calibration on the sulfur isotope fractionation of other

relevant pathways such as sulfide re-oxidation are obtained, and as a better understanding of the behavior of multiple sulfur isotopes is obtained for exchange of sulfate between seawater and sedimentary pore waters.

The next three chapters present a long term analysis of the sulfur cycle over the Phanerozoic Eon and the latest Neoproterzoic Era that draws on the multiple sulfur isotope records. Chapter 4 discusses the chemistry and data statistics during data collection. Chapter 5 presents a view of sulfur cycling and its relation to the oxidation state of Ediacaran oceans. Chapter 6 has been previously published (Wu et al., 2010), but includesa reanalysis that takes into consideration additional observations and data collected in the interval since publication. In summary, the primary goals of this study are to:

1) Construct a $\Delta^{33}S$ record of oceanic sulfate since the latest Neoproterzoic Era (Chapters 5, 6)
2) Constrain the sulfur isotope fractionations between oceanic sulfate and pyrite over the Phanerozoic Eon (Chapter 6)
3) Identify the possible mechanism for time-series sulfur isotopic shifts (Chapters 5, 6)

Chapter 4: Samples and Analytical Methods

Abstract: This chapter describles the samples studied, procedures of chemical extraction of carbonate associated sulfate and the isotopic measurement using mass spectrometry. The analytical uncertainty associated with these procedures is also assessed by monitoring IAEA reference materials. The long-term uncertainties determined for this study (2σ) aree 0.3‰ for $\delta^{34}S$ and 0.018‰ for $\Delta^{33}S$.

4.1 Sample Sets

Two sample sets were collected and analyzed for sulfur isotopes. A brief description for these is listed below and detailed information about their geological setting can be found in individual chapters.

1. The sample set for the Neoproterozoic study was prepared for studies by Fike et al. (2006, 2008). Rock samples were originally taken from two drill cores: Miqrat-1 wells, from the north Huqf region and TM-6 wells in the Eastern Flank of South Oman Salt Basin. The CAS extracts were available as $BaSO_4$ and CRS (chromium-reducible sulfur) as Ag_2S.
2. The sample set for the Phanerozoic study consists of archived carbonate rocks from collection located at Ruhr-Universität Bochum in Germany. Obviously weathered samples, weathered portions of sample, and samples with vein were not used for analysis. The detailed procedure for CAS extraction at the Stable Isotope laboratory, University of Maryland is described below.

4.2 Chemical approach for CAS Extraction

Carbonate associate sulfate (CAS) is thought to be a lattice-bound trace component in carbonate minerals and this proxy has been verified to record the sulfur isotope compositions of Modern and ancient oceanic sulfate (Burdett et al., 1989; Kampschulte et al., 2001; Kampschulte

and Strauss, 2004; Gill et al., 2007). In this study, the carbonate associated sulfate in biogenic carbonate and whole carbonate rock has been used to reconstruct the sulfur isotopic composition of seawater sulfate. The method for CAS extraction is modified from Goldberg et al. (2011) and Kampschulte and Strauss (2004).

The carbonate rocks were cut using a water-cool saw into small pieces to remove weathered portions and vein portions. These chips were further broken so they fit into a SPEX shatter box. The inside of the shatter box holder is made of ceramic, and the grain size of the crushed rock powder was generally smaller than 75 mesh after 3-minute vibration.

Approximately 3 to 60 grams rock powder was immersed in 50 to 150 ml (dependent on sample size) 5% NaOCl solution for 24 hours in a 500 ml glass beaker. The mixture was stirred 4-5 times using a glass rod for ~ 5 minutes during the 24-hour period. The NaOCl supernatant was carefully decanted. The wet powder was immersed and stirred in 150 to 400 ml Milli-Q water for 2-3 hours and then the Milli-Q water supernatant was decanted. This rinse procedure using Mill-Q water was repeated 4-5 times to remove any water soluble sulfate and reduced sulfur oxidized by NaOCl solution. The wet powder was then transferred to a 0.2 micron (25 mm) cellulose nitrate filter paper that was held by a 500 ml funnel. 1000-2500 ml Milli-Q water was added into the funnel to further rinse the carbonate powder, and then it was set in a rack overnight to leach and dry.

The dried powder on the filter paper was reacted with approximately 30-300 ml of 5N HCl solution added slowly to the carbonate, which released the sulfate in solution that collected in a pyrexflask below the funnel. It took approximately 1-2 hours to finish the acidification procedure.

The collected solution was filtered through a 0.2 micron 25 mm cellulose nitrate filter paper to remove particulates.

Approximately 5 ml 1.24M $BaCl_2$ was added into the filtered sulfate solution. The container was covered with Parafilm and heated at 100 ℃ for 1-2 hours. After this, the sample was allowed to cool to room temperature and sit for 24-36 hours to precipitate barium sulfate.

The solution with $BaSO_4$ precipitation was then transferred to either 50 or 15 ml plastic tubes, which were centrifuged and rinsed with Milli-Q water 5 times, then soaked in Milli-Q water for 2-3 hours. After a final centrifugation, the plastic tubes with $BaSO_4$ were put in an oven at 60 ℃ to dry for 72 hours.

4.3 Thode Reduction

Approximately 5 mg of dried $BaSO_4$ powder was reduced to hydrogen sulfide (H_2S) using a heated and actively purged (by nitrogen gas) solution of $HI+H_3PO_4+HCl$ (Thode et al., 1961). Product hydrogen sulfide was carried in a stream of nitrogen through a water-cooled condenser and then passed through a water trap filled with Milli-Q water to remove chloride, and sulfur was chemically trapped as silver sulfide using 14 mL of a ~0.02M solution of silver nitrate with 2 ml of 1.55M HNO_3. The solution with precipitated silver sulfide was set in the dark for approximately seven days, then filtered and rinsed with ~250 ml Milli-Q water and ~5 ml 1N ammonia solution (NH_4OH). Samples were aged to allow for the dissolution of oxygen-bearing contaminants that precipitate with the silver sulfide during Thode reductions. The black Ag_2S precipitate was collected and transferred to an aluminum packet and dried in the oven for approximately 48 hours prior to preparation for fluorination.

There are two types of uncertainty on $\delta^{34}S$ and $\Delta^{33}S$ associated with chemical sulfate reduction. The sample sulfur may be contaminated by sulfur from the analytical blank (Thode solution). The measured sulfur isotopic abundance is that of the sample sulfur plus the blank sulfur. In principle, this type of uncertainty can be corrected using a blank correction. However, there is no detectable Ag_2S precipitation during the Thode reduction without sample (blank test). In addition, the amount of sample used in chemical reduction is approximately 5 mg, which is large enough not to have its sulfur isotopic abundance influenced by a blank sulfur contaminant. The other type of uncertainty is derived from the fractionation of sulfur isotope during the Thode reduction, which is monitored by characterizing the composition of known standards and by measuring yields.

To accurately characterize the sulfur isotopic abundance in unknown samples, a critical step is to convert the targeted sulfur with 100% yield. In this study, the standard, NBS-127 (barium sulfate) was used to quantify the uncertainty associated with Thode reduction, fluorination, and mass spectrometric measurement. This reference material was prepared by ion exchange of sulfate in seawater from Monterey Bay, California, USA (Hut, 1987; Halas and Szaran, 2001), and $\delta^{34}S$ value of NBS-127 is reported to be 20.30 ± 0.40‰ (1σ, SO_2-based mass spectrometric measurement).

There is a systematic difference between values from the SO_2 mass spectrometric measurements and SF_6 mass spectrometric measurements due to scale compression and memory effects of the SO_2-based method (Rees et al., 1978). The calibration for the mass spectrometer (Thermo Finnigan 253) at University of Maryland is derived using sulfur isotope data for Neoproterozoic samples, and the regression equation is $\delta^{34}S_{SF6} = 1.011(\pm 0.008;\ 1\sigma) \times \delta^{34}S_{SO2}$ -

0.125(±0.185; 1σ) with a value of regression correlation coefficient 0.994. Therefore, the corrected sulfur isotopic abundance of NBS-127 is 20.38±0.28‰ (1σ), assuming the SO_2 compression scale for reported NBS-127 (20.30±0.40‰, 1σ) is the same as for the Neoproterozoic sulfur isotope dataset.

NBS-127 sulfur isotope data are listed in Table 4.1; the standard has an average isotopic composition of 21.15‰ and 0.038 for $\delta^{34}S$ and $\Delta^{33}S$, respectively. The reproducibility of this measurement procedure are ±0.21‰ (1σ) for $\delta^{34}S$ values and 0.012‰ (1σ) for $\Delta^{33}S$ values. However, $\Delta^{36}S$ will be not discussed in this study due to its larger uncertainty.

At the 95% confidence level, the SF6-based $\delta^{34}S$ composition of NBS-127 in this study is not statistically distinct from the value based on the SO_2 method (20.38±0.28‰, 1σ, correction for the difference between these two approaches). If this is the case, then it is difficult to identify the systematic error from chemical extraction, the IAEA-S2 standards are then measured to evaluate the possible source of uncertainty from the fluorination procedures and mass spectrometric measurements.

The sulfur isotope fractionation in chemical reduction from sulfate to sulfide was first studied by Harrison and Thode (1957), and the magnitude of sulfur isotope fractionation was found to be approximately 20‰ at temperatures between 17-50℃ for small degrees (2%) of sulfate reduction. At the temperature (~ 300℃) of Thode reduction, the kinetic isotope effect is approximately 10‰. If the yield of NBS-127 is above 95%, the uncertainties associated with sulfate reduction are smaller than 1.6‰ and 0.005‰ for $\delta^{34}S$ and $\Delta^{33}S$, respectively. If the yield of NBS-127 is above 99%, the uncertainty associated with sulfate reduction are smaller than 0.5‰ and 0.002‰ for $\delta^{34}S$ and $\Delta^{33}S$, respectively.

4.4 SF_6 Method

Approximately 1-3 mg dried Ag_2S was wrapped in aluminum foil and was loaded into a nickel metal vessel. The reaction vessel was filled with 10-fold excess (molar by reaction stoichiometry) of fluorine gas and heated at ~300 ℃ overnight, producing sulfur hexafluoride (SF_6). The target gas (SF_6) was purified using a cold trap at approximately -110 ℃ to -115 ℃ to remove condensable gases (mostly HF). Further purification was conducted using a gas chromatograph with one 1/8 in. O.D. 4.8 m Haysep Q column with a helium carrier flow rate of 20 mL/min. SF_6 gas was collected into two glass coils out of the carrier helium flow and finally transferred to the sample bellows of the Finnigan 253 mass spectrometer. The bellows introduces sample to the ion source of the mass spectrometer via a ~1 meter capillary that is crimped at its exit. The SF_6 is ionized to SF_5^+ and other SF_x fragments by electron impact. The SF_5^+ ions are formed into an ion beam in the source that is transmitted through the magnetic sector of the instrument where it is separated into four ion beams determined by the mass of the four sulfur isotopes. The four sulfur isotopes are simultaneously detected by ion beams with ratios of mass/charge of 127, 128, 129 and 131 daltons ($^{32}SF_5^+$, $^{33}SF_5^+$, $^{34}SF_5^+$, $^{36}SF_5^+$ respectively).

In this study, the uncertainty on $\delta^{34}S$ and $\Delta^{33}S$ values associated with the fluorination and purification of SF_6 is monitored by repeatedly measuring the IAEA reference materials over a mulit-year period. We also calculated the converted yields of fluorinated silver sulfide for each analysis, and the yields for IAEA-S2/S3 reference materials were mostly in the range of 97%-102%. The summary of IAEA reference materials sulfur isotope is listed in Table 4.2.

There is no difference between the IAEA material sulfur isotopes for the two separated periods, and these data ($\delta^{34}S$) are comparable to those measured by different techniques. The long term

reproducibility for IAEA-S2 sulfur isotope compositions over nearly four years are 22.16‰, and 0.041‰ for $\delta^{34}S$ and $\Delta^{33}S$ values, respectively. The reproducibility of fluorination and mass spectrometric measurement is ±0.16‰ (1σ) for $\delta^{34}S$ measurement and 0.011‰ (1σ) for $\Delta^{33}S$ measurements. There is ~1‰ difference between the $\delta^{34}S$ for NBS-127 and IAEA-S2. This is a statistically resolvable difference that may be due to the preparation procedure for these two standards by NBS and IAEA affiliated laboratories, or it may also reflect natural heterogeneity between the samples and the settings from which they were collected.

Table 4.1 NBS-127 Sulfur isotope data

Lab #	Sample	$\delta^{33}S$	$\delta^{34}S$	$\delta^{36}S$	$\Delta^{33}S$	$\Delta^{36}S$
SF6457	NBS-127	10.76	20.93	40.42	0.039	0.279
SF6460	NBS-127	11.16	21.73	41.79	0.023	0.096
SF6464	NBS-127	10.97	21.33	41.04	0.044	0.136
SF6465	NBS-127	10.81	21.03	40.57	0.028	0.234
SF2394	NBS-127	10.86	21.16	40.42	0.023	-0.159
SF2437	NBS-127	10.94	21.29	40.74	0.027	-0.103
SF2499	NBS-127	10.83	21.08	40.39	0.032	-0.046
SF2500	NBS-127	10.81	21.01	40.33	0.049	0.037
SF2519	NBS-127	10.87	21.10	40.45	0.056	-0.028
SF2543	NBS-127	10.83	21.05	40.37	0.046	-0.008
SF2544	NBS-127	10.87	21.12	40.57	0.051	0.065
SF2589	NBS-127	10.83	21.04	40.01	0.051	-0.349
SF3182	NBS-127	10.83	21.09	39.94	0.027	-0.517

Table 4.2 Summary of sulfur isotope data for IAEA-S2 and IAEA-S3

	IAEA-S3 ($\delta^{34}S$)	IAEA-S3 ($\Delta^{33}S$)	IAEA-S2 ($\delta^{34}S$)	IAEA-S2 ($\Delta^{33}S$)	IAEA-S1 ($\delta^{34}S$)	IAEA-S1 ($\Delta^{33}S$)
1	−32.30 ±0.20‰		22.70±0.20‰		−0.30‰	
2	−32.49 ±0.16‰		22.62 ±0.16‰			
3	−32.41 ±0.41‰ (13)	0.070 ±0.013‰ (13)	22.06 ±0.17‰ (21)	0.046 ±0.010‰ (21)		
4	−32.59 ±0.12‰ (4)	0.075 ±0.005‰ (4)	22.24 ±0.09‰ (25)	0.037 ±0.010‰ (25)	−0.49 ±0.04‰ (3)	0.094 ±0.007‰ (3)

1: IAEA Isotopic Data; 2: Data from Mann et al 2009; 3: Data collected from Sept. 2011 to Oct. 2011; 4: Data collected from Feb. 2008 to April 2011; number in brackets is the analysis number

Chapter 5: Ediacaran sulfur cycle: Insights from sulfur isotope measurements ($\delta^{34}S$ and $\Delta^{33}S$) on paired sulfate-pyrite in the Huqf Supergroup, Oman

Abstract: The covariations of $\delta^{34}S$ and $\Delta^{33}S$ of carbonate associated sulfate and pyrite from the Huqf Supergroup of Oman show evolution that progresses from a system that appears to track the global oceanic sulfate and possibly pyrite to a system that appears to track more of the systematics of the basin itself. In the upper sequences of the Oman basin, the sulfur source appears to have changed. This may reflect a change in the sulfur source to the oceans as a whole, largely from the weathered evaporite minerals, or it may reflect a change in the sulfur source to the basin itself as a result of intermittent closing. If the basin closed or was restricted with respect to transfer sulfate from the oceans, the source of sulfate to the basin would be from the oceans, but the isotopic compositions would have evolved as a result of processes that occurred in the basin. The modeling presented here suggests that drawdown of sulfate concentrations due to the weakening of sulfide reoxidation or weakening of other physical processes that mix sulfate in sediment pore water with sulfate overlying oceans in marine setting may provide an explanation for the isotopic records of the upper parts of the Huqf Supergroup.

5.1. Introduction

Earth's surface environments, its biology, and its ecology underwent a series of dramatic changes between the Ediacaran and early Cambrian periods. The late Neoproterozoic deep oceans became progressively oxygenated since ~580 Ma, but oxygenation may not have been global in extent, especially in marine restricted evironments (Canfield et al., 2007, Canfield et al., 2008, Dahl et al. 2010) . These environmental changes are believed to trigger the evolution of a number of groups of benthic eukaryotic organisms (Canfield et al., 2007, McFadden et al., 2008), and provided conditions favorable for bioturbation of sediments. Bioturbation by marine organisms is thought to have enhanced oxidation of sedimentary sulfide, and played an important role in regulating oceanic sulfate levels, as well as the sulfur isotopic compositions of both oceanic sulfate and buried pyrite (Canfield and Farquhar, 2009).

Constraints on oceanic sulfate concentrations at this time come from fluid inclusion studies in rocks from the Ara Group of the Huqf Supergroup in Oman (Horita et al., 2002; Lowenstein et

al., 2003), from sulfur isotope evidence of the Doushantuo Formation in the Nanhua Basin, South China(McFadden et al., 2008, Li et al., 2010), and from modeling results based on the rate of change in sulfate-sulfur isotopic compositions within carbonate strata of Sorona, Mexico and Death Valley, California(Loyd et al., 2012). Three types of studies come up with different interpretations.Fluid inclusion evidence points to high concentrations of oceanic sulfate (~17mM), whereas sulfur isotopic evidence suggests much lower levels (~200 μM), and simulation results suggesting sustained low sulfate conditions (~2.0mM or lower). These differences have been interpreted by some workers to reflect real changes in oceanic sulfate concentrations in the late Proterozoic (Fike et al., 2006, Fike and Grotzinger, 2008).

A number of scientific questions have risen from studies of the Ediacaran sulfur cycle that are linked to isotopic measurements of sulfide and sulfate. These include questions about the levels of sulfate in oceans basins, the evolution of sulfide oxidation in the sediments, the role of bioturbation, and whether the isotopic records of sulfide and sulfate from different basins preserve global or regional signals. Here, new sulfur isotope measurements ($\delta^{34}S$ and $\Delta^{33}S$) of paired carbonate associated sulfate (CAS) and sedimentary pyrite are presented for samples previously studied from the Huqf Supergroup in Oman (Fike et al., 2006, Fike and Grotzinger, 2008) that provide empirial and modeling constraints on the response of the oceanic sulfur cycle at this time. Existing hypotheses about the role of processes associated with drawdown of oceanic sulfate are evaluated and new insights into the ocean chemistry of late Neoproterozoic ocean basins are described. I argue that connections between sulfur isotope fractionations, sulfate concentrations, and sulfide reoxidation revealed by the rare sulfur isotopes are generally consistent with existing models, with a few subtle differences. I also explore how this data

provides evidence for links between sulfide reoxidation and bioturbation during this geological time interval (635-540Ma).

5.2. Geological Setting

The stratigraphic focus of this study, the Huqf Supergroup of Oman (Figure 5.1), is a mostly thick sequence of strata consisting of the Abu Mahara, Nafun and Ara groups, with several recognized unconformities in the succession (Fike et al., 2006, Fike and Grotzinger, 2008) .

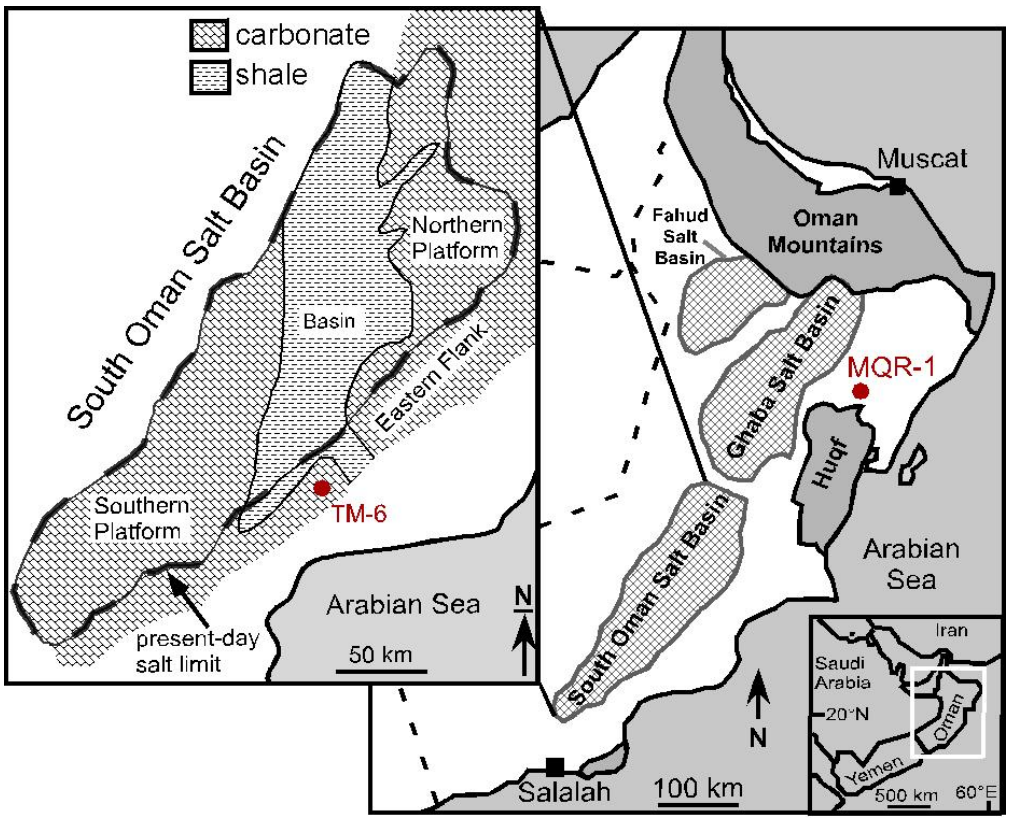

Figure 5.1. Map of Oman basins showing the locations of drilling wells (TM-6 and MQR-1) that provided samples in studies of Fike et al. (2006) and Fike and Grotzinger (2008).

The oldest part of the Huqf Supergroup, the Abu Mahara Group, overlies ~800 Ma crystalline basement and may contains glacial deposits of Marinoan age (~635Ma, Bowring et al., 2007). The Nafun Group overlies the Abu Mahara Group and was deposited during the late

Ediacaran (ca. 580-547 Ma; Amthor et al., 2003, Schröder et al., 2004). The Nafun Group was deposited in a shallow marine environment and outcrops laterally over a distance of several hundred kilometers (Mattes and Conway-Morris,1990; McCarron, 2000; Grotzinger et al., 2002; LeGuerroue et al., 2006). The strata of the Nafun Group consist of two clastic-to-carbonate shallowing-upward cycles that are divided by an unconformity at the contact between the Khufai and the Shuram formations. The older cycle is defined by the Masirah Bay and Khufai formations, and the younger cycle is defined by the Shuram and Buah formations. The Shuram excursion from the basal Shuram Formation through the mid-Buah Formation overlies the unconformable contact between the Khufai and the Shuram, which is thought to include the interval of Gaskiers glaciation (~580 Ma) (McCarron, 2000, Bowring et al., 2002, Bowring et al., 2007).

The Ara Formation overlies the Nafun Group and was deposited between ~547 Ma and 540 Ma in a subsiding, fault-bounded basin (South Oman Salt Basin, Bowring et al., 2007). This formation consists of a series of six carbonate shallowing upwards cycles (A0-A6) with evaporites discontinuously present in the upper five, suggesting basin restriction. In the eastern flank of the South Oman salt basin, the Ara Group does not preserve evaporites and there may have been a connection with the open ocean. The thickness of the Ara Group (A0-A6) is approximately 200-300 meters.

The Ara Group in the eastern flank shares an unconformable contact with the underlying Buah Formation. Age constraint for upper Buah Formation is ~ 548Ma (Grotzinger et al., 1995) and the age of the ash horizon in the middle of the Ara A0 carbonate unit has been determined to be 546.72±0.21Ma (Bowring et al., 2007). These ages constrain the unconformity at the Buah-Ara boundary to a ~1 Ma time interval. The base of the A4 carbonate unit is correlated with the

interior carbonate units in the South Oman Salt Basin, which is dated to 541 Ma by the bedded ash. This corresponds with the Ediacaran-Cambrian boundary (~541 Ma), which is also marked by a negative carbon isotope excursion (~ 7‰). (Amthor et al., 2003, Bowring et al., 2007).

5.3. Analytical Methods

CAS (carbonate associated sulfate) and CRS (chromium-reducible sulfur) samples for this study come from the studies by Fike et al. (2006) and Fike and Grotzinger (2008). Carbonate associated sulfate samples were provided by David Fike who precipitated $BaSO_4$ from the samples for the two previous studies. Chromium reducible sulfur had been prepared by David Fike as Ag_2S. Details of the procedures used to extract sulfur from rock samples that were originally taken from drill cores (Miqrat-1 wells from the north Huqf region, TM-6 wells in the Eastern Flank of South Oman Salt Basin) are reported in the studies by Fike et al. (2006) and Fike and Grotzinger (2008). A brief description of CAS extraction is summarized here to evaluate the possibility of contamination from soluble non-CAS sulfur, and uncertainties in data analysis and interpretation. Ten to thirty grams of powdered core samples, which were crushed in the SPEX 8510 shatterbox were rinsed with 3X deionized water and/or 10% NaCl solution to remove water soluble sulfate. There was no noticeable difference in $\delta^{34}S_{CAS}$ data generated from these two leaching solutions. The dried powdered samples were then soaked in 6N HCl for 2 hours at ~60 ℃ under an anoxic condition of continuous flushing of nitrogen gas stream or in 6N HCl for 12-24 hours. Following dissolution, filtrate were filtered and excess 1M $BaCl_2$ solution was added to the filtrate to precipitate $BaSO_4$ and the residue was used to extract chromium reducible sulfur. The Thode reduction method that is used to convert CAS samples ($BaSO_4$ powders) to Ag_2S and the protocol for multiple sulfur isotopic measurement and assoacited uncertainties for $\delta^{34}S$ and $\Delta^{33}S$ are described in Chapter 4.

5.4. Results

Sulfur isotope measurements are reported in tables (Table 5.1 and Table 5.2) for CRS and CAS sulfur isotope data. Figure 5.2 presents the carbon and sulfur isotope data along the stratigraphic column in the Huqf Supergroup, which is normalized to the MQR-1 well depths.

Table 5.1 Sulfur isotopic data for pyrite

Strata Unit	Well	Composite Depth	$\delta^{34}S\_SF_6$	$\Delta^{33}S$	$\delta^{34}S\_SO_2$
Ara	TM-6	2400	9.6	0.081	8.7
Ara	TM-6	2450	7.9	0.094	8.5
Ara	TM-6	2490	9.9	0.092	9.9
Ara	TM-6	2520	8.0	0.065	7.9
Ara	TM-6	2525	10.7	0.039	11.9
Ara	TM-6	2545	10.1	0.087	9.9
Ara	TM-6	2560	9.0	0.063	8.7
Ara	TM-6	2580	6.2	0.095	5.5
Ara	TM-6	2605	10.8	0.061	10.9
Ara	TM-6	2615	10.0	0.076	10.4
Ara	SHM-1	2890	-2.1	0.064	-2.1
Ara	SHM-1	2950	4.4	0.045	4.4
Buah	MQR-1	3200	-26.5	0.088	-25.5
Buah	MQR-1	3206	-24.8	0.099	-24.1
Buah	MQR-1	3208	-24.5	0.093	-24.1
Buah	MQR-1	3224	-25.2	0.085	-24.0
Buah	MQR-1	3280	-12.4	0.058	-13.7
Buah	MQR-1	3326	-12.9	0.053	-12.6
Buah	MQR-1	3404	-13.8	0.064	-13.9
Buah	MQR-1	3420	-8.5	0.050	-13.6
Shuram	MQR-1	3450	-11.8	0.065	-11.5
Shuram	MQR-1	3468	-7.8	0.081	-7.5
Shuram	MQR-1	3490	-15.4	0.053	-13.6
Shuram	MQR-1	3510	-15.3	0.053	-14.9
Shuram	MQR-1	3520	-15.4	0.048	-14.5
Shuram	MQR-1	3530	-19.5	0.055	-17.8
Shuram	MQR-1	3550	-24.0	0.057	-22.5
Shuram	MQR-1	3610	-3.0	0.053	-3.0
Khufai	MQR-1	3830	-10.6	0.056	-10.7
Khufai	MQR-1	3860	-3.4	0.185	-1.8
Khufai	MQR-1	3870	-3.6	0.077	-3.5
Khufai	MQR-1	3880	-1.9	0.060	-1.5
Khufai	MQR-1	3910	-5.1	0.032	-4.5
Khufai	MQR-1	3950	-1.5	0.014	-1.2
Khufai	MQR-1	3968	1.4	0.004	1.4
Khufai	MQR-1	3980	-0.4	0.003	-0.2
Khufai	MQR-1	3990	0.5	-0.002	1.6
Khufai	MQR-1	4050	-2.9	0.008	-3.1
Masirah Bay	MQR-1	4072	-1.1	0.014	1.1
Masirah Bay	MQR-1	4100	11.5	0.010	5.8
Masirah Bay	MQR-1	4120	12.1	0.023	12.1
Masirah Bay	MQR-1	4200	9.2	-0.031	10.6

Table 5.2 Sulfur isotopic data for carbonate associated sulfate

Strata Unit	Well	Correlation Depth	$\delta^{34}S\_SF_6$	$\Delta^{33}S$	$\delta^{34}S\_SO_2$
Ara	TM-6	2400	42.4	0.062	41.2
Ara	TM-6	2450	38.8	0.065	39.3
Ara	TM-6	2480	39.6	0.010	39.3
Ara	TM-6	2490	42.2	0.021	41.3
Ara	TM-6	2505	39.7	0.056	38.9
Ara	TM-6	2520	39.8	0.030	40.0
Ara	TM-6	2525	40.9	0.043	40.3
Ara	TM-6	2530	41.6	0.065	41.1
Ara	TM-6	2545	40.3	0.027	39.7
Ara	TM-6	2560	41.3	0.060	39.7
Ara	TM-6	2580	40.0	0.046	38.9
Ara	TM-6	2605	39.7	0.027	38.3
Ara	TM-6	2615	40.4	0.028	39.4
Ara	TM-6	2850	41.6	0.010	41.6
Ara	SHM-1	2890	40.0	0.049	40.0
Ara	SHM-1	2950	40.3	0.055	40.3
Ara	TM-6	3000	33.4	0.017	33.4
Buah	MQR-1	3200	26.8	0.014	24.7
Buah	MQR-1	3206	27.4	0.023	26.2
Buah	MQR-1	3208	27.2	0.012	26.0
Buah	MQR-1	3224	26.7	0.011	26.0
Buah	MQR-1	3280	25.9	0.035	25.3
Buah	MQR-1	3326	25.7	0.023	23.8
Buah	MQR-1	3360	22.0	0.008	21.3
Buah	MQR-1	3380	22.1	0.007	21.4
Buah	MQR-1	3404	23.3	0.025	22.7
Buah	MQR-1	3420	23.6	0.010	23.3
Shuram	TM-6	3430	26.2	-0.013	25.7
Shuram	MQR-1	3460	24.0	0.030	23.9
Shuram	MQR-1	3468	18.2	0.035	23.9
Shuram	MQR-1	3490	24.7	0.017	24.1
Shuram	MQR-1	3510	23.9	0.026	23.3
Shuram	MQR-1	3520	22.3	0.023	23.8
Shuram	MQR-1	3530	24.2	0.022	23.4
Shuram	MQR-1	3550	23.2	0.023	22.3
Shuram	MQR-1	3610	21.3	0.027	22.0
Shuram	MQR-1	3690	25.2	0.039	24.6
Shuram	MQR-1	3720	24.4	0.024	23.1
Shuram	MQR-1	3740	25.7	0.012	24.6
Shuram	MQR-1	3780	24.2	0.026	23.6
Khufai	MQR-1	3810	27.9	0.008	27.0
Khufai	MQR-1	3820	27.8	-0.007	27.3
Khufai	MQR-1	3830	21.5	0.066	28.0
Khufai	MQR-1	3850	23.6	0.018	28.0
Khufai	MQR-1	3860	26.5	-0.007	26.8
Khufai	MQR-1	3880	25.2	-0.007	25.1
Khufai	MQR-1	3910	21.5	0.020	21.0
Khufai	MQR-1	3950	19.1	0.010	21.6
Khufai	MQR-1	3968	23.8	-0.004	23.8
Khufai	MQR-1	3980	23.0	-0.009	21.8
Khufai	MQR-1	4020	20.6	0.048	22.3
Khufai	MQR-1	4050	22.2	0.019	21.7
Masirah Bay	MQR-1	4072	18.4	-0.001	18.2
Masirah Bay	MQR-1	4100	22.3	0.000	21.9
Masirah Bay	MQR-1	4120	21.0	0.036	23.1
Masirah Bay	MQR-1	4200	22.7	-0.053	21.8

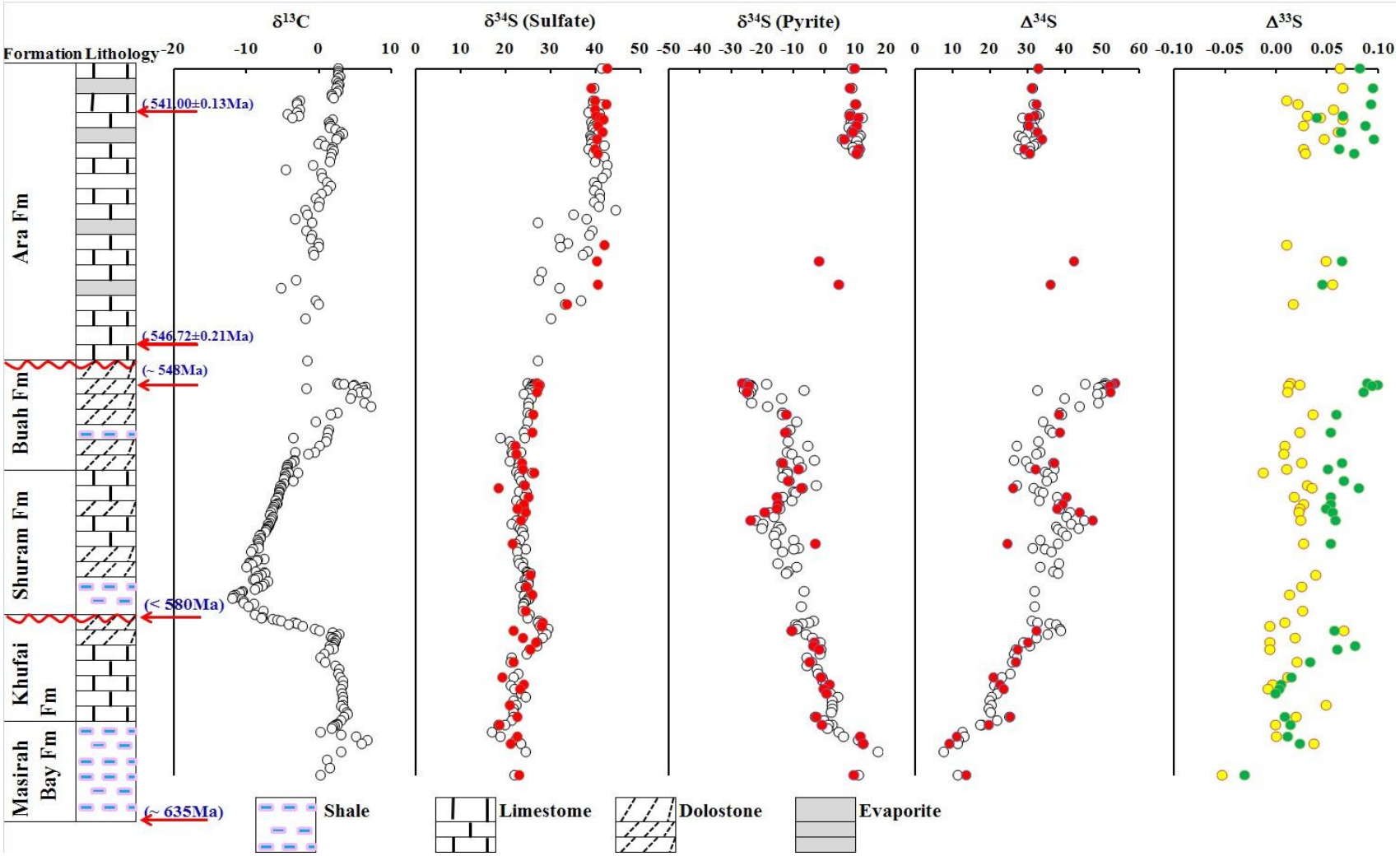

Figure 5.2. $\delta^{13}C$, $\delta^{34}S$ and $\Delta^{33}S$ depth profiles of carbonate, sulfate and pyrite along the normalized strata depth. It also include the new SF_6-based analyses of sulfur isotope data (red circles). The 4th panel are the sulfur isotope fractionations ($\Delta^{34}S$) between sulfate and pyrite. The error bar (0.3‰, 2σ) in $\delta^{34}S$ profiles are smaller than the data symbol, and the error bar (2σ) in $\Delta^{33}S$ profiles are 0.020‰.

$\delta^{13}C_{carb}$ record of carbonate provides a way to understand pertubations of the global carbon cycle and a context for interpreting the changes in the sulfur cycle. $\delta^{13}C_{carb}$ rises from 0‰ to ~6‰ in the Masirah Bay Formation, and then fall to 0‰ just below the Masirah Bay-Khufai boundary. $\delta^{13}C_{carb}$ then rises to 3‰ and and oscillates a value of 3‰ for most of the Khufai Formation,except for a negative shift to 0‰ in the mid-Khufai Formation. A decrease to -12‰ in the lower Shuram Formation was followed, which is known as the Shuram excursion and is attributed to oxidation of organic matter in the deep ocean (Fike et al., 2006). Above this level, $\delta^{13}C_{carb}$ values progressively increase to 6‰ in the upper Buah, and then decrease to 0‰ at the uppermost Buah. $\delta^{13}C_{carb}$ shows several cycles of rising and falling, but oscillates about a mean of 0‰ throughout the Ara, and the Precambrian and Cambrian boundary (~541Ma) is marked by a negative excursion in $\delta^{13}C_{carb}$ (up to ~ 7‰).

Figure 5.3 presents the sulfur isotopic data ($\delta^{34}S$ and $\Delta^{33}S$) using the SF_6 method and also includes the isotopic data ($\delta^{34}S$) reported in Fike et al. (2006) and Fike and Grotzinger (2008) collected using an on-line combustion technique coupled with isotope ratio monitoring of SO_2. A cross plot of SF_6 measurements against previous SO_2-based analyses at the stable isotope lab of Indiana University yields a relationship of $\delta^{34}S_{SF6}=1.011(\pm0.008;\ 1\sigma) \times \delta^{34}S_{SO2}-0.125(\pm0.185;\ 1\sigma)$, where the value of the regression correlation coefficient is 0.994. Any differences between these two methods are thought to be due to scale compression and memory effects associated with the SO_2-based method (Rees et al., 1978). The comparison of the results based on these two methods shows that the general match is good for analyses made in my study and those of Fike et al. (2006) and Fike and Grotzinger (2008) on the same samples. The data analysis and interpretation is based on the sulfur isotope data measured by SF_6 method.

$\delta^{34}S_{CAS}$ rises from 21‰ to ~24‰ in the Masirah Bay Formation, and then fall to 16‰ just below the Masirah Bay-Khufai boundary. $\delta^{34}S_{CAS}$ then rises to ~29‰ in the upper Khufai Formation, followed by a fall to ~23‰ at the Khufai-Shuram boundary. $\delta^{34}S_{CAS}$ oscillates a mean of 24‰ for most of the Shuram and Buah Formation, and rises to ~26‰ in the upper Buah. At the Buah-Ara boundary, a positive shift (10‰) in the $\delta^{34}S$ of sulfate is observed, which has been called the Ara anomaly. $\delta^{34}S_{CAS}$ remains constant (~40‰) throughtout the Ara Formation. $\delta^{34}S_{PY}$ increases from ~9 ‰ to ~17‰ in the Masirah Bay Formation, and then fall to -3‰ just below the Masirah Bay-Khufai boundary. $\delta^{34}S_{PY}$ gradually decrease to -10‰ just prior to the Khufai-Shuram boundary. $\delta^{34}S_{PY}$ rises slightly in the basal Shuram and then falls to -23‰ in the upper Shuram. $\delta^{34}S_{PY}$ then increases to -10‰ in the uppermost Shuram and lower Buah, followed by a decrease to -25‰ in the uppermost Buah. There is a positive shift (up to ~30‰) in $\delta^{34}S_{PY}$ at the Buah-Ara boundary, and $\delta^{34}S_{PY}$ remains positive and constant (~10‰) throughout the Ara Formation.

$\Delta^{33}S_{CAS}$ gradually rises from -0.053‰ to 0.048‰ in the Masirah Bay Formation and lower Khufai, and $\Delta^{33}S_{CAS}$ then falls to -0.009‰ followed by an increase to 0.066‰ in the uppermost Khufai. $\Delta^{33}S_{CAS}$ then falls to -0.007‰ and rises to 0.026‰ just prior to the boundary of Khufai-Shuram. $\Delta^{33}S_{CAS}$ then oscillates a mean of 0.020‰ for most of the Shuram and Buah Formation. There is a slightly positive shift in $\Delta^{33}S_{CAS}$ (up to 0.020‰) at the boundary of Buah-Ara. $\Delta^{33}S_{PY}$ tracks the $\Delta^{33}S_{CAS}$ record, except $\Delta^{33}S_{PY}$ reach maxium of 0.099‰ in the uppermost Buah.

The sulfur isotope fractionations between sulfate and pyrite ($\Delta^{34}S_{SW\text{-}PY}$) increases from a smaller value of approximately 10‰ in the Masirah Bay Formation to approximately 47‰ in the

mid Shuram. Following this, $\Delta^{34}S_{SW\text{-}PY}$ decreases to 26‰ in the uppermost Shuram, and $\Delta^{34}S_{SW\text{-}PY}$ then rises and reach a maximum value of ~51‰ in the upper Buah. A quick drop in the magnitude of $\Delta^{34}S_{SW\text{-}PY}$ occurs at the boundary of Buah-Ara to reach a fractionation of approximately 30‰. There appears to be no direct relationship between the records of $\delta^{34}S$ and $\Delta^{33}S$ of pyrite and CAS. The stratigraphic profiles for $\delta^{34}S$ and $\Delta^{33}S$ of pyrite and CAS diverge throughout the Masirah Bay Formation and Buah Formation, suggesting an increase in fractionation. These profiles then parallel each other in the Ara Formation, indicating constancy in the magnitude of fractionation. On the other hand, stratigraphic profiles for $\Delta^{33}S_{py}$ and $\Delta^{33}S_{CAS}$ covary throughout the Huqf Supergroup. $\delta^{34}S$ of pyrite and CAS generally maintains relatively constant positive values near 10‰ and 40‰, respectively; $\Delta^{33}S$ of pyrite and CAS similarly show relatively constant values near 0.060‰ and 0.040‰, respectively in the Ara Formation. In order to capture the first-order feature of the sulfur isotopic records and simplify the interpretation of the isotopic records for CAS and CRS, $\delta^{34}S$ and $\Delta^{33}S$ provided in this study have been grouped into selected intervals throughout the stratigraphy that is normalized to the MQR-1 well depths (Figure5.3). These lumped strata are mostly based on the geological observations (lithostratigraphic transitions and unconformities observed in the cores). These averages are summarized and shown in Table 5.3 and Table5.4.

Table 5.3 averages of $\delta^{34}S$ and $\Delta^{33}S$ of CRS for lumped strata

Sequence	Correlation Depth (m)	Strata Unit	$\delta^{34}S$ (‰)	$\Delta^{33}S$ (‰)
6	2615 to 2400	Ara Fm	9.2	0.075
5	2950 to 2890	Ara Fm	1.1	0.054
4	3224 to 3200	Buah Fm	-25.3	0.091
3	3530 to 3280	Shuram Fm, Buah Fm	-13.3	0.058
2	3680 to 3550	Khufai Fm, Shuram Fm	-13.5	0.055
1	4200 to 3830	Khufai Fm, Masirah Fm	0.3	0.032

Table 5.4 averages of $\delta^{34}S$ and $\Delta^{33}S$ of CAS for lumped strata

Sequence	Correlation Depth (m)	Strata Unit	$\delta^{34}S$ (‰)	$\Delta^{33}S$ (‰)
6	2615 to 2400	Ara Fm	40.5	0.042
5	3000 to 2850	Ara Fm	38.9	0.033
4	3280 to 3200	Buah Fm	26.8	0.019
3	3530 to 3326	Shuram Fm, Buah Fm	23.3	0.018
2	3820 to 3550	Khufai Fm, Shuram Fm	25.0	0.019
1	4200 to 3830	Khufai Fm, Masirah Fm	22.2	0.010

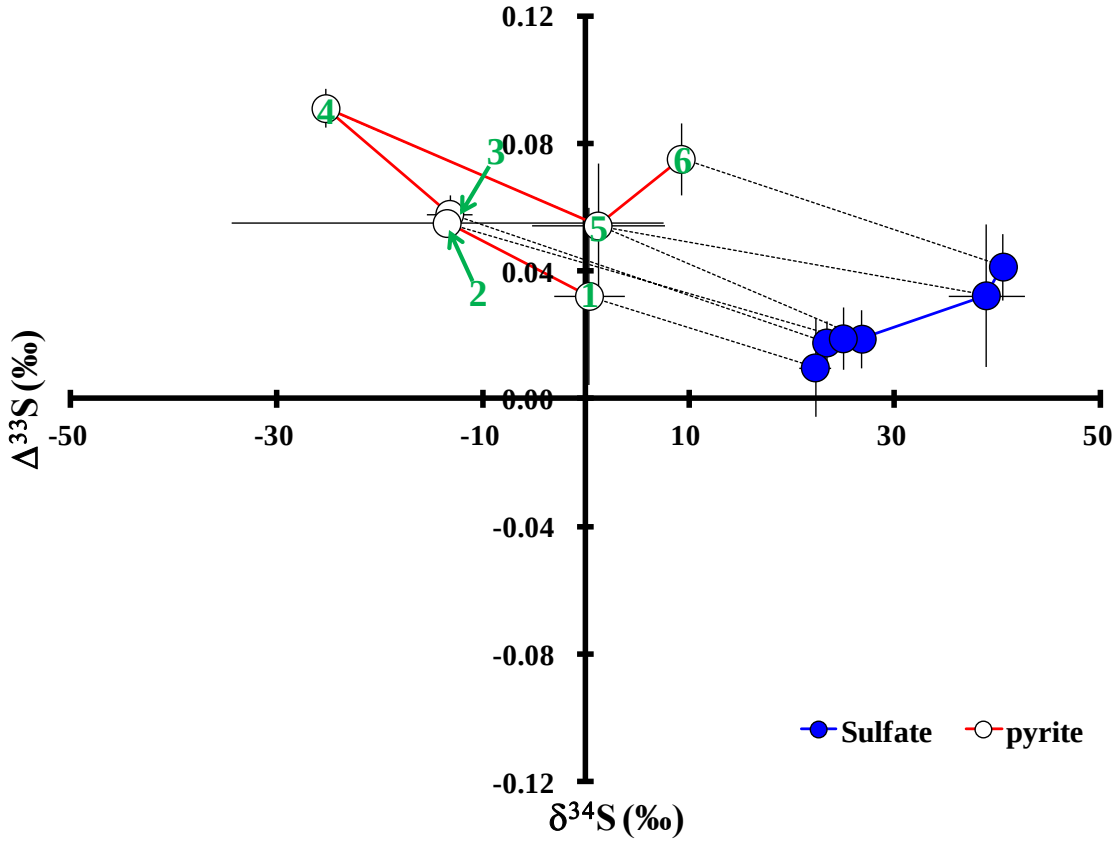

Figure 5.3 this plot shows the data averages for different stratigraphic intervals (from sequence 1 to sequence 6). Bars on points represent the two standard error (2σ)for the different stratigraphic horizons. The gray dashed lines link the composition of corresponding sulfate and pyrite for each stratigraphic interval. This figure illustrates the evolution of oceanic sulfate (CAS) from $\delta^{34}S$ values near 22‰ and $\Delta^{33}S$ values near 0.009‰ to higher values. This plot also shows a clockwise evolution of pyrite sulfur moving up section.

The averages for $\delta^{34}S$ and $\Delta^{33}S$ values in CAS progress from low values to high values moving up section. The averages for $\delta^{34}S$ values of CRS show a decrease between the depth of 4200m and 3200m, and then shift to positive values at the depth of 3200m. The averages for $\Delta^{33}S$ of CRS show a general increase between the depths of 4200m and 3200m, and reach a

maximum at the depth of 3200m. Averages for $\Delta^{33}S$ of CRS then may shows a slightly fall, but remain high values.

5.5 Discussion

The primary aim of this study is to understand the first order observations made from the $\delta^{34}S$ and $\Delta^{33}S$ records of the Huqf Supergroup. I use model under various assumptions to provide systems in which ideas about mechanism involved in regulating the sulfur isotopes of oceanic sulfate and sedimentary pyrite can be tested and simulated. These assumptions include 1) there are three major sulfur pools (pyrite-sulfur, seawater sulfate-sulfur and evaporite sulfate minerals), and other sulfur pools is negligible, 2) the sulfur cycle is closed in terms of exchange of sulfur between mantle and the Earth surface,and 3) the sulfate concentrations may change with time.

Before data analysis and interpretation is made, the sulfur isotopic data should be evaluated as to 1) whether diagenesis of carbonate influences the sulfur isotopic compositions of CAS, 2) whether the CAS extraction method is efficient in removing non CAS sulfate, and 3) whether non-CAS sulfate affect the final isotopic compositions of samples. The relationship between $\delta^{34}S$ and indicators of diagenesis ($\delta^{18}O_{carb}$, Mn/Sr, $\delta^{13}C_{carb}$, and the concentration of carbonate-associated sulphate) has been examined and no correlations were found (Fike et al., 2006), so it is believed depositional $\delta^{34}S$ are preserved. The non CAS sulfate may come from post-depositional pyrite oxidation and reduced sulfur oxidation in the lab extraction procedure. A mixed $\delta^{34}S$ and $\Delta^{33}S$ compositions will be produced if non CAS sulfate is not eliminated from samples. The CAS samples studied here were rinsed and soaked in deionized water for 24 hours to remove non CAS sulfate, but it is difficult to quantitatively evaluate how non-sulfate influence the final isotopic analysis due to paucity of data (e.g., the concentration of reduced sulfur in

samples and oxidized rate of reduced sulfur in lab environments). As seen from the depth profiles of $\delta^{34}S$, the $\delta^{34}S$ of CAS is generally higher than that of pyrite, therefore, the corrected $\delta^{34}S$ values of oceanic sulfate, if possible, would be more higher if measured $\delta^{34}S$ values of CAS are mixture with the sulfate derived from the oxidized pyrite. This logic is also applied to the $\Delta^{33}S$ of CAS because the line of binary mixing of sulfur pools in $\delta^{34}S$- $\Delta^{33}S$ space is curved. Further, the $\delta^{34}S$ of CAS in carbonate units of the Ara Formation is consistent with the $\delta^{34}S$ of anhydrites that are interlayed by carbonate units(Fike and Grotzinger, 2008; Schro ̈der et al.,2004). Thus we believe that the analytical procedure is not likely to affect the data analysis and interpretation.

A common way to describe the relationship between the isotopic composition and the fluxes of the sources and sinks is given by:

$$\delta^{34}S_{SW} = \delta^{34}S_{in} + f_{PY} \times \Delta^{34}S_{SW-PY} \qquad \text{(Eq 5.1)}$$

This steady state equation relates the sulfur isotopic compositions of oceanic sulfate ($\delta^{34}S_{SW}$) to the sulfur isotopic composition of the sulfate sulfur influx to the oceans ($\delta^{34}S_{in}$), the fraction of sulfur buried as sedimentary pyrite (f_{Py}), and the sulfur isotope fractionation between oceanic sulfate and coeval sedimentary pyrite ($\Delta^{34}S_{SW\text{-}PY}$). This equation is the basis for interpretation of time-series sulfur isotope data from Ediacaran and Early Cambrian successions (Fike et al., 2006, Fike and Grotzinger, 2008). Application of this equation to describe the isotopic compositions of the oceanic sulfate pool requires information about 1) the isotopic composition of the source sulfate, 2) the fraction of sulfur buried as sedimentary pyrite (f_{Py}), and 3) the fractionation associated with pyrite burial ($\Delta^{34}S_{SW\text{-}PY}$).

Holser (1988) suggests that the isotopic composition of sulfate sulfur ($\delta^{34}S$) fluxing into the oceans has been relatively constant at ~5‰ over the Mesozoic and Cenozoic, but this influx may have ranged between 4 to 12‰ during the Paleozoic and the latest Neoproterozoic (Garrels and Lerman, 1981, Canfield, 2004). Variations in $\delta^{34}S_{in}$ may relate to the rapid recycling of short lived sulfur pools, such as evaporite sulfate minerals and younger deposited pyrite sulfur (Berner, 1987). Recently, Havely et al (2012) has used a different type of sulfur model to estimate the input flux to the oceans. His model uses data from the reconstruction of evaporite deposition rates at various geologic times to constrain f_{py} and $\delta^{34}S_{in}$, suggesting strong negative $\delta^{34}S_{in}$ values for influx sulfur to the oceans. It is difficult to reconcile these results with the long term sulfur influx to the oceans insofar as the volcanic sulfur flux has near zero $\delta^{34}S$ compositions. Thus the sulfur model here uses the range of input values suggested by earlier authors.

Changes in the fraction of sulfur buried as sedimentary pyrite (f_{Py}) have been invoked as the principal variable that controls the observed isotopic variations of seawater sulfate, but changes in f_{Py}, through time have not been linked to specific changes in the oceanic environment perhaps related to the extent of areas of anoxia in marine sediments and the water column, if the Ediacaran deep oceans did become progressively oxygenated (Fike et al., 2006), one might expect a more prominent role for sulfide oxidation, and hence a change in the isotopic composition of oceanic sulfate. It also has been proposed that bioturbation by benthic organisms may have enhanced the oxidation of sulfide, reducing the fraction of sulfide buried as pyrite and shifting the balance to evaporites with higher oceanic sulfate levels (Canfield and Farquhar, 2009).

The magnitude of $\Delta^{34}S_{SW\text{-}PY}$ reflects the combined effects of sulfur isotope fractionations by microbial sulfate reducers, including pathways associated with sulfide oxidation and disproportionation, as well as other environmental factors such as temperature, sulfate concentration, sulfate supply and the type and abundance of reactive organic carbon. The use of sulfur by these organisms may also respond to changes in these environmental factors, with changes in sulfate reduction rate and sulfur isotope fractionation that may reflect different oceanic settings such as the limiting availability of sulfate, (Canfield, 2001, Detmers et al., 2001; Habicht et al., 2002).

Constraints on the magnitude of sulfur isotope fractionation between seawater sulfate and pyrite over geologic time have been placed in number of ways. One of these is described by Strauss (1999) who uses paired sulfur isotope records of oceanic sulfate and pyrite (minimum values for global average of pyrite-sulfur isotopes). Another approach developed by Wu et al., (2010) uses the $\Delta^{33}S$ of seawater sulfate and $\delta^{34}S$ of pyrite to calculate the magnitude of fractionation between oxidized and reduced reservoirs and the flux of pyrite burial. Model runs using these two different types of constraints on sulfur isotope fractionation yield different results for pyrite burial fluxes in different intervals of Phanerozoic Eon. Other earlier approaches assumed a constant sulfur isotope fractionation (Garrel and Lerman, 1981) and/or assumed that sulfur isotope fractionation is dependent on atmospheric oxygen levels (Berner, 2001).

A steady state equation that relates the ^{33}S to ^{32}S in the sulfur cycle can also be derived to further test the existing hypothesis about the evolution of the sulfur cycle. This equation coupled with another two equations listed below can be used to infer changes in $\Delta^{33}S$ of sulfate to the

oceans over geologic times. The changes in the $\Delta^{33}S$ of influx sulfur to the oceans may carry information about the changes in weathering pattern (e.g. preferred weathering of evaporite minerals or global averaging of weathered of pyrite and evaporite minerals) and exchange between Earth surface sulfur and mantle sulfur.

$$\delta^{34}S_{SW} = \frac{\delta^{34}S_{in} + 1}{f_{py} \times (^{34}\alpha - 1) + 1} - 1$$
$$\delta^{33}S_{SW} = \frac{\delta^{33}S_{in} + 1}{f_{py} \times (^{33}\alpha - 1) + 1} - 1 \qquad \text{(Eq 5.2)}$$
$$^{33}\alpha = {}^{34}\alpha^{\lambda}$$

where $\delta^{34}S_{in}$ and $\delta^{33}S_{in}$ represent the sulfur isotopic compositions of the sulfur influx to the oceans. The f_{Py} is the fraction of sulfur buried as sedimentary pyrite. The $^{34}\alpha$ is the sulfur isotope fractionation between oceanic sulfate and coeval sedimentary pyrite. Finally, the parameter λ relates $^{34}S/^{32}S$ to $^{33}S/^{32}S$. All parameters in these three equations are dimensionless, and for a box model with a single oceanic sulfate box, $^{34}\alpha$ is the global average fractionation.

One estimate of modern $\Delta^{33}S$ of influx sulfate-sulfur is constrained using data from measurements of the NBS-127 standard (see Chapter 3). The isotopic compositions of NBS-127 are taken as an estimate for the isotopic composition of sulfur in the oceans today, where the fraction of pyrite burial is assumed to be between 0.17 and 0.40 (Berner, 1982; Ono et al., 2006). The sulfur isotope fractionations are assumed to be 40‰, which is similar to the estimates for the Cenozoic Era (Wu et al., 2010). Using these constraints the model yields a range of $\Delta^{33}S$ of 0.012 to 0.017‰ for modern riverine sulfate with $\delta^{34}S_{in}$ ranging from 4.8 to 12.9‰. Other estimates of $\Delta^{33}S$ of influx sulfur have been made using models for times in the geologic past (Wu et al., 2010). These estimates have been reconstructed assuming a relationship between $\Delta^{33}S$

and $\delta^{34}S$ for sedimentary pyrite-sulfur and using this in combination with the modeled compositions of the sedimentary flux of pyrite-sulfur to determine the $\Delta^{33}S$ of that end member. The other two end members are the sulfur isotopic composition of juvenile sulfur determined from an oceanic floor spreading model, and the sulfur isotopic compositions of weathered evaporite minerals using a weathering model that takes into account estimated residence times for sedimentary pyrite sulfur and sulfate sulfur on the continents (Wu et al., 2010).

5.5.1 Evaluating the sulfur cycle in the Oman basin using steady state models

Use of a steady state model to constrain the sulfur cycle during deposition of Huqf Supergroup is justified on the basis of two lines of reasoning. The first is made by the comparing of sampling density with estimates made about residence time of oceanic sulfate. The second is made through examination of the sulfur cycle in continuous but transient steady conditions that would stand alone as a way dependent only on sulfur isotopes of seawater sulfate. The assumption of the sulfur cycle at steady state condition does not imply oceanic sulfate levels may not change over geologic times, however it implies that the response time of oceanic sulfate-sulfur due to the perturbation of the sulfur cycle is equal to the residence time of oceanic sulfate-sulfur.

Based on the assumed age of the basal diamictite and radiometric constraints within the Huqf succession, the resolution of sampling for time intervals of 635-580 Ma (4200 m to 3830 m), 580-548 Ma (3830 m to 3200 m) and 548-540 Ma (3200 m to 2400 m) is on the order of one to a few million years. This sample resolution is comparable to the turnover times estimated for low sulfate (<5 mM) oceans by Kah et al. (2004) and Canfield and Farquhar (2009). Canfield and Farquhar (2009) arrive at similar order of magnitude residence times using a relationship relating the sulfate sink to evaporite formation, reoxidation and sulfate reduction rates, which depend on

the reactive organic carbon flux and penetration of sulfate into the sediments. The way to deal with the sulfur cycle under steady state condition is informative and is the first step to quantitatively understand the evolution of the sulfur cycle over geologic time.

Non-steady state processes (e.g. changes in sulfate concentrations) may contribute to noise in the studied isotope signatures. A series of transient steady state can also be explored for evaluating the sulfur isotope data described herein in terms of the fraction of pyrite burial (f_{Py}) and the fractionation between sulfate and buried pyrite ($\Delta^{34}S_{SW\text{-}PY}$) to provide insights about the evolution of the sulfur cycle at this time.

5.5.2 Role of pyrite burial using steady state equations

The parameter of f_{Py} is calculated using the steady state equation (Eq. 5.1) with assumed values for the influx sulfur isotopes. Figure 5.4 presents two scenarios using $\delta^{34}S_{in}$ = 5‰ and $\delta^{34}S_{in}$ = 10‰ respectively. The overall trends of f_{Py} with time are similar under these two scenarios. The uncertainties associated with f_{Py} can be evaluated by its standard devivation, and is calculated by:

$$\sigma_{f_{py}} = \frac{\sigma_{SW}{}^2 + \sigma_{in}{}^2}{\Delta^{34}S_{SW-PY}{}^2} + (\sigma_{SW}{}^2 + \sigma_{PY}{}^2) \times \left(\frac{\delta^{34}S_{SW} - \delta^{34}S_{in}}{\Delta^{34}S_{SW-PY}{}^2}\right)^2 \quad \text{(Eq 5.3)}$$

where σ_{SW},σ_{PY} and,σ_{in} are uncertainties associated with estimates of $\delta^{34}S_{SW}$, $\delta^{34}S_{PY}$ and $\delta^{34}S_{in}$ averages, and $\Delta^{34}S_{SW\text{-}PY}$ is the sulfur isotope fractionation between oceanic sulfate and coeval sedimentary pyrite in the sulfur cycle.

The uncertanties in f_{py} is primarily from the uncertainty in $\delta^{34}S_{in}$, and σ_{fpy} is smaller than 0.08 if we adopt that the maximum uncertainty in $\delta^{34}S_{in}$ is 10‰. The estimates of standard deviation of

f_{py} for the Huqf Supergroup in the Oman basin are not likely to affect the data interpretation and infererence from variations in f_{py}.

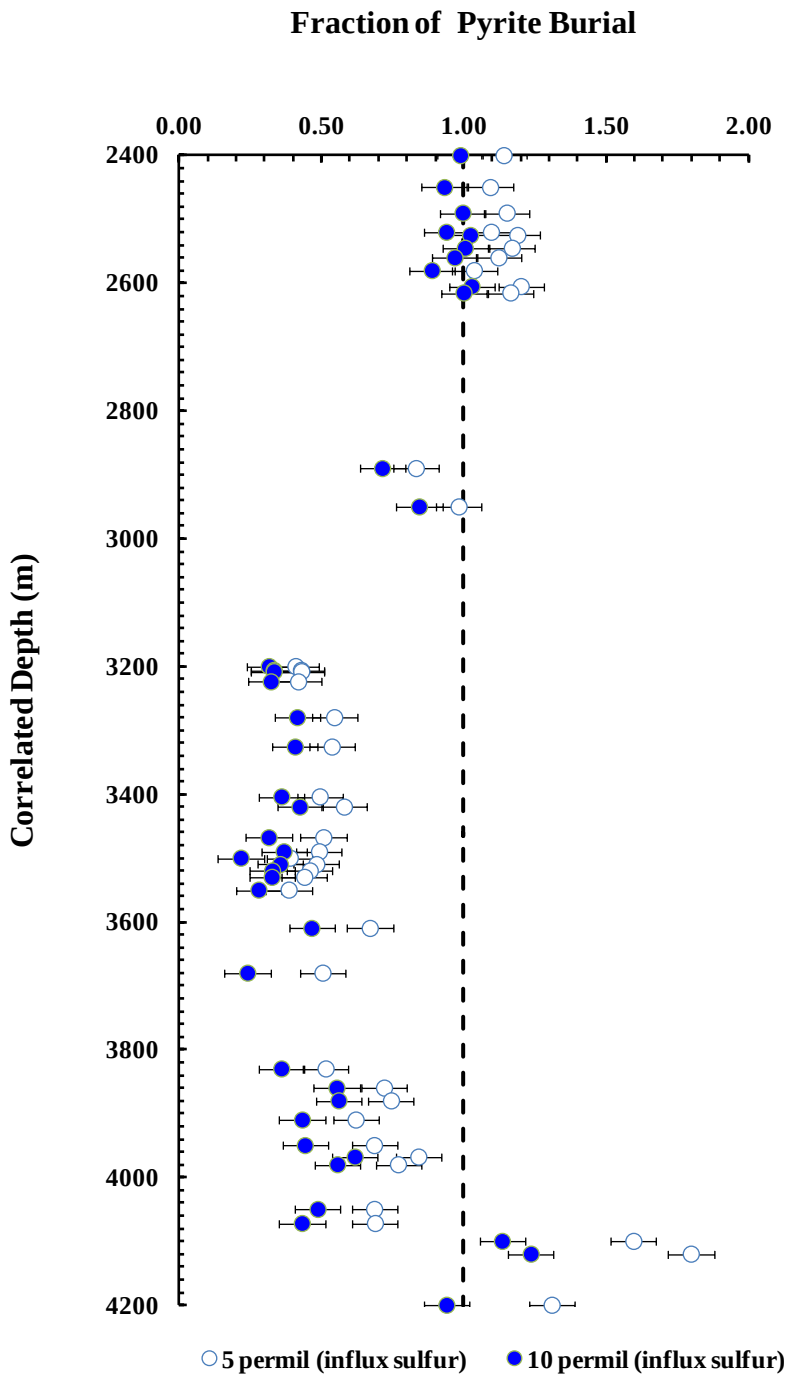

Figure 5.4 Variations in f_{py} underr two scenarios using $\delta^{34}S_{in}$ = 5‰ (open circle) and $\delta^{34}S_{in}$ = 10‰ (blue circle). The error bar is the maximum estimates of stadnard deviation in f_{py} using Eq(5.3). Detailed discussion is in section 5.5.2.

The values of f_{Py} are greater than one just above the glacial deposits (~635 Ma), which may reflect the sulfur influx to the oceans deposited exclusively as sedimentary pyrite at the basinal scale in the sulfur cycle when oceanic sulfate may be low. The values of f_{Py} progressively become smaller than one, but are slightly larger than the modern estimate value of f_{Py} (0.36, Berner, 1982; 0.17 to 0.26, Ono et al., 2006) in the time interval of 635-548 Ma (4200m to 3200m). Today, oceanic sulfate is thought to be under non-steady state and sulfate levels are in a growth phase (Ivanov, 1983). These mean values for f_{Py} smaller than unity do not require deposition of evaporite sulfate minerals, but instead may reflect changes of seawater sulfate concentrations. If evaporite minerals are not selectively preserved and/or weathered at a specific point in geologic time, a change in seawater sulfate concentration may result in a fraction of pyrite burial being calculated either less than or greater than one. The calculated fraction of pyrite burial in the Huqf Supergroup may point to periods when the sulfate concentrations rose (fraction of pyrite burial less than one without evaporite formation) or fell (fraction of pyrite burial greater than 1). Factors that may influence pyrite burial and evaporite formation include: changes in benthic bioturbation, changes in the amounts and rates of sulfide oxidation, and other changes related to the interface between oceanic sediments and the overlying oceanic water column.

The values of f_{Py} seen in Figure 5.5 start changing from values of 0.41-0.51 at a depth of 3200m to values of 0.90-1.20 at a depth of 2600 m and above. This may reflect a decrease in seawater sulfate concentrations. Sulfate levels estimated from the amount of change of $\delta^{34}S_{CAS}$ for the short time interval (approximately 3 Ma) are around 7 mM, which is in the same order of magnitude suggested consistent with the evidence from fluid inclusion study that indicate a decrease of seawater sulfate concentration across the Precambrian-Cambrian transistion

(Lowenstein et al., 2003). The two methods of tuning sulfate concentrations from fluid inclusion chemistry and the rate of change in $\delta^{34}S_{CAS}$ are, however, subject to large uncertainty. Even given these large uncertainties, the changes are thought to be real and may be due to the weakening of benthic bioturbation and the extinction of Ediacaran biota (Canfield and Farquhar 2009) and/or other weakening of other physical processes (e.g., turbulence) in marine sediments that lead to a progressively smaller role for sulfide oxidation in the cycling of sulfur.

5.5.3 Implication of sulfur isotope fractionation

The present interpretation attributes the small sulfur isotope fractionation in the oldest parts of the succession to sulfate reduction under low sulfate conditions. It is generally thought that there is a threshold for the expression of sulfur isotope fractionation produced by microbial sulfate reduction. This threshold is controlled by sulfate levels, and it is generally accepted that the sulfur isotope fractionation is not suppressed when the sulfate levels are above 0.2 mM, but the magnitude of sulfur isotope fractionations show large ranges of 3‰ to 46‰ in culture studies (Canfield 2001). Recently, Sub Sim et al., (2011) and Canfield et al., (2010) presented results from two laboratory culture experiments that yielded even large fractionation (up to ~75‰). It is also noted that the sulfur isotope fractionation was inverted when the sulfate concentration further decreased down to 0.01 mM (Harrison and Thode, 1957). This correlation has been applied to calibrate the oceanic sulfate levels during the Archean when the inferred sulfate concentrations are thought to be below 0.2 mM (Habicht et al., 2002).

Studies have shown that the magnitude of the biological fractionation associated with sulfate reduction is dependent on the sulfate concentrations in the growth medium. Sulfate reducers have shown a capability of producing very large isotopic fractionation when sulfate concentrations are

above 0.2 mM (Canfield 2001, Habicht et al., 2002, Canfield et al., 2010). Studies also have shown that sulfate reducers metabolizing sulfate in settings where the sulfate concentrations are low, express much smaller sulfur isotope fractionations (Habicht et al., 2002). This arises because at low sulfate concentration the sequence of metabolic steps associated with sulfate reduction is unidirectional, so that large fractionations are not expressed in the final metabolic product.

Fike et al. (2006) and Fike and Grotzinger (2008) have interpreted the smaller fractionations in the lower parts of the Huqf Supergroup in terms of sulfate limitation, with estimates of concentrations in the range of 0.2mM to 5mM. Values of $\Delta^{34}S_{SW\text{-}PY}$ as high as ~51‰ are very large and it is possible that they represent a single step of sulfate reduction, but it is also possible they reflect an added role of sulfur disproportionation in a more complex model of sulfur cycling (Fike et al, 2006). The environmental and ecological forcing for such a transition is unclear. The coeval depleted ^{34}S pyrite may indicate that the water column was euxinic. The sulfur isotope fractionation drops to ~30‰ in the Ara Formation and is also associated with positive $\delta^{34}S$ values of pyrite. The shift from negative to positive $\delta^{34}S$ values has been interpreted to indicate either a shift to very positive $\delta^{34}S$ composition for influx sulfate to the system (see section 5.5.4) or to suggest the existence of a sulfate drawdown and distillation of sulfur isotopes in both sulfate and pyrite (Canfield and Farquhar 2009).

5.5.4 Implication of non-zero $\Delta^{33}S$

The observation that non-zero $\Delta^{33}S$ values can be produced by microbes metabolizing various sulfur compounds in nature has made it possible to obtain new information about sulfur cycling. The $\Delta^{33}S$ of oceanic sulfate has been used to argue for sulfide oxidation and sulfur

disproportionation in ancient geologic records (Johnston et al., 2005), and in modern environmental systems of the Cariaco Basin (Li et al., 2010).

The $\Delta^{33}S$ has also been used to explore mixing and un-mixing of sulfur between sulfur pools in the oceanic sulfur cycle (Ono et al., 2006). In this study, I use a slightly more complex sulfur cycle box modelto study the cycling of sulfur in the Ediacaran Period. This model includes additional steps that relate to sulfide oxidation and the exchange of sulfate between seawater and pore water sulfate pools. Parameters that are explored in this model include: 1) the fraction of pyrite burial, 2) the fraction of sulfide oxidation, and 3) the fraction of sulfate exchange between seawater and pore-water. Model results (Figure 5.6) are compared with the isotopic data from the Huqf Supergroup in order to evaluate whether the model can be used to reproduce the results, and whether assumptions such as the steady state and the components in the model are valid.

Geochemical evidence shows that the Oman basin was linked to the open ocean inferred from the global correlation in $\delta^{13}C_{carb}$ of these carbonate units (Nanfun and Ara groups) and facies independent $\delta^{34}S$ values. However, it is possible that the deposition of Ara carbonate units interbedded with evaporites occurred in a periodically restriction basin (Fike and Grotzinger, 2008). An additional argument that supports this assertion is based on the calculation of mixing time for sulfate between the two sulfur pools with different sulfate levels (refer to chapter 4), which is shorter than our sampling resolution for Oman strata. The sulfur isotope records of CAS from the Oman basins may reflect the sulfur isotope records of oceanic sulfate of the open oceans at the time when these carbonate were deposited. With this assumption, the values of f_{py} and $\Delta^{33}S$ of influx sulfur are estimated using steady state sulfur models.

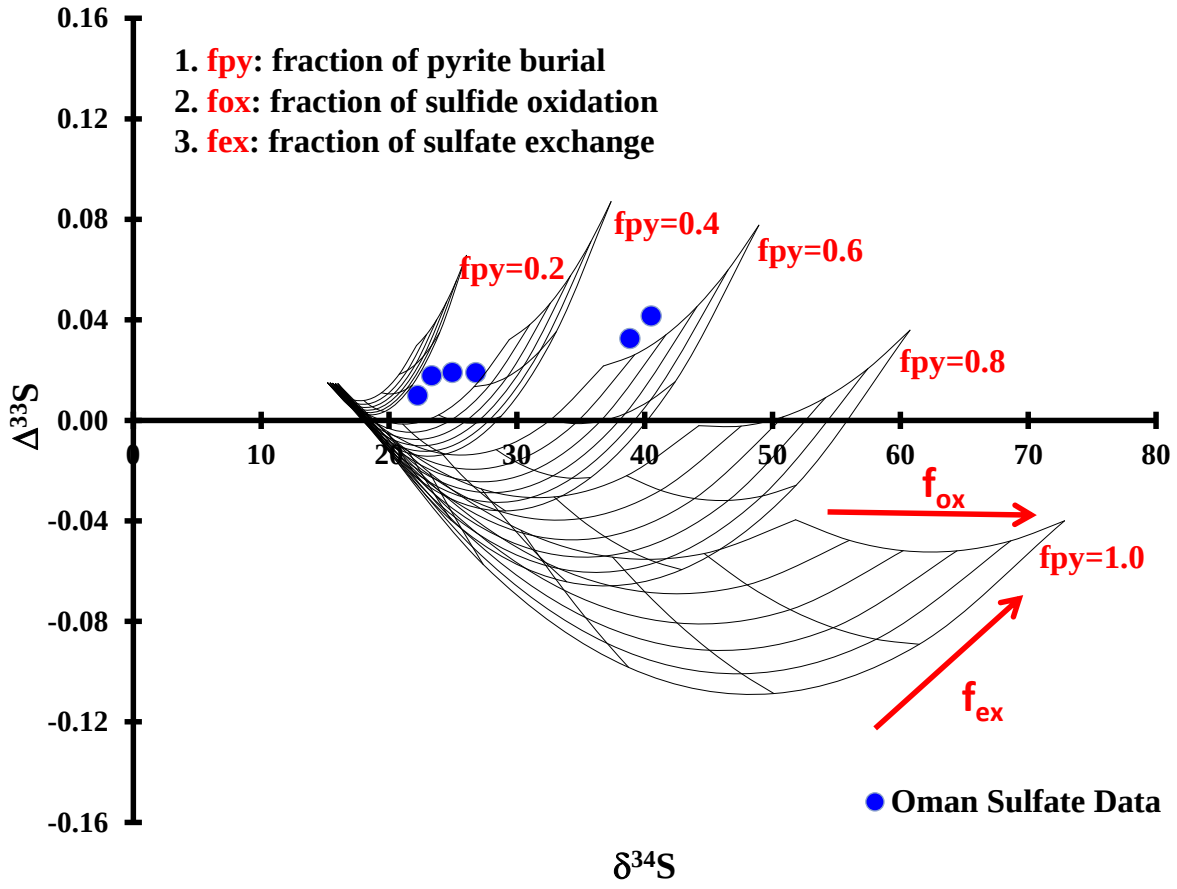

Figure 5.5. The plot shows the calculated field for the oceanic sulfate. For the individual network, the configuration is constrained by three parameters, including the fraction of pyrite burial, fraction of sulfate exchange and fraction of sulfide oxidation. The localities of these networks are primarily controlled by the fraction of pyrite burial. The isotopic compositions of influx of sulfur to the oceans are 15‰ and 0.015‰ for $\delta^{34}S$ and $\Delta^{33}S$, respectively. The blue dots represent the averages of oceanic sulfate for the lumped strata in Table 5.1.

The results (Fig. 5.5) show that changes in the fraction of sulfate exchange (f_{ex}) can cause the same effect as variation on the fraction of pyrite burial (f_{py}) for the $\delta^{34}S$ of oceanic sulfate, but the two parameters generate different signatures for the $\Delta^{33}S$ of oceanic sulfate. The $\Delta^{33}S$ decreases as the f_{py} parameter increases, whereas the $\Delta^{33}S$ has no consistent pattern as the f_{ex} parameter changes. The f_{ox} parameter has the same role in controlling the $\delta^{34}S$ and $\Delta^{33}S$ of seawater sulfate as the f_{ex} parameter in this model simulation.

The f_{py} values (0.2-0.4) for strata between 4200 m and 3224 m derived from this approach are consistent with those values using the common steady state equation. However, these values (0.4-0.6) are inconsistent with the values calculated from the paired $\delta^{34}S$ of pyrite and sulfate, which are generally greater than 1.0 between 3200 m and 2400 m (See Figure 5.4). This discrepancy may imply that the data collected for the pyrite and CAS from the Huqf Supergroup preserve a fractionation that is not representative of the global average. This may also imply that the steady state assumption is not valid. For instance, if there were changes in sulfate concentrations in parallel with the isotopic changes, the data can be alternatively explained using a different model (see section 5.5.5).

The model results shown here are difficult to use in evaluating any long term trend of changes in the fraction of sulfide oxidation and the fraction of sulfate exchange during the latest Neoproterozoic in the Oman basin. The results also indicate that the prescribed fractionation factor between product sulfate and reactant sulfide should be greater than 1.0 in order to contain the isotopic data from Oman basins. This implies that a mechanism other than the direct oxidation of sulfide is involved in regulating sulfur cycling and production of large sulfur isotope fractionations.

The compositions of sulfur that fluxed into the oceans are estimated using data for fractionations involving $^{34}S/^{32}S$ and $^{33}S/^{32}S$. This is done to evaluate the existing hypothesis that suggests the isotopic records of the latest Neoproterozoic changed as a result of a change in the isotopic compositions of sulfur that has fluxed into the oceans. $\Delta^{33}S$ of influx sulfur to the oceans can be estimated using the steady-state coupled equations (Eq. 5.2), the estimated global average fractionation (approximately 25‰) during the latest Neoproterozoic, and global averages of f_{py}

(0.2 to 0.4) between 4200 m and 3200m, and global averages of f_{py} (0.4 to 0.6) between 3200 m to 2400 m inferred from graphic presentation in Figure 5.5. The results are shown in Figure 5.6.

Estimates of $\delta^{34}S$ and $\Delta^{33}S$ of influx sulfur to the oceans for the lower sedimentary sequences (4200 m to 3200 m) are approximately between 7‰ and 19‰, and between 0.004‰ and 0.022‰, respectively. Estimates of $\delta^{34}S$ and $\Delta^{33}S$ of influx sulfur to the oceans for the upper sedimentary sequences (3200 m to 2400 m) made the same approach are approximately between 23.0‰ and 32.0‰, and between 0.027‰ and 0.045‰, respectively.

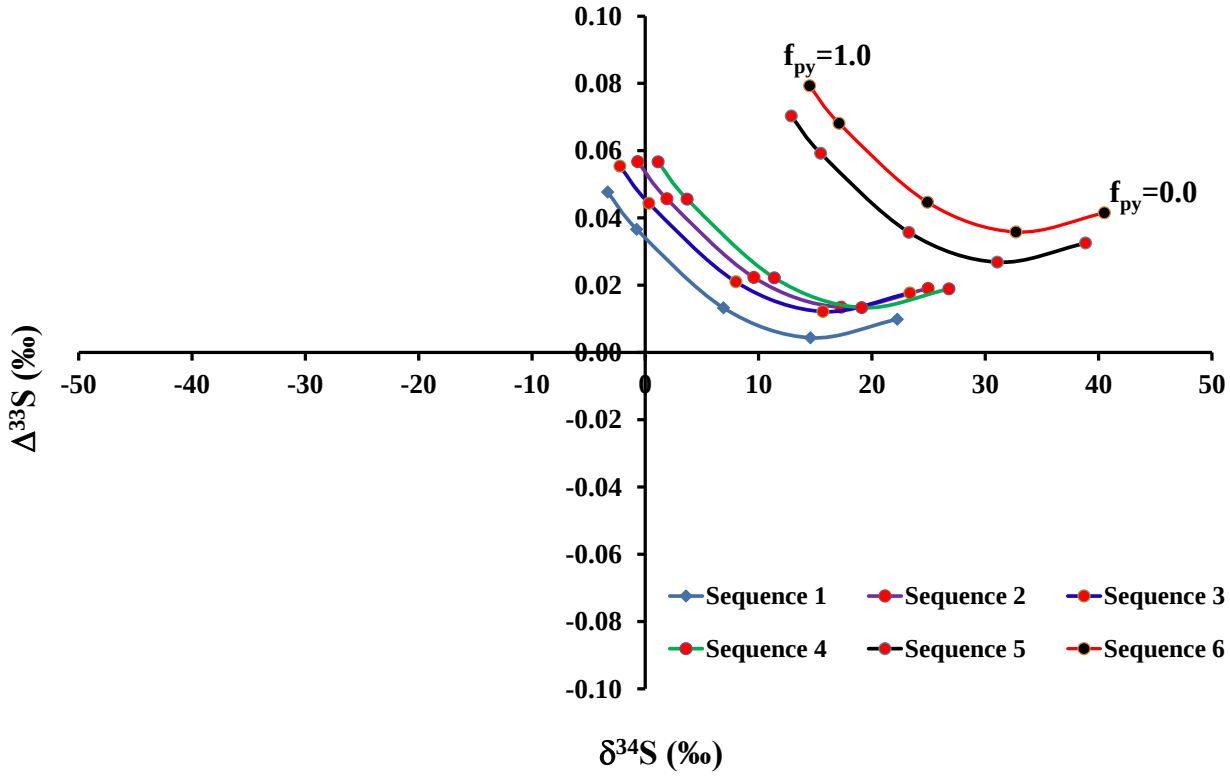

Figure 5.6. The graph shows the estimates of $\delta^{34}S$ and $\Delta^{33}S$ of influx sulfur to the oceans during the latest Neoproterozoic determined by steady state equations of 5.2. The individual lines are estimates for different stages within the Huqf Supergroup with different with fraction of pyrite burial between 0 and 1 represented by the points within each line.

These estimates may imply that the isotopic composition of sulfur sources to the oceans may change from lower to higher values during the Ediacaran Period. It also implies that the isotopic data from the lower sedimentary sequences in the Oman basin can be interpreted in the framework of a global sulfur cycle, and those values can be viewed as global averages that represent the buried pyrite-sulfur isotopes that conserve the isotope mass balance.

Two mechanisms have been suggested to generate the high values of $\delta^{34}S$ for influx sulfur to oceans during the latest Neoproterozoic. A prolonged subduction of ^{32}S-enriched pyrite into deep Earth during Proterozoic has been proposed and the sulfur on Earth's surface generally should enrich ^{34}S sulfur, and hence the influx sulfur to the oceans derived from weathered pyrite and evaporate minerals is expected to carry enriched ^{34}S sulfur (Canfield, 2004). Another way to increase the $\delta^{34}S$ for influx sulfur is through the rapid cycling of younger sedimentary deposits (newly formed pyrite and evaporite minerals) and preferential weathering of evaporite minerals (Berner, 2006).

However, one inference with the Canfield (2004) model is that $\Delta^{33}S$ of Earth's surface sulfur pool experienced a long term depleted trend along with an increase in $\delta^{34}S$ since ~2.0Ga. The sulfur influx to the oceans is mostly a combination of weathered pyrite and evaporite minerals. Evidence from the Proterozoic pyrite suggests positive $\delta^{34}S$ is associated with negative $\Delta^{33}S$ (Johnston et al., 2006) that may represent the sulfur isotopic compositions of influx to the oceans when oceanic sulfate was low and burial of pyrite was the dominant sink in the surface sulfur cycle. The effect of binary mixing on $\Delta^{33}S$ of influx sulfur to the oceans is balanced by the fraction of pyrite weathered. The $\Delta^{33}S$ of buried pyrite during the Proterozoic may cause a general decreasing trend in the global average value of $\Delta^{33}S$ of influx sulfur to oceans. This is

inconsistent with high and positive values of $\Delta^{33}S$ for the upper sedimentary sequences in the Oman basin.

Alternatively, the Oman basins may have been connected with the open ocean during the late Ediacaran Period, and sulfate from the open ocean is possibly the primary influx of sulfur to the Oman basin. The Oman basin may have experienced intermittent closure, and the formation of evaporite minerals may have become a more important pathway for removal of sulfur from the Oman basin. The distillation and drawdown in sulfate concentration thus regulated the sulfur isotopic compositions of sulfate, and this may have been the primary driver for the observed isotopic data of sulfate and pyrite from the upper sequence of Huqf Supergroup. Distillation and drawdown of sulfate concentrations in the Oman basin would be a non-steady state process. It has been shown that distillation trends result in a higher $\Delta^{33}S$ (Johnston et al., 2005). The wide occurrence of evaporite deposits in the Oman basin during this short time interval may also indicate local drawdown of sulfate. Drawdown of sulfate may reflect closure of the Oman basin or a process that drawdown in a basin with a limited but not completely cutoff communication with the open ocean. This scenario requires a non-steady state sulfur cycle model which is examined in the next section (5.5.5).

5.5.5 Using non-steady state model to study the sulfur cycle in the Oman basin

Heterogeneous distributions of sulfur isotopes of sedimentary pyrite have been observed along the modern continental shelf and slope (Vokov and Rozanov, 1983). This heterogeneity may be linked to factors that influence the sulfur cycle, including the openness of the sediments, organic carbon cycling, and the intensity of vertical bioturbation. The processes that generate this type of heterogeneous distribution may also be relevant to other settings such as the Oman basin, and the

sulfur isotope records of pyrite from the Ara Formation may not reflect the average isotopic composition of buried pyrite on a global scale.

Starting with the context of a basinal control on sulfur isotopes, non-steady state modeling of the sulfur cycle is used to study the evolution of oceanic sulfate concentrations and sulfur isotopic compositions of sulfate. The non-steady state model is initialized at steady state and the simulation is forced by the imbalance between sulfur transfer into and out of the oceans. The simulation results provide a framework to interpret the first-order characteristic of the observed sulfur isotopic records and to evaluate those factors that influence the sulfur isotopes of sulfate and pyrite.

This model is used to study the possible response of $\delta^{34}S$ and $\Delta^{33}S$ as well as sulfate concentrations to changes in the intensity of sulfide reoxidation. The model is initialized for 10 million years in order to establish steady state. Following initialization, the model is forced to two stages: first by enhancing sulfide reoxidation to the level seen today and then by returning the sulfide reoxidation to its initial level. The inputs and calibrated values are from Canfield and Farquhar (2009), and the rate of microbial sulfate reduction is thought to be dependent on sulfate levels, but follows exponential functions with a value of 0.30 (also used in Canfield and Farquhar 2009). The exponential function with exponential value 0.30 is thought to mostly fit with results that studied the relationship between sulfate reduction and the sulfate levels (Canfield and Farquhar, 2009, Habitch et al., 2002).

The simulation results are used to illustrate the way that factors in the sulfur cycle control the coevolution of sulfate concentration and sulfur isotopes. The model results provide a first order context for evaluating the variations in sulfate levels and sulfur isotopes of the Oman basin. The

uncertainty associated with the simulation is primarily controlled by the exponential values mentioned above. Here, only one case of modeled evolutionary trajectories of oceanic sulfate levels and its sulfur isotopes is shown in Figure 5.7A and Figure 5.7B

As the intensity of sulfide reoxidation increases, the sulfate levels (red line) increase to a magnitude that is limited by the exponential value. Sulfate concentrations (blue line) reach a maximum magnitude that is established and controlled due to the formation of evaporite sulfate minerals. Sulfate concentrations (purple line) dramatically drop in a short time period as intensity of sulfide reoxidation is weakened (Figure 5.7A). The coevolution of $\delta^{34}S$ and $\Delta^{33}S$ at different simulation stages is shown in Figure 5.7B.

The isotope data from lower sequence in Oman basin (4200 m to 3200 m) are clustered at values (~25‰ of $\delta^{34}S$ and ~ 0.010‰ of $\Delta^{33}S$) and show a dramatic positive shift to values (~40‰ of $\delta^{34}S$ and ~ 0.040‰ of $\Delta^{33}S$) over a very short interval period. In the simulated sulfur cycle, $\delta^{34}S$ and $\Delta^{33}S$ show a dramatic positive shift between the 3rd and 4th stages. However, the simulation results are not set to fit the observed data, considering that there is no unique combination of variables in the simulated sulfur cycle to reproduce the observation. Given this context, the data from the Oman basin may imply that a change in the intensity of sulfide reoxidation occurs either due to weakening of vertical bioturbation or weakening of other physical processes that involve in mixing of marine sediments. It also implies that the sulfate levels drop at this transition, and significant deposition of evaporite sulfate minerals occurred at this time (Fike and Grotzinger, 2008).

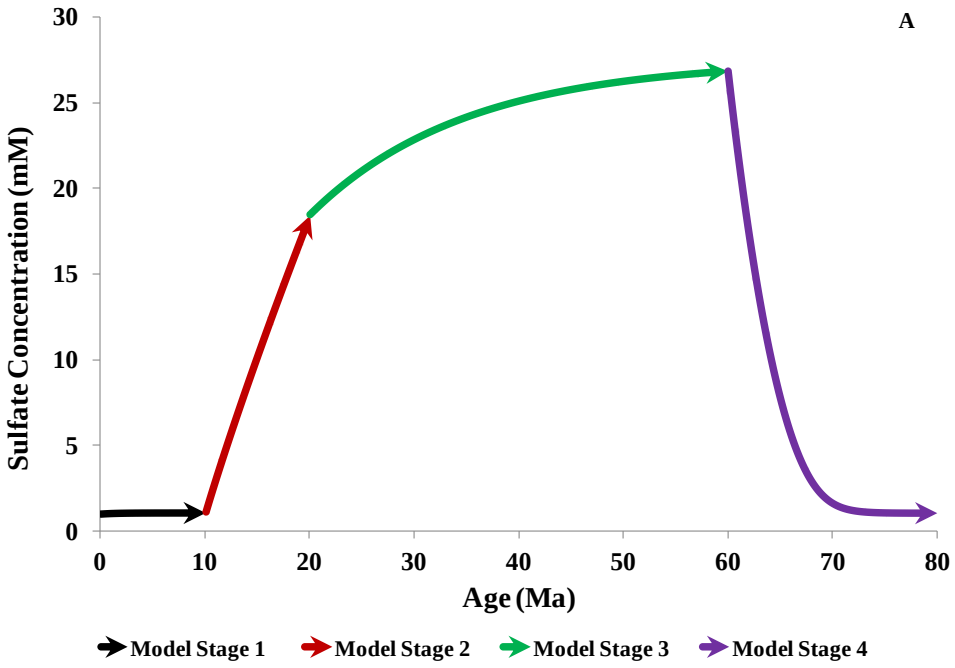

Figure 5.7A. The lines of different color represent the sulfate levels in response to the change in intensity of sulfide reoxidation at different stages in the model

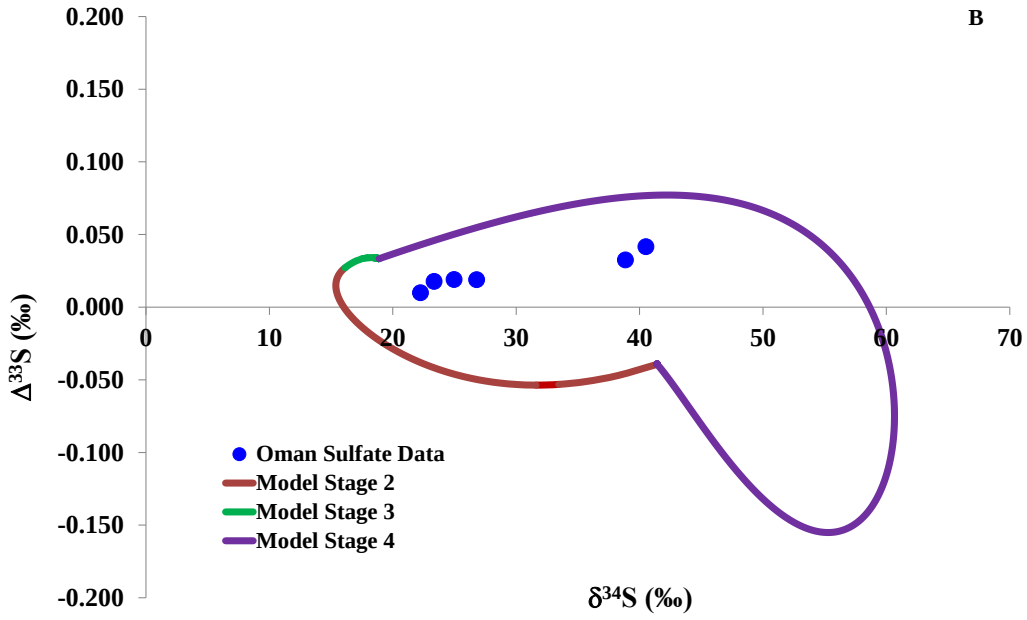

Figure 5.7B. The lines of different color represent the evolution of isotopic composition of oceanic sulfate in response to the change in intensity of sulfide-reoxidation at different model stages. The blue dots present the averages for different sedimentary sequence in Oman basin (refer to Table5.4 and Figure 5.4).

5.6 Summary

Multiple sulfur isotopes ($\Delta^{33}S$ and $\delta^{34}S$) of carbonate associated sulfate (CAS) and sedimentary pyrite from the Huqf Supergroup in Oman are presented here. These data are evaluated in the context of oceanic sulfur cycle models under both steady state and non-steady state conditions. These models have been designed to evaluate the first order observations of these new sulfur isotopic data.

The steady state model suggests that pyrite data from upper parts of Huqf Supergroup are not representative of the global pool of buried pyrite. They may imply that the isotopic compositions of sulfur flux to the Oman basin changed from values with low $\delta^{34}S$ and near zero $\Delta^{33}S$ to values with higher $\delta^{34}S$ and more positive $\Delta^{33}S$ during the latest Neoproterozoic. The origin of the $\delta^{34}S$ and $\Delta^{33}S$ in sulfate may reflect a change to a greater weathering of evaporite minerals, or to a different $\delta^{34}S$ and $\Delta^{33}S$ enriched source, such as an oceanic sulfate pool that fed the Oman basin. It also may imply the isotopic compositions of sulfate in the Oman basin evolved independently of the greater oceanic sulfate pool reflecting partial closure.

The inferences from the non-steady state simulation also suggest that the weakening of sulfide reoxidation can produce a large positive shift in both $\delta^{34}S$ and $\Delta^{33}S$ and drawdown in sulfate levels. The $\Delta^{33}S$ data from the upper sequences of the Oman basin (Ara Formation) is tracked by the general trajectories of the simulation, which with existing models argue for connections between sulfur isotope fractionations, sulfate concentrations, and sulfide reoxidation.The modeled results and the data presented here thus suggest the sulfur cycle in the Oman basin firstly behaviored like a status that was similar to the global sulfur cycle at the time sediments of lower strata of Huqf Supergroup were deposited. The sulfur cycle then evolved to a sulfur cycle

that was disconnected or partially was disconnected from the open ocean sulfur cycle and recorded dynamics that were more specific to the Oman basin.

Chapter 6: $\delta^{34}S$ and $\Delta^{33}S$ records of Phanerozoic seawater sulfate and the sulfur isotope fractionation associated with Phanerozoic pyrite burial[1]

Abstract: This chapter presents a new temporal record of $\delta^{34}S$ and $\Delta^{33}S$ of Paleozoic and Ediacaran seawater sulfate, based on data from carbonate associated sulfate (CAS). Additional data included in the analysis is from Cenozoic marine barites. Long term variations in $\delta^{34}S$ and $\Delta^{33}S$ are clearly discernible, and high frequency variations are also observed. These isotopic records are used to calibrate an important parameter in the global sulfur cycle, the sulfur isotope fractionation ($^{34}\alpha$) between oceanic sulfate and coeval sedimentary pyrite throughout the Phanerozoic. The calibrated sulfur isotope fractionation between sulfate and pyrite appears to have varied widely, between 25‰ to 40‰ over the course of Phanerozoic. For the earlier part of Phanerozoic, the values of sulfur isotope fractionation are approximately 35‰. The fractionation then decreases to 25‰ in the Carboniferous. Following this, the sulfur isotope fractionations progressively increase, reaching approximately 40‰ during the Cenozoic. The change in the magnitude of sulfur isotope fractionations with time is interpreted to reflect a systematic change in the role of sulfur reoxidation and sulfur disproportionation in cycling of sulfur over the course of Phanerozoic.

6.1 Introduction

Sulfur has four stable isotopes ^{32}S, ^{33}S, ^{34}S and ^{36}S, and there are three isotopic ratios ($\delta^{34}S$, $\Delta^{33}S$ and $\Delta^{36}S$) that can be determined and used as a diagnostic tool for deciphering the evolution of the sulfur cycle throughout geologic time (Farquhar et al., 2000; Farquhar and Wing 2003; Johnston et al., 2005; Johnston et al., 2006; Ono et al., 2006; Johnston 2011). Studies have been carried out to characterize and to interpret the long term sulfur isotopic compisitions ($\delta^{34}S$) of oceanic sulfate, using proxies for ancient oceanic sulfate, including evaporite minerals, carbonate associated sulfate, and marine barite (Claypool et al., 1980, Paytan et al., 1998, 2004, Kampschulte and Strauss, 2004, Gill et al., 2007). The variations of sulfur isotopic compositions of seawater sulfate may reflect the isotope mass balance associated with sulfur fluxes into and

---

Significant part of this chapter has been published as **Wu, N.**, et al., 2010. But the text is modified from this published paper, including new data and new analysis.

out of the oceans. Changes in sulfur fluxes are thought to be linked with the related paleo-environmental variability (Garrels and Lerman 1984, Berner, 1987).

The fluctuations of sulfur isotopic compositions of seawater sulfate are generally considered to be regulated by the fraction of pyrite burial because the large magnitude of sulfur isotope fractionation between oceanic sulfate and burial pyrite ($\Delta^{34}S_{SW\text{-}PY} = \delta^{34}S_{SW} - \delta^{34}S_{PY}$) is propagated via mass transfer in the cycling of sulfur (Claypool et al., 1980; Garrels and Lerman, 1981, 1984; Berner and Raiswell, 1983; Berner, 1987, 2006; Kampschulte et al., 2001; Canfield, 2004; Kampschulte and Strauss, 2004). Therefore, calibration of the sulfur isotope fractionation ($\Delta^{34}S_{SW\text{-}PY}$) is an important part of sulfur models and carries implications for the model predictions. Here, two questions are asked. First, *has the sulfur isotope fractionation between oceanic sulfate and coeval pyrite varied significantly over the Phanerozoic*? Second, *if so, what biogeochemical and geological information might those variations provide*?

Several approaches have been used to estimate the magnitude of the sulfur isotope fractionation ($\Delta^{34}S_{SW\text{-}PY}$) associated with pyrite formation and burial over geologic time. These include values constrained using experimental results from laboratory culture experiments with sulfate reducers (e.g., Garrels and Lerman, 1984), values constrained using paired isotopic records of sedimentary pyrite and sulfate (e.g., Strauss, 1999; Canfield, 2004; Kampschulte and Strauss, 2004), and values constrained using assigned relationships between $^{34}S/^{32}S$ and $^{33}S/^{32}S$ for marine sulfate (Ono et al., 2006). Here, sulfur isotopic compositions of sedimentary pyrite and marine sulfate are compiled to constrain a record of $\Delta^{34}S_{SW\text{-}PY}$ over the course of the Phanerozoic. Constraints are also placed on the magnitude of $\Delta^{34}S_{SW\text{-}PY}$ over geologic time by drawing on the $\Delta^{33}S$ of marine sulfate. I also examine how the $\Delta^{34}S_{SW\text{-}PY}$ calibration can be used to estimate the

sulfur sinks with time and to examine implications for the mechanisms that control the magnitude of the sulfur isotope fractionation ($\Delta^{34}S_{SW-PY}$) .

6.2 Results

A subset of the archived extracts of carbonate associated sulfate from the Kampschulte and Strauss (2004) study in the form of barite, have been measured and reported for $\delta^{34}S$ and $\Delta^{33}S$ (Table 6.1). Cambrian samples are from the Kuljumbe section in northwestern Siberia (Ebneth et al., 1994), and Triassic samples are from sections in Italy, Hungary and Slovakia (Korte, 1999). A detailed chemical extraction procedure for carbonate associated sulfate is described in Kampschulte and Strauss (2004). The associated uncertainty is estimated by monitoring measurements of IAEA reference materials and can be found in chapter 4.

Table 6.1 Sulfur isotope data for carbonate associated sulfate

Sample	Age (Ma)	Epoch	Biozone	Locality	$\delta^{34}S$ (‰)	$\Delta^{33}S$ (‰)
Tr49	211.8	Tr3	*Pargvigondolella andrusovi*	Slovakia	19.6	0.037
Tr55	213.3	Tr3	*Mockina bidentata*	Slovakia	19.8	0.009
Tr61	214.7	Tr3	*Mockina Postera*	Slovakia	18.2	0.018
Tr64	218.8	Tr3	*Epigondolella triangularis*	Slovakia	18.8	0.012
Tr75	224.2	Tr3	*Epigondolella pseudodiebeli*	Slovakia	20.0	0.027
Tr77	224.7	Tr3	*Epigondolella nodosa*	Slovakia	19.1	-0.008
Tr150	236.2	Tr2	*Budurovignathus mungoensis*	Hungary	18.0	0.033
Tr239	241.2	Tr1	*Chiosella gondolelloides*	Italy	27.8	0.023
Tr245	241.4	Tr1	*Neospathodus sosioensis*	Italy	27.6	0.038
Tr252	244.4	Tr1	*Neospathodus dieneri*	Italy	17.0	0.041
Tr253	244.8	Tr1	*Hindeodus postparvus*	Italy	17.2	0.038
Tr256	244.9	Tr1	*Isarcicella isarcica*	Italy	24.5	0.066
KKU-71	510.3	Mer	*Dolgeuloma Kaninia*	Sibirian	37.9	-0.001
KKU-57	511.7	Mer	*Dolgeuloma Kaninia*	Sibirian	29.6	-0.007
KKU-53	512.9	Mer	*Kujandaspis*	Sibirian	29.5	-0.023
KKU-43	518.1	Std	*Maspakites Idahoia Raashellina*	Sibirian	35.2	-0.050
KKU-17	557.4	Crf	*Judomia Uktaspis*	Sibirian	31.9	-0.002
KKU-4	561.3	Crf	*Dokidocyathus regularis*	Sibirian	38.6	0.016

The data from Cambrian samples yield a range of $\delta^{34}S$ values from 29.5‰ to 38.6‰. The $\Delta^{33}S$ ranges from -0.050‰ to 0.016‰ and an average of -0.011 ± 0.046‰. An average $\Delta^{33}S$ of -0.006 ± 0.036‰ for Cambrian samples is obtained when combined with data published in Johnston et al. (2005a, b). The data from Triassic samples yield a range of $\delta^{34}S$ value from 17.0‰ to 27.8‰. All Triassic sulfur isotopic data are consistent with this part of the Phanerozoic record (Kampschulte and Strauss, 2004), except three samples, which are Tr239, Tr245, and Tr256. These three data points show higher $\delta^{34}S$ values than are predicted by the evolutionary curve that has been fitted to the data set as a whole. These anomalous values are attributed to a combination of local depositional environment and/or high frequency variations in isotopic compositions. The $\Delta^{33}S$ of Triassic samples yield a range of -0.008‰ to 0.066‰ and an average of 0.028 ± 0.038‰.

6.3 Data Compilation

Evaluation of $\Delta^{34}S_{SW\text{-}PY}$ over the course of Phanerozoic requires knowledge of both $\delta^{34}S_{SW}$ and $\delta^{34}S_{PY}$. Literature data for isotope analyses of marine sulfate and sedimentary pyrite are compiled from various sources (Canfield 2005; Canfield and Farquhar 2009 and used to construct the evolution curves of marine sulfate and sedimentary pyrite.

Since the mixing time scale for oceanic sulfate is short and there exists a buffer effect on sulfur isotopes of seawater sulfate due to its high concentrations over the Phanerozoic (Refer to Chapter 3), the averaging of Phanerozoic $\delta^{34}S_{SW}$ records derived from proxies (e.g. carbonated associated sulfate) is less problematic for constructing a continous isotopic records thant that for pyrite-sulfur isotopes. However, it will require sampling all reduced sulfur (mostly pyrite-sulfur) which is not accessible and practically possible, in order to accurately reconstruct the $\Delta^{34}S_{SW\text{-}PY}$ over the course of Phanerozoic and fluxes among sulfur pools. Global averaging of Phanerozoic $\delta^{34}S_{PY}$

records is more challengable to be solved before a reliable estiamtes of the distributions of reduced sulfur along the ocean basins and a reliable estimates of the abundances of reduced sulfur and their sulfur isotopic compositions over geologic time, and refinement of $\delta^{34}S_{PY}$ records is necessary and recommeneded.

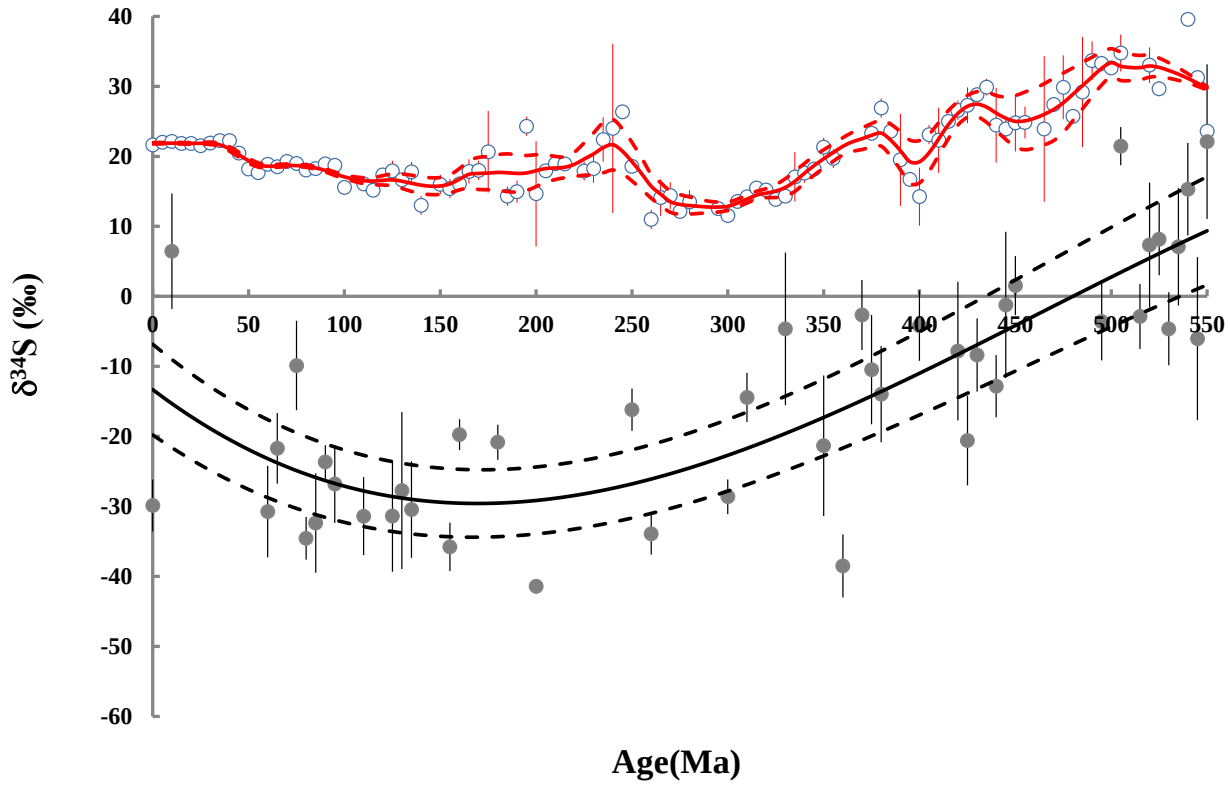

Figure 6.1 Plot of $\delta^{34}S$ versus age for binning groups of marine sulfate dataset (open circle) and marine sulfate fitting curve (red lines), and for binning groups of sedimentary sulfide dataset (gray circle) and sedimentary sulfide fitting curve (black lines). The error bars represent standard error (3σ) of binning groups of data in 5Ma time windows, and dashed lines represent the uncertainties associatied with the fitting method, and these envelopes are dependent on the sampling density.

The geologic time interval examined here is from the latest Neoproterozoic (550Ma) to the Holocene. The sample age and related stratigraphical information are reported in each study. The evolution curves of $\delta^{34}S_{SW}$ and $\delta^{34}S_{PY}$ records are produced using a built-in Sigmaplot inversing smoothing method and built-in Matlab curvilinear regression method for a polynomial of degree

2. The curve of $\delta^{34}S_{SW}$ is considered to preserve the first order features of these isotopic records, though the rapid changing in $\delta^{34}S_{SW}$ may not be recognized in this smoothed curve. In this study, the smoothed curve of $\delta^{34}S_{PY}$ records is thought to be estimates of global averages of buried reduced sulfur over the course of Phanerozoic. The compiling $\delta^{34}S_{PY}$ records also reflects biases from the interests of original studies and from the method of data collection used here, and these imperfections impose the most significant uncertainty associated with the smoothed curve of $\delta^{34}S_{PY}$ records. Althought the imcompleteness exists in this compiling data set, it is my initial step to estimate the continous records of global averages of pyrite-sulfur isotopes.

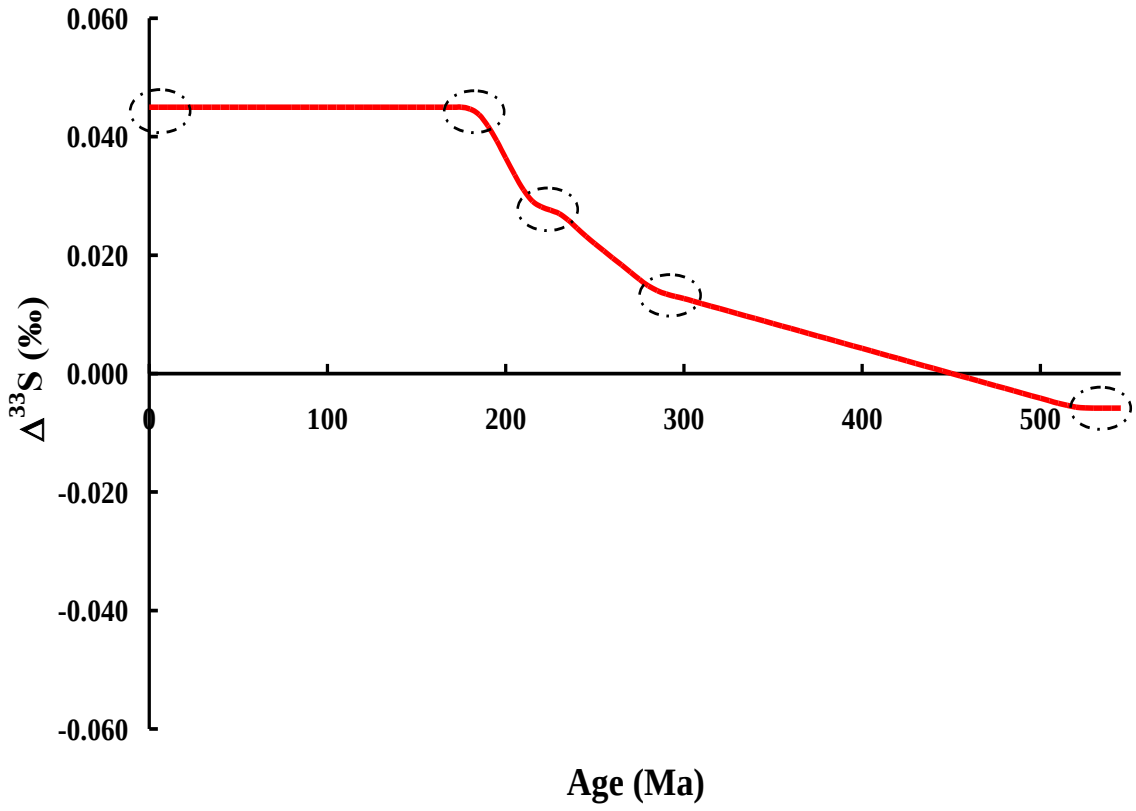

Figure 6.2 Plot of $\Delta^{33}S$ versus age for marine sulfate used by Wu et al., 2010. The circle is the measured data. The red line is the fitting curve of $\Delta^{33}S$ of oceanic sulfate used in calculations. Note that this is our initial step towards the estimates of $\Delta^{33}S$ of oceanic sulfate. The most significant bearing on this record comes from the limit of sampling. Modified from Wu et al, 2010.

Knowledge of $\Delta^{33}S_{SW}$ (Figure. 6.2) throughout the Phanerozoic is estimated from the results of isotope analyses presented in this study, and also from previously published data presented in Johnston et al. (2005a) (Cambrian) and Domagal-Goldman et al. (2008) (Pennsylvanian), as well as in Rouxel et al. (2008) (Jurassic). The $\Delta^{33}S_{SW}$ of modern seawater sulfate is taken to be an average of analyses of IAEA-S2 and NBS-127 (refer to chapter 4), but this value is also similar to a value previously presented in Ono et al. (2006) when corrected for a difference in laboratory calibration of CDT. The evolutionary curve of $\Delta^{33}S_{SW}$ herein is our first estimate on the basis of sparsely sampled isotope analyses, but this is interpreted to be a real feature of $\Delta^{33}S_{SW}$ record over a long time period.

6.4 Discussion

6.4.1 Estimates of $\Delta^{34}S_{SW\text{-}PY}$ using paired $\delta^{34}S_{SW}$ and $\delta^{34}S_{PY}$ isotope records

Figure 6.1 presents the binned isotopic data for marine sulfate and sedimentary sulfide over the course of the Phanerozoic. The difference between $\delta^{34}S$ of marine sulfate and the $\delta^{34}S$ minimum for coeval sedimentary pyrite appears to be a constant (51 ±8‰) throughout the Phanerozoic and has been suggested to be the magnitude of the sulfur isotope fractionation associated with pyrite burial (Strauss, 1999). These high values (~50‰) have also been used in sulfur models (Kampschulte and Strauss, 2004).

Other suggestions have also been made about the magnitude of the sulfur isotope fractionation associated with pyrite burial. It has been proposed that the average value for $\delta^{34}S$ of sedimentary pyrite may be a more representative record of the global averages (Canfield 2004), and that $\Delta^{34}S$ should be assigned to the difference between $\delta^{34}S$ of marine sulfate and the average $\delta^{34}S$ of

coeval sedimentary pyrite: the difference between the regressed lines in figure 6.1. We find that the magnitude of $\Delta^{34}S_{SW\text{-}PY}$ is $43 \pm 3‰$ since approximately 270Ma, and $32 \pm 4‰$ (2σ) in the time interval of 550Ma to 270Ma (Figure 6.3). Figure 6.3 also presents other estimates of $\Delta^{34}S_{SW\text{-}PY}$ used in other studies (Garrels and Lerman, 1981; Kampschulte and Strauss, 2004). These studies assumed a constant value for the sulfur isotope fractionation over the Phanerozoic. Figure 6.3 shows that our estimates are consistent with those by Garrels and Lerma (1981) in the time interval of 550Ma to 250Ma, while our estimates are consistent with those by Strauss (1999) during the Mesozoic. For the Cenozoic, the sulfur isotope fractionations show slightly drops to values of ~ 35‰.

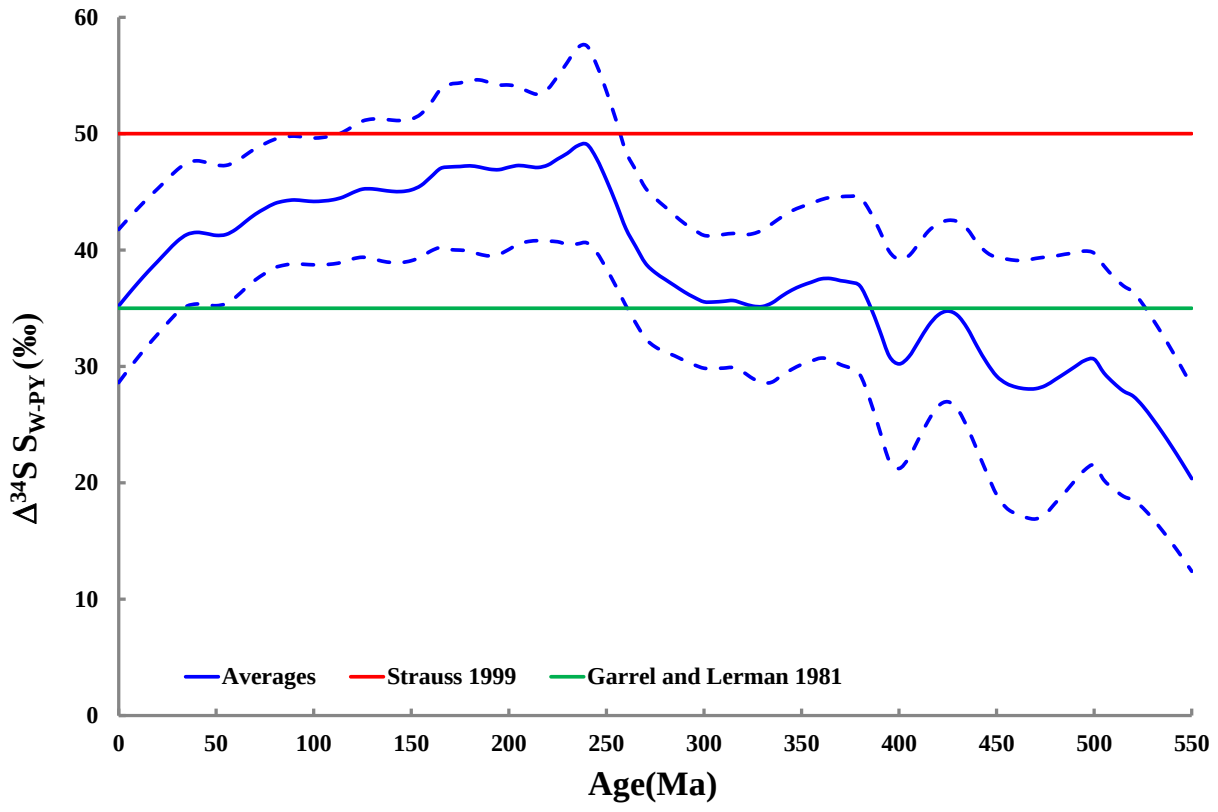

Figure 6.3. Plot of the sulfur isotope fractionation between the seawater sulfate and pyrite ($\Delta^{34}S_{SW\text{-}PY}$) throughout the Phanerozoic. The blue line is the arithmetic difference between $\delta^{34}S$ of oceanic sulfate and $\delta^{34}S$ of coeval pyrite, and the dashed blue lines are the uncertainties (3σ) associated with the data fitting. The red line is the estimate by

Strauss (1999) that assumes a constant fractionation of ~50‰. The green line is used by Garrel and Lerman (1981) for the isotope mass balance model and assumes a constant fractionation of 35‰.

The arithmetic approach implies that the values taken from the regressed curve for $\delta^{34}S$ of sedimentary pyrite are the global averages of the buried pyrite sulfur reservoir and that there are no other major sulfur sinks with large associated sulfur isotope fractionation. However, several other studies (Zaback and Pratt, 1992; Werne et al., 2004; Bottrell and Newton, 2006) have suggested that buried organic sulfur may be an important sulfur sink with large associated sulfur isotope fractionation, which implies that the two component (evaporite sulfate and sedimentary pyrite) un-mixing may not conserve the isotope mass balance. Here, another approach on the basis of $\Delta^{33}S$ and $\delta^{34}S$ of seawater sulfate will be explored to study the sulfur isotope fractionation between oceanic sulfate and pyrite and to identify other possible sulfur sinks taking advantage of the isotope mass balance.

6.4.2 Estimates of $\Delta^{34}S_{SW\text{-}PY}$ using $\Delta^{33}S$ of oceanic sulfate

Ono et al (2006) have argued that $\Delta^{33}S$ and $\delta^{34}S$ of seawater sulfate can be used to determine $\Delta^{33}S$ and the fraction of pyrite burial (f_{py}) on the basis of an assumed relationship between $^{33}S/^{32}S$ and $^{34}S/^{32}S$. This approach is expanded in this study using a system of equations similar to those that have been described elsewhere (Garrels and Lerman, 1981, 1984; Kampschulte and Strauss, 2004) but solved in terms of R ($^{34}S/^{32}S$) and $\alpha_{a\text{-}b}(=R_a/R_b)$ rather than δ and $\Delta_{a\text{-}b}(\delta_a - \delta_a)$.

The standard equation is described the conservation of mass in terms of flux as below:

$$\frac{dM}{dt} = f_{ew} + f_{pw} + f_j - f_{pb} - f_{eb}, \qquad (1)$$

t: time

M: moles of the oceanic dissolved sulfate,

f_{ew} : influx from weathering of evaporites,

f_{pw} :influx from oxidation of sedimentary pyrite,

f_j :influx from juvenile sources (mid-ocean ridge hydrothermal sources, terrestrial volcanics, submarine eruptions)

f_{pb} : out-flux of sulfur lost to burial of pyrite in sediments,

f_{eb} : out-flux of sulfur lost to other sources such as evaporites and carbonate associated sulfate

The equation of the isotope mass balance is described in terms of isotope ratios ($^{34}R_{SW}=^{34}M/^{32}M=^{34}S/^{32}S$) as below:

$$\frac{d\left({}^{34}R_{SW}\,{}^{32}M\right)}{dt} = {}^{32}f_{ew}\,{}^{34}R_{ew} + {}^{32}f_{pw}\,{}^{34}R_{pw} + {}^{32}f_{j}\,{}^{34}R_{j} - {}^{32}f_{pb}\,{}^{34}R_{pb} - {}^{32}f_{eb}\,{}^{34}R_{eb}\,. \quad (2)$$

Where $^{34}R_{sw}$ is the sulfur isotopic composition of dissolved sulfate and $^{34}R_{ew,}\ ^{34}R_{pw,}\ ^{34}R_{j,}\ ^{34}R_{pb}$ and $^{34}R_{eb}$ represent the isotopic ratios of sulfur associated with the fluxes entering and leaving the oceanic sulfate pool. $^{32}f_{ew}$, $^{32}f_{pw}$, $^{32}f_{j}$, $^{32}f_{pb}$, $^{32}f_{eb}$ represent the ^{32}S fluxes into and out of the oceans.

The mass balance and isotope balance equations can be combined using:

$$\frac{d\left({}^{34}R_{SW}\,{}^{32}M\right)}{dt} = {}^{32}M\,\frac{d\left({}^{34}R_{SW}\right)}{dt} + {}^{34}R_{SW}\,\frac{d\left({}^{32}M\right)}{dt},\ \alpha = \frac{{}^{34}R_{pb}}{{}^{34}R_{SW}},$$

and noting $^{34}R_{eb=}\ ^{34}R_{sw}$, to yield:

$$^{32}M\,\frac{d\left({}^{34}R_{SW}\right)}{dt} = \left(\sum {}^{32}f_{n}\left({}^{34}R_{n} - {}^{34}R_{SW}\right)\right) - {}^{32}f_{pb}\,{}^{34}R_{SW}\left(\alpha - 1\right) \quad (3)$$

where the subscript *n* refers to the input fluxes (*ew*, *pw*, *and j*). Similar equations can be written for ${}^{33}R={}^{33}M/{}^{32}M$ using ${}^{33}\alpha = \alpha^{\,{}^{33}\lambda}$, e.g.,

$$ {}^{32}M\,\frac{d({}^{33}R_{SW})}{dt} = \left(\sum {}^{32}f_n\left({}^{33}R_n - {}^{33}R_{SW}\right)\right) - {}^{32}f_{pb}\,{}^{33}R_{SW}\left(\alpha^{\lambda}-1\right) \qquad (4) $$

These equations can then be combined to yield:

$$ \frac{\left(\alpha^{\,{}^{33}\lambda}-1\right)}{(\alpha-1)} = \frac{{}^{34}R_{SW}\left(\frac{d({}^{33}R_{SW})}{dt} - \frac{\left(\sum {}^{32}f_n\left({}^{33}R_n - {}^{33}R_{SW}\right)\right)}{{}^{32}M}\right)}{{}^{33}R_{SW}\left(\frac{d({}^{34}R_{SW})}{dt} - \frac{\left(\sum {}^{32}f_n\left({}^{34}R_n - {}^{34}R_{SW}\right)\right)}{{}^{32}M}\right)}, \qquad (5) $$

The solution of this equation requires a number of constraints on fluxes, isotopic compositions associated with the fluxes and on the isotopic composition of oceanic sulfate .

For calculations presented below, the mass of the seawater sulfate pool over the course of the Phanerozoic was estimated by Lowenstein et al (2003). The flux of juvenile sulfur (f_j) was set to ~ 5.0×10^{11} mol/yr (present-day flux, Canfield, 2004) and its magnitude is set to be proportional to the normalized amount of crust production (Gaffin, 1987) during geologic time. For the parameterization of evaporite weathering and pyrite weathering, values are used that are similar to those used by Kampschulte and Strauss (2004)

The isotopic compositions of seawater sulfate (R_{sw} and $d(R_{sw})/dt$) are derived from the curves described in figure 6.1 and figure 6.2. The isotopic compositions of weathering products ($\delta^{34}S_{ew}$, $\Delta^{33}S_{ew}$, and $\delta^{34}S_{pw}$) are also derived from these curves using reasoning similar to that presented in Berner (1987). The $\Delta^{33}S_{pw}$ was estimated using an empirical relationship ($\Delta^{33}S_{pw}$ = -0.00221 $\delta^{34}S_{pw}$ + 0.0449) that was derived by regression of published and unpublished data for

sulfides (Johnston et al., 2005a, 2006, 2008; Farquhar et al., 2008). For juvenile sulfur, $\delta^{34}S$ is set at 2‰, which is chosen to match values used by Kampschulte and Strauss (2004). $\Delta^{33}S$ is set at 0‰, assuming the composition of juvenile sulfur is similar to CDT.

We can see that Eq. (5) describes a relationship between $\Delta^{34}S_{SW\text{-}PY}$, $^{33}\lambda$, the sulfur influxes and their associated isotopic compositions. This equation can be used in several ways with different assumptions and constraints on the parameters. Ono et al. (2006) used an equation like this one to calibrate the $\Delta^{34}S$ values by assuming a range of $^{33}\lambda$ values. One also can use the observed $\Delta^{34}S_{SW\text{-}PY}$ to place limits on $^{33}\lambda$; or if another relationship can be found between $\Delta^{34}S_{SW\text{-}PY}$ and $^{33}\lambda$ which will be discussed in the following text.

Recent studies have examined the relationship between $^{34}S/^{32}S$ and $^{33}S/^{32}S$ for sulfate-reducing, sulfur-disproportionating, and sulfide oxidizing bacteria (Farquhar et al., 2003, 2007, 2008; Johnston et al., 2005a,b, 2007, 2008; Zerkle et al., 2009). The results of these studies can be used to calibrate a relationship that describes the way that α and $^{33}\lambda$ may covary in the sulfur cycle. This approach is also extended to the sulfur cycle at global scale similar to the flow network method discussed in Hayes et al (2001).

The isotopic composition of any sulfur pool in the network is controlled by the flow of sulfur into and out of the sulfur pool, the isotope effects associated with sulfur transformations from pool to pool, and the isotopic composition of the upstream sulfur pool. By solving for the fractionation between the sulfate and pyrite as a function of the proportions of sulfur reduced directly to pyrite and of sulfide oxidized and disproportionated, the equation that describes this relationship is obtained:

$$\frac{R_{sw}}{R_{py}} = \frac{\left[(1 - f_{reox} - f_{dis} \times (1 - f_6)) + \alpha_{reox-interm} \times f_{dis} + \alpha_{reox} \times f_{reox} - \alpha_{reox-interm} \times \frac{f_{dis} \times f_6}{\alpha_{dis} \times (1 - f_6) + f_6}\right]}{\alpha_{sr}} \quad (6)$$

Where α_{disp} is the fractionation factor associated with disproportionation, α_{sr} is the fractionation factor associated with sulfate reduction, α_{reox} is the fractionation factor associated with oxidation of sulfide to sulfate and $\alpha_{reox\text{-}interm}$ is the fractionation factor associated with oxidation of sulfide to sulfur intermediate compounds. The terms f_{reox} and f_{disp} are the fractions of ^{32}S in the sulfide pool that are directly reoxidized to sulfate, and the fraction of the reoxidized ^{32}S that is subject to disproportionation. The experimental results from available sulfate reduction data (except those for the thermophile Archaeoglobus fulgidus), sulfur disproportionation data, and sulfide oxidation data (Johnston et al., 2005a, b, 2007; Farquhar et al., 2008; Zerkle et al., 2009) are used to define a field of fractionations between sulfate and buried pyrite as a function of the fraction of sulfide that is reoxidized and disproportionated.

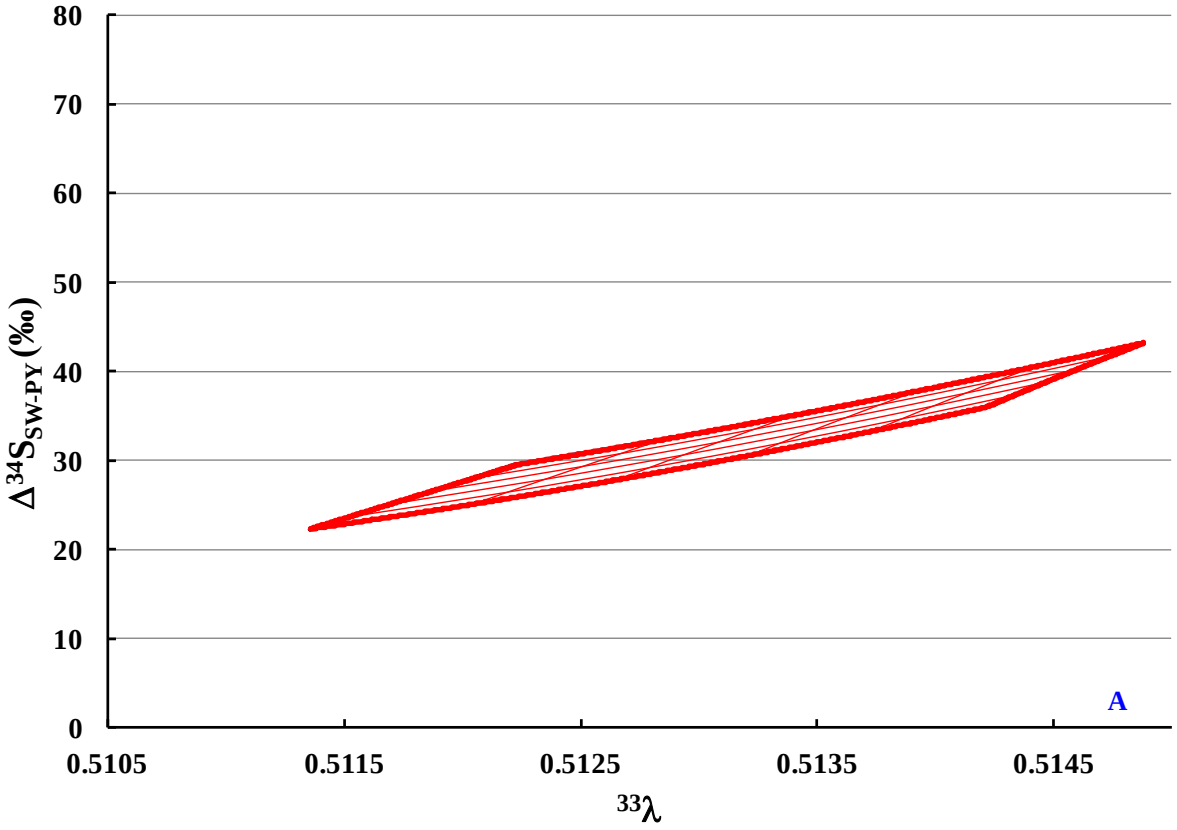

Figure 6.4A. Plot of $\Delta^{34}S_{SW-PY}$ and $^{33}\lambda$ with outlines of the field using a sulfur model similar to that used in Johnston et al., 2005. This field is calibrated with fractionations measured in laboratory culture experiments (Farquhar et al.,2003; Johnston et al., 2005b, 2007). The red lines are results of by varying the proportion of sulfide reoxidation and sulfur disproportionation.

A representative plot that assumes a single set of sulfur isotope fractionations (average values of the experiments with sulfate reducers, elemental sulfur disproportionators, and fractionations for sulfide oxidation) is presented in Figure 6.4A. For this plot, the role of disproportionation increases moving toward the upper right hand side of the field.

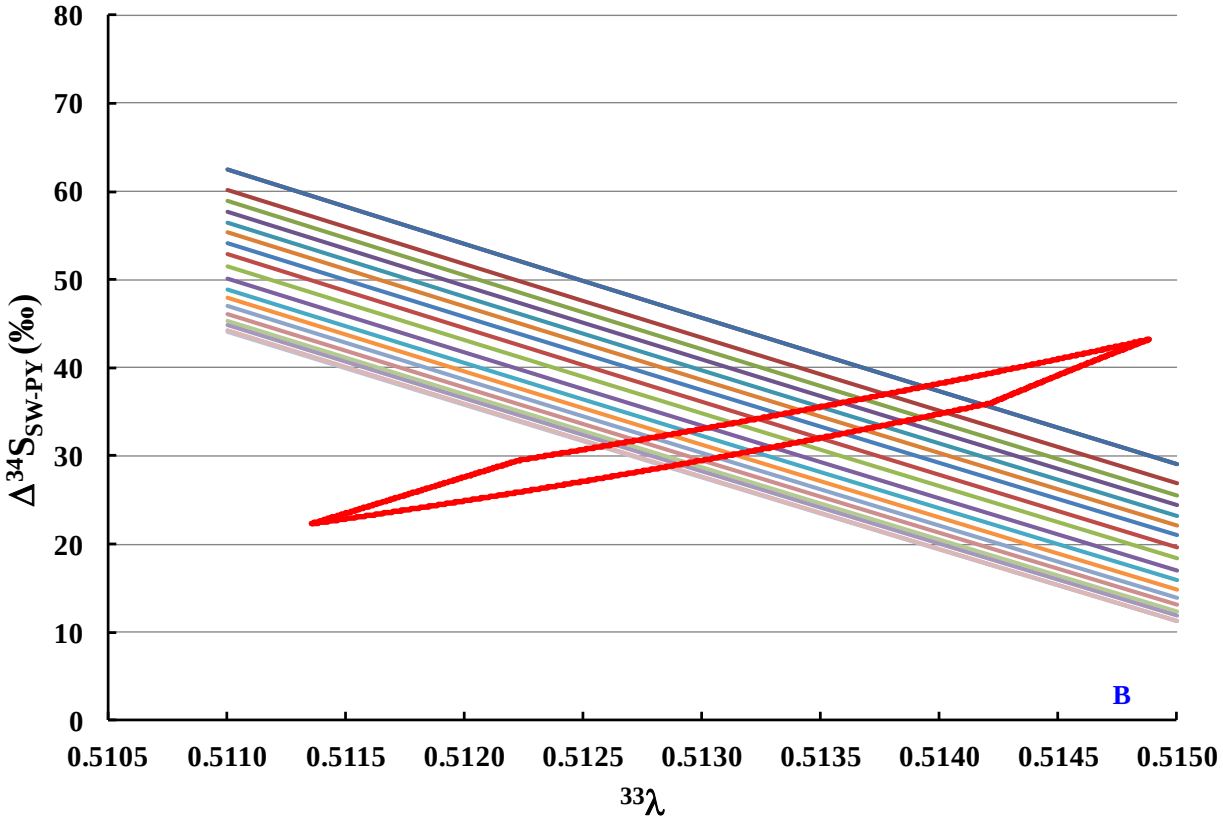

Figure 6.4B. The plot shows the intersection of results of model calculations using Eq. (5) and calculations of the relationship (Eq.(6)) between $\Delta^{34}S_{SW\text{-}PY}$ and $^{33}\lambda$ in Figure 6.4A (red field). The colored lines represent the solutions that satisfy the sulfur model described by Eq. (5), and each line is a snap short of every 5 Ma over the Phanerzoic.

The covariation between $\Delta^{34}S_{SW\text{-}PY}$ and $^{33}\lambda$ with time provided by Eq. (5) trend from the lower right to upper left of the predicted field in Fig. 6.4B. The intersections of these solutions represent the collection of solutions that satisfy the sulfur cycle of Eq. (5) and Eq. (6). These results also support a change in the fractionation associated with pyrite burial between 200Mya and 300 Mya and are consistent with an increase in the $\Delta^{34}S_{SW\text{-}PY}$ and/or $^{33}\lambda$ associated with pyrite burial and with an increase with time in the proportion of sulfur cycled through disproportionation (Johnston et al., 2005a, 2006).

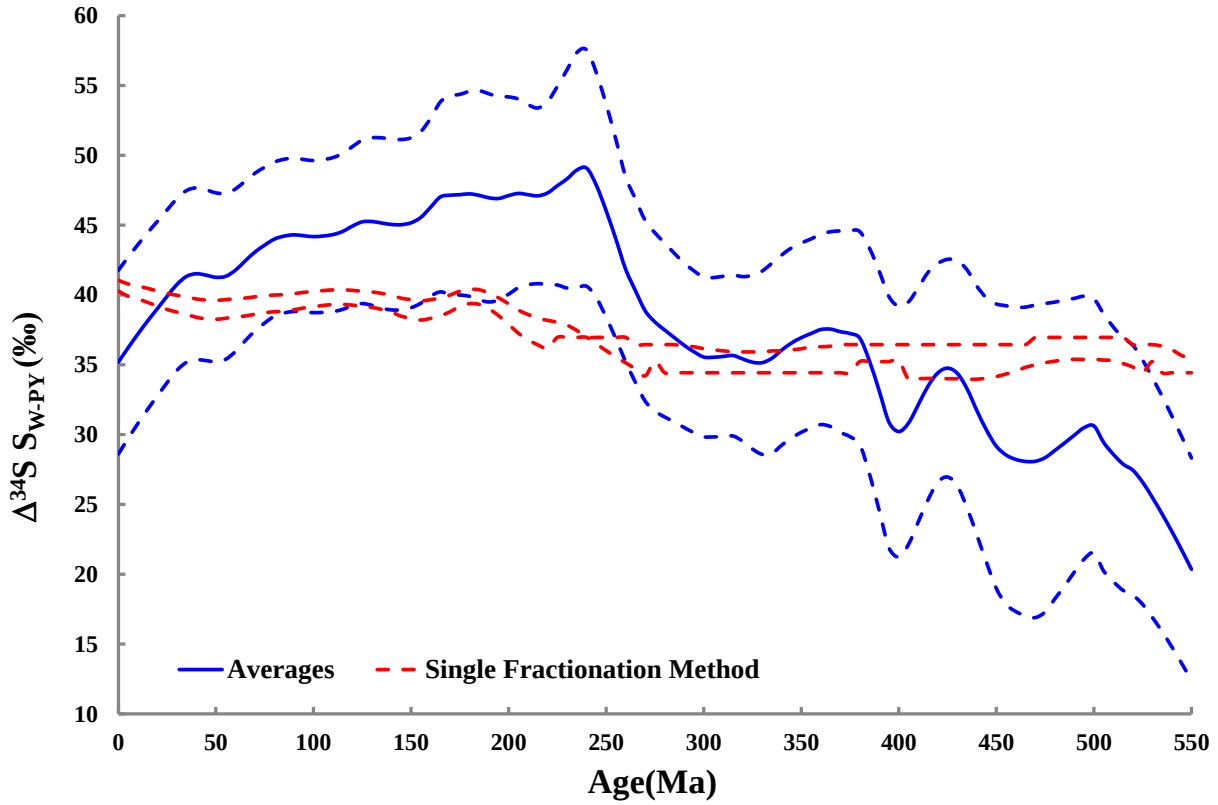

Figure 6.5. Plots of $\Delta^{34}S$ versus age. The field between the ed dash lines represents the intersection of results of model calculations using Eq. (5) and calculations of the relationship using Eq. (6). blue lines are solutions using the arithmetic difference between $\Delta^{34}S_{SW\text{-}PY}$ of sulfate and coeval pyrite (see figure 6.3).

Figure. 6.5 shows the variation of $\Delta^{34}S_{SW\text{-}PY}$ with geologic time for the results of the arithmetic difference method and the results derived from the single set of sulfur biological fractionations. The range in results arises mostly from the proportion of sulfur cycled through disproportionation at any time point. This figure also illustrates common features of all of these solutions. All are consistent with a change in the values of $\Delta^{34}S_{SW\text{-}PY}$ from lower values in the early Phanerozoic and higher values since about 200 million years ago. All of these results imply a fundamental change in the way that sulfur isotopes were fractionated in the sulfur cycle. Average values for $\Delta^{34}S$ provided by these models suggest a change in the magnitude of $\Delta^{34}S_{SW\text{-}PY}$ from values of approximately 35±1‰ in the Paleozoic to values of approximately 40±1‰

since 200 million years ago. It is not clear which evolution of $\Delta^{34}S_{SW\text{-}PY}$ is closer to captureing the true nature of the variations

There is a discrepancy between the estimates of $\Delta^{34}S_{SW\text{-}PY}$ evolution through geologic time made using these two approaches (arithmetic difference between $\delta^{34}S$ of sulfate and coeval pyrite versus method based on $\Delta^{33}S$ of oceanic sulfate). The values of $\Delta^{34}S_{SW\text{-}PY}$ are lower than those estimated on the basis of $\Delta^{33}S$ of oceanic sulfate in the time interval of 300-545Ma, but higher since 270Ma. The apparent discrepancy may arise from inaccuracy associated with reconstruction of the sulfur isotopic records of sedimentary pyrite. It is not clear whether the measurements used to constrain the global average composition for pyrite sulfur are sufficient for this purpose. If there are significant biases in sampling of sedimentary pyrite, adjustment to the $\Delta^{34}S_{SW\text{-}PY}$ throughout time will result. The same considerations also apply to the approach that uses the $\delta^{34}S$ and $\Delta^{33}S$ of oceanic sulfate where the underlying assumptions, including those about averages of fractionations associated with sulfate reduction, sulfide reoxidation and sulfur disproportionation, are also made in this approach. The data set for $\Delta^{33}S$ of oceanic sulfate is also small. In spite of these uncertainties, both methods show generally the same form and would suggest the changes in $\Delta^{34}S_{SW\text{-}PY}$ and potentially in the fractionation involving ^{33}S associated pyrite burial. These models are relatively simple and do not include organic sulfur burial. Future work should focus on this.

6.5 $\Delta^{33}S$ record of the Phanerozoic seawater sulfate

Since the first analysis we did on this topic about the long term variation in sulfur isotope fractionation ($\Delta^{34}S_{SW\text{-}PY}$) over the course of the Phanerozoic (Wu et al., 2010), new sulfur

isotope data ($\Delta^{33}S$ and $\delta^{34}S$) of oceanic sulfate have been collected, and prompt us to revisit this issue of the variation of sulfur isotope fractionation, and to explore the possible mechanism that could produce the high frequency fluctuation in $\Delta^{33}S$ and $\delta^{34}S$ of oceanic sulfate.

The samples for this study are selected from archived samples of the Bochum-Ottawa carbonate samples, which have been used to establish high-resolution isotopic records for Phanerozic seawater $^{87}Sr/^{86}Sr$, $^{13}C/^{12}C$, and $^{18}O/^{16}O$ (Veizer et al., 1999). Samples covering geological time intervals from the Cambrian to the Triassic periods were selected with a goal of establishing a long-term record for $\Delta^{33}S$ of Paleozoic oceanic sulfate that is a complimentary isotopic record for oceanic sulfate-sulfur. The age model for the selected sample is updated to the geological time scale of 2004. The carbonate samples in this study that are used to reconstruct the sulfur isotopic records for Cambrian, Ordovician, and Devonian are whole rocks, and those for Carboniferous, Permian, and Triassic are biogenic carbonate, including brachiopods and conodonts. The time resolution for different geological periods varies. The time resolution is limited by sampling density of the Bochum-Ottawa carbonate samples. Detailed sample information such as the sampling locality, the sample age and fossil type are listed in the appendix. Figure 6.6 present the sulfur isotopic records ($\Delta^{33}S$) since 635Ma. The Cenozoic data include analysis of marine barite, and the late Neoproterozoic data consist of Oman carbonate. Other data comes from analysis of selected samples of Bochum-Ottawa carbonate (Veizer et al., 1999). The underlying assumption for data interpretation is that the sulfur isotopic records reflect the sulfur isotopic compositions of ancient seawater sulfate of open oceans.

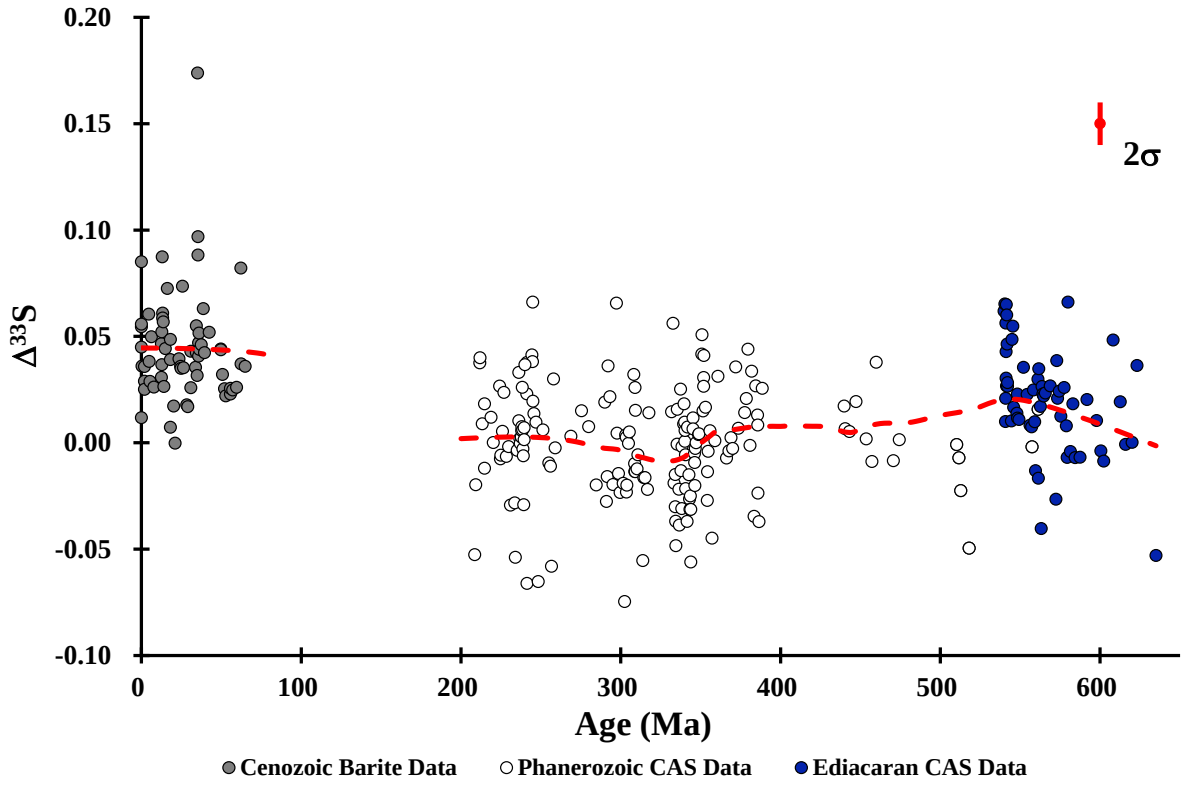

Figure 6.6. Plots of $\Delta^{33}S$ versus age. The sulfur isotopic compositions (Cambrian to Triassic) are derived from carbonate associated sulfate (CAS) in low-Mg calcite (whole rock) and biogenic carbonate. The data for Cenozoic are from marine-origin barite. The red dashed line is the modeled estimate of oceanic sulfate since the late Neoproterozoic using Sigmaplot bulit-in inverse smoothing method. The model age of these samples are updated to geological time scale of 2004.

The $\Delta^{33}S$ record from the Oman carbonate sequences shows a positive shift at the Pre-Cambrian and Cambrian boundary to an average of 0.040‰. This is followed by a drop to -0.050‰ that occurs during the middle Cambrian (~518Ma). An increasing trend is observed and extends up until the Ordovician. The values of $\Delta^{33}S$ oscillate around 0.000‰ for the Devonian, Carboniferous and Permian-Triassic periods. During the early Triassic when $\delta^{34}S$ shows a positive excursion, the $\Delta^{33}S$ shows quite low negative values. During the Cenozoic, the values of $\Delta^{33}S$ oscillate around 0.045‰. A re-analysis of the long term variations of $\Delta^{34}S_{SW\text{-}PY}$ is evaluated on the basis of new $\Delta^{33}S$ data of oceanic sulfate. Figure 6.7 illustrates the modeled results that are derived from these two approaches.

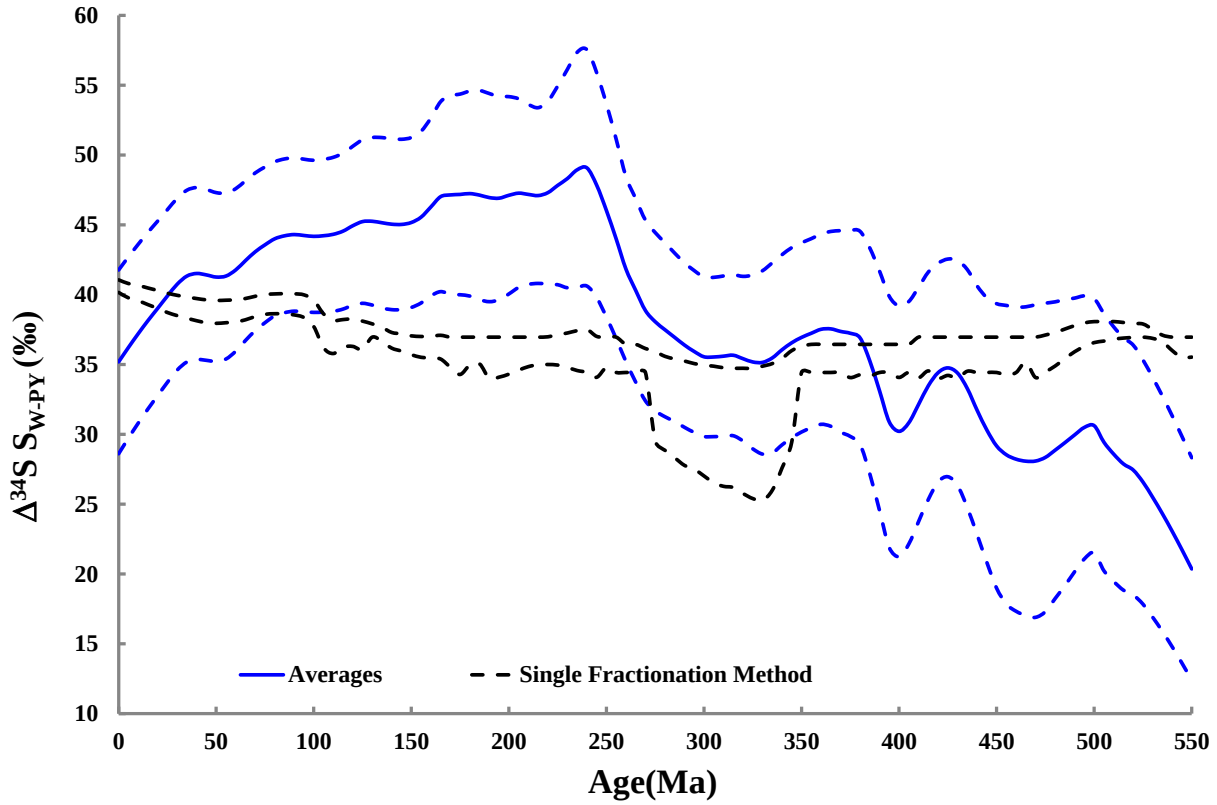

Figure 6.7. Plots of $\Delta^{34}S_{SW\text{-}PY}$ versus age. blue lines are solutions using the arithmetic difference between $\delta^{34}S$ of sulfate and coeval pyrite. The field between the black dash lines represents the intersection of results of model calculations using Eq. (5) and calculations of the relationship using Eq. (6), which are calculated from new $\Delta^{33}S$ data.

It is noticed that the new estimates of sulfur isotope fractionation on the basis of $\Delta^{33}S$ data are similar to those constrained by Wu et al. (2010). However, there are significant differences of $\Delta^{34}S_{SW\text{-}PY}$ for the Carboniferous Period when $\Delta^{34}S_{SW\text{-}PY}$ reach lowest values of approximately 25‰. Both methods with two different calibrations of $\Delta^{33}S$ (one is used by Wu et al (2010) and the one used here) provide subtle different history for the $\Delta^{33}S$ of oceanic sulfate. The discrepancy may imply that the assumptions or the data underlying either these two methods are not completely valid or the sample set for either the global averages for pyrite or the sulfate is incomplete.

The newly calibrated $\Delta^{34}S_{SW\text{-}PY}$ values are used to determine pyrite burial flux as shown in Figure 6.8. It is observed that there are two time intervals (0-30Ma and 300-380Ma) when the estimates of pyrite burial rate are negative. These negative values may imply that the seawater sulfate concentration increased, which is consistent with the estimates from fluid inclusion chemistry (Horita et al., 2002). The negative values do not necessarily imply there is no pyrite burial during these two time intervals. It may indicate that the influx of sulfur to the oceans was greater than the out flux of sulfur from the oceans. The increased weathering of either sulfide or sulfate minerals is testable by indicators of weathering intensity.

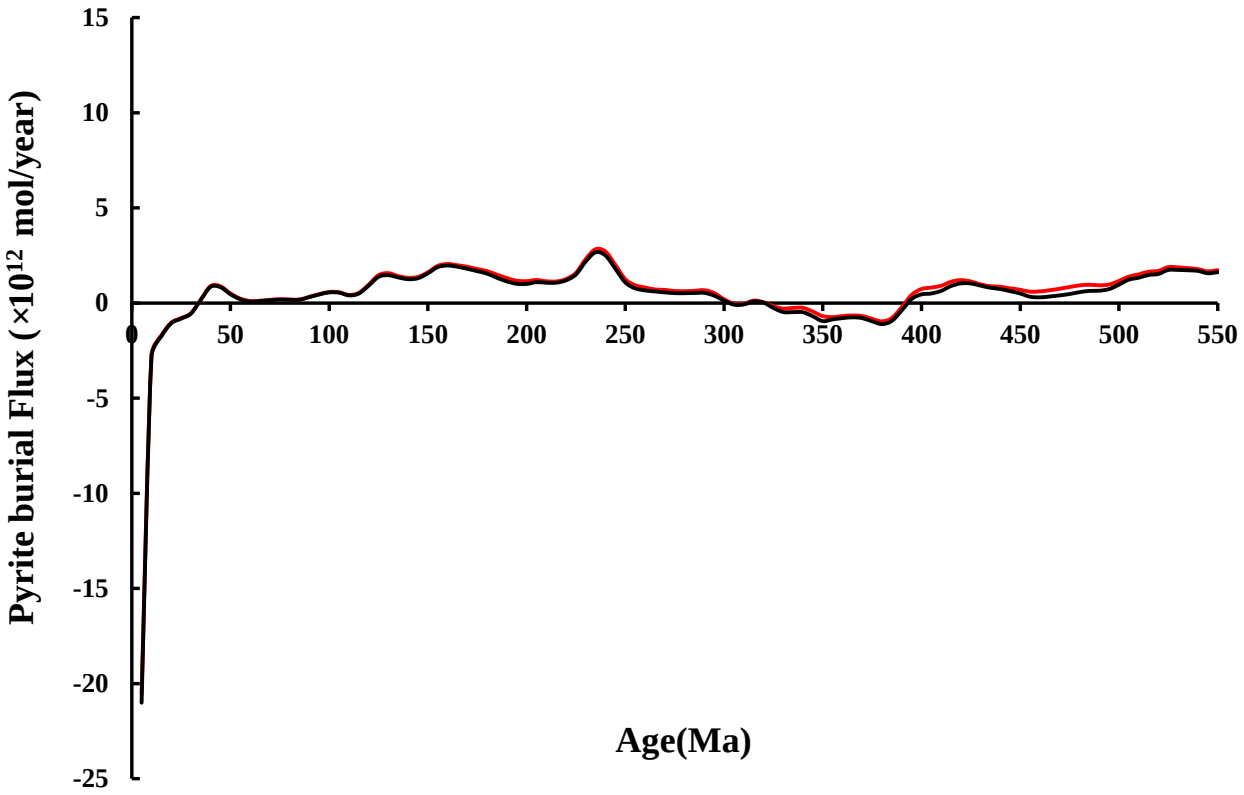

Figure 6.8. Plots of pyrite burial rate versus age. The rated are determined by the newly calibrated $\Delta^{34}S_{SW\text{-}PY}$ data.The black and red line represents the calculation results using the upper and lower limits of newly calibrated $\Delta^{34}S_{SW\text{-}PY}$ in Figure 6.7.

Another explanation for the negative values of pyrite burial rate for the time interval of 300-380 Ma may be a change in the role of direct sulfide oxidation. The role of direct sulfide oxidation may be also much more prominent. This is consistent with the conclusion made from newly calibrated $\Delta^{34}S_{SW\text{-}PY}$.

Given the context provided by the results of the sulfur cycle (Johnston 2005, 2006), the changes in $\Delta^{34}S_{SW\text{-}PY}$ with geologic time require different role of sulfur disproportionation in cycling of sulfur. Canfield and Farquhar (2009) argued that the magnitude of sulfur isotope fractionation between sulfate and buried pyrite would be larger when sulfide oxidation was higher because of a relationship with sulfate concentration. Another process that would be associated with greater sulfide oxidation would be a different role for sulfur disproportionation. In this way, the $\Delta^{34}S_{SW\text{-}PY}$ calibration for the Phanerozoic may indicate a more prominent role for sulfur disproportionation in the later and earlier parts of the Phanerozoic, but a smaller role for sulfur disproportionation during the Carboniferous. It may imply that the role of direct sulfide oxidation is more prominent during the Carboniferous potentially as a result of a maximum in atmospheric oxygen levels (Berner, 2001). The biogeochemical factors that influence the role of disproportionation and oxidation are not clear and this hypothesis needs to be tested further.

6.6 Summary

Our new sulfur isotope data ($\delta^{34}S$ and $\Delta^{33}S$) measured for carbonate associated sulfate (CAS) in stratigraphically well-constrained biogenic and whole rock carbonates, and additional data from Cenozoic marine barites, provide a new temporal record for the sulfur isotopic compositions of Phanerozoic seawater. Secular variations in $\delta^{34}S$ and $\Delta^{33}S$ are clearly observed, and high frequency variations are also discernible.

These sulfur isotope records are used to place constraints on the average global fractionation ($\Delta^{34}S_{SW\text{-}PY}$) associated with pyrite burial (Wu et al. 2010 and this study). The calibrated values show that $\Delta^{34}S_{SW\text{-}PY}$ has varied widely between 25‰ to 40‰, reaching lower values for the Carboniferous (25‰), and higher values for the Cenozoic (40‰), and a long term average (35‰) for other Phanerozoic periods.

The sulfur isotope fractionation between sulfate and pyrite is thought to be a combination of fractionations by processes such as microbial sulfate reduction, which produce large metabolic isotope effects (>40‰), and other processes including sulfide oxidation (sulfide oxidized to form sulfur intermediate compounds), as well as subsequent reductive, oxidative, and disproportionative biological and abiological pathways which complete the sulfur cycle (Canfield, 2001). The findings of changing $\Delta^{34}S_{SW\text{-}PY}$ throughout the Phanerozoic likely reflect a change in the ecology of the oceanic sulfur cycle. This change may reflect either changes in fractionations associated with sulfate reduction and fractionations associated with sulfide oxidation or a shift in the fractionation that would reflect a change in the role of disproportionation and oxidation of sulfur in the sulfur cycle. It is not clear at present how to differentiate between these two possibilities.

Chapter 7: Conclusions and Directions

7.1 General Conclusions

The primary goal of this study was to characterize sulfur isotopic compositions ($\delta^{34}S$ and $\Delta^{33}S$) of seawater sulfate over the course of the latest Neoproterozoic and Phanerozoic, and use these isotopic records to understand the evolution of the sulfur cycle and geochemical and geological factors that control isotopic compositions of seawater sulfate. Carbonate associated sulfate (CAS), thought to be a proxy of seawater sulfate, was extracted and confirmed the long term variations in $\delta^{34}S$ records throughout the Phanerzoic observed from other proxies (e.g. sulfur isotopic records from evaporite, Figure 3.6), whereas the $\Delta^{33}S$ isotopic record shows no discernible long term trend and indicates high frequency variations over geologic times (Figure 6.6). These sulfur isotopic records are interpreted in a framework of $\delta^{34}S$-$\Delta^{33}S$ dynamics afforded by the isotope mass conservation (Chapter 2) to exmine existing hypotheses inferred from $\delta^{34}S$ records, and extract new information about temporal changes in the sulfur cycle.

The average global fractionation ($\Delta^{34}S_{SW\text{-}PY}$) associated with pyrite burial were constrained using the newly $\Delta^{33}S$ isotopic record derived from proxy of CAS. The calculation shows that $\Delta^{34}S_{SW\text{-}PY}$ has varied widely between 25‰ to 40‰ over the course of Phanerozic, reaching lower values for the Carboniferous (~ 25‰), and higher values for the Cenozoic (~ 40‰), and a long term average (~ 35‰) for other Phanerozoic periods (Chapter 6). Study of the multiple sulfur isotopic records ($\delta^{34}S$ and $\Delta^{33}S$) of paired sulfate and pyrite from the Huqf Supergroup of Oman shows the character of the basin-scale sulfur cycle. The isotopic compositons of sulfur source to the Oman baisn appears to have changed from a set of lower values to a set of higher values (Figure 5.7). Another explanation for the isotopic records of the

upper parts of the Huqf Supergroup is invoked by drawdown of sulfate concentrations due to the weakening of sulfide reoxidation and/or weakening of other physical processes that mix sulfate in sediment pore water with sulfate overlying oceans in marine setting (Figure 5.8). These studies provide a way to evaluate the connection between sulfur isotopes, sulfate concentration, sulfide reoxidation and sulfur isotope effects associated with microbial sulfate reduction and sulfur disproportionation. It is relevant to understanding the environmental changes and their response to changes in geochemical and geological processes over geologic times.

7.2 Directions for future research

This study provides a first look at the systematics of $\delta^{34}S$ and $\Delta^{33}S$ of Phanerozoic seawater sulfate. The calibrated sulfur isotope fractionation using the approach developed here may be refined in future. Ways that can be refined include:

1) Improving data from missing temporal records. $\delta^{34}S$ and $\Delta^{33}S$ records from Jurassic and Cretaceous oceanic sulfate are missing from these records and represent an important target for future research. Oceanic anoxic events occurred during Jurassic and Cretaceous and played an important role in controlling of marine chemistry and marine ecology. The multiple sulfur isotope data will provide information about the cycling of hydrogen sulfide.

2) Experimental study on the isotope effects associated with processes in the sulfur cycle. More experiments on isotope effects associated with sulfide oxidation and sulfur disproportionation will provide data that improve the application of models, the understanding of uncertainties associated with the models and conclusions that can be made from models.

3) Investigation of key intervals in the geological records. These studies may provide information about connection between sulfate levels, sulfur isotopes and ocean chemistry. The

connection between sulfate levels, sulfur isotopes of oceanic sulfate, and the intensity of sulfide reoxidation deserve further study. Our data from the Permian/Triassic boundary interval generally follow the evolution path of $\delta^{34}S$ and $\Delta^{33}S$ from model predictions, but more work is needed to link the sulfur isotopes with biological events. This may provide a framework to understand the origin of high frequency changes in $\delta^{34}S$ and $\Delta^{33}S$ of oceanic sulfate that appears to be present in this data.

4) Understanding the long term compositional trend for sulfate flux into the oceans. Long term subduction of sulfide from the exogenic sulfur cycle would result in accumulation of a sedimentary sulfur pool with positive $\delta^{34}S$ at the Proterozoic suggested by Canfield (2004). Canfield's argument was made for the Paleoproterozoic and Mesoproterozoic which preceded Ediacaran time when the Oman basin deposition occurred. A complimentary evolution of $\Delta^{33}S$ for the surface sulfur pool may also exist. Work to address this possibility is warranted. Note that our data from the Huqf Supergroup, Oman basin suggest that this process has not been important.

All of these questions and others form the basis for future research in this area. These latter studies will allow for more application of $\Delta^{33}S$ dynamics to understand the complexity of the global sulfur cycle and to understand the variations of sulfur isotopes related to the paleoenvironmental changes, as is based on establishing the analytical protocol for extration of carbonate assoicated sulfate for seawater sulfate-sulfur isotopes and mutually calibrating and validating of CAS-based and evaporite-based sulfur isotopic records.

Appendix

Table 1 Sulfur isotope data for IAEA-S2

Lab #	Sample	$\delta^{33}S$	$\delta^{34}S$	$\delta^{36}S$	$\Delta^{33}S$	$\Delta^{36}S$
SF3557	IAEA-S2	11.4	22.2	42.4	0.038	-0.231
SF3613	IAEA-S2	11.4	22.2	42.3	0.036	-0.300
SF3635	IAEA-S2	11.4	22.1	42.2	0.048	-0.234
SF3661	IAEA-S2	11.4	22.1	42.2	0.036	-0.261
SF4094	IAEA-S2	11.5	22.3	42.7	0.056	-0.128
SF4104	IAEA-S2	11.4	22.2	42.3	0.044	-0.320
SF4114	IAEA_S2	11.5	22.3	42.5	0.024	-0.341
SF4123	IAEA-S2	11.5	22.3	42.4	0.047	-0.385
SF4140	IAEA-S2	11.5	22.3	42.6	0.050	-0.208
SF4188	IAEA-S2	11.4	22.2	42.4	0.006	-0.153
SF4188-A	IAEA-S2	11.4	22.2	42.6	0.045	-0.004
SF4230	IAEA-S2	11.5	22.4	43.0	0.043	0.020
SF4345	IAEA-S2	11.4	22.2	42.5	0.040	-0.097
SF4457	IAEA-S2	11.5	22.3	42.6	0.034	-0.184
SF4894	IAEA-S2	11.4	22.3	42.5	0.038	-0.194
SF4911	IAEA-S2	11.5	22.3	43.0	0.039	0.164
SF5088	IAEA-S2	11.4	22.2	42.7	0.050	-0.018
SF5126	IAEA-S2	11.4	22.2	42.5	0.031	-0.142
SF5556	IAEA-S2	11.4	22.3	42.5	0.029	-0.187
SF5617	IAEA-S2	11.3	22.1	42.7	0.029	0.295
SF5940	IAEA-S2	11.4	22.2	43.6	0.036	0.963
SF5955	IAEA-S2	11.5	22.3	43.0	0.032	0.159
SF5979	IAEA-S2	11.5	22.3	42.9	0.032	0.153
SF6782	IAEA-S2	11.4	22.1	42.0	0.023	-0.449
SF6897	IAEA-S2	11.5	22.4	42.9	0.041	-0.182
SF7063	IAEA-S2	11.3	22.1	42.2	0.040	-0.084
SF7076	IAEA-S2	11.3	22.0	41.7	0.036	-0.460
SF7086	IAEA-S2	11.3	21.9	41.5	0.046	-0.486
SF7087	IAEA-S2	11.2	21.8	41.3	0.039	-0.594
SF7089	IAEA-S2	11.5	22.3	41.7	0.048	-1.067
SF7103	IAEA-S2	11.4	22.1	41.8	0.055	-0.641
SF7116	IAEA-S2	11.4	22.1	41.9	0.041	-0.528
SF7126	IAEA-S2	11.4	22.1	42.0	0.047	-0.527
SF7143	IAEA-S2	11.3	22.1	42.0	0.038	-0.318
SF7158	IAEA-S2	11.3	22.0	41.8	0.041	-0.378
SF7178	IAEA-S2	11.2	21.9	41.5	0.051	-0.414
SF7201	IAEA-S2	11.2	21.8	41.8	0.068	-0.046
SF7205	IAEA-S2	11.2	21.7	41.4	0.058	-0.294
SF7208	IAEA-S2	11.4	22.1	41.6	0.059	-0.810
SF7208	IAEA-S2	11.3	22.1	41.6	0.040	-0.798
SF7209	IAEA-S2	11.4	22.1	41.9	0.033	-0.492
SF7211	IAEA-S2	11.4	22.1	41.8	0.039	-0.660
SF7211	IAEA-S2	11.4	22.1	41.9	0.065	-0.465
SF7240	IAEA-S2	11.5	22.3	42.3	0.037	-0.507
SF7255	IAEA-S2	11.5	22.3	42.3	0.048	-0.501
SF7277	IAEA-S2	11.5	22.3	42.5	0.036	-0.332

Table 2 Sulfur isotope data for IAEA-S3

Lab #	Sample	$\delta^{33}S$	$\delta^{34}S$	$\delta^{36}S$	$\Delta^{33}S$	$\Delta^{36}S$
SF4176	IAEA-S3	-16.8	-32.5	-62.2	0.074	-1.347
SF7068	IAEA-S3	-16.8	-32.5	-61.7	0.083	-0.835
SF7068	IAEA-S3	-16.8	-32.5	-61.7	0.083	-0.835
SF7095	IAEA-S3	-16.9	-32.6	-61.6	0.075	-0.542
SF7095	IAEA-S3	-16.9	-32.6	-61.6	0.075	-0.542
SF7112	IAEA-S3	-16.9	-32.8	-61.7	0.070	-0.351
SF7112	IAEA-S3	-16.9	-32.8	-61.7	0.070	-0.351
SF7135	IAEA-S3	-16.6	-32.0	-60.0	0.055	0.037
SF7150	IAEA-S3	-17.0	-32.9	-61.6	0.070	0.029
SF7164	IAEA-S3	-17.1	-33.0	-61.8	0.064	0.011
SF7170	IAEA-S3	-16.5	-32.0	-60.0	0.064	-0.059
SF7191	IAEA-S3	-16.6	-32.0	-60.2	0.058	-0.209
SF7207	IAEA-S3	-16.6	-32.1	-60.4	0.066	-0.305
SF7232	IAEA-S3	-16.4	-31.6	-59.3	0.059	-0.018
SF7248	IAEA-S3	-16.8	-32.5	-61.4	0.084	-0.589
SF7270	IAEA-S3	-16.8	-32.5	-61.8	0.057	-0.843
SF7285	IAEA-S3	-16.8	-32.6	-61.2	0.102	-0.222

Table 3 Sulfur isotope data for NBS-127

Lab #	Sample	$\delta^{33}S$	$\delta^{34}S$	$\delta^{36}S$	$\Delta^{33}S$	$\Delta^{36}S$
SF6457	NBS-127	10.8	20.9	40.4	0.039	0.279
SF6460	NBS-127	11.2	21.7	41.8	0.023	0.096
SF6464	NBS-127	11.0	21.3	41.0	0.044	0.136
SF6465	NBS-127	10.8	21.0	40.6	0.028	0.234
SF2394	NBS-127	10.9	21.2	40.4	0.023	-0.159
SF2437	NBS-127	10.9	21.3	40.7	0.027	-0.103
SF2499	NBS-127	10.8	21.1	40.4	0.032	-0.046
SF2500	NBS-127	10.8	21.0	40.3	0.049	0.037
SF2519	NBS-127	10.9	21.1	40.5	0.056	-0.028
SF2543	NBS-127	10.8	21.1	40.4	0.046	-0.008
SF2544	NBS-127	10.9	21.1	40.6	0.051	0.065
SF2589	NBS-127	10.8	21.0	40.0	0.051	-0.349
SF3182	NBS-127	10.8	21.1	39.9	0.027	-0.517

Table 4 Sulfur isotope data for Triassic CAS

Lab #	Sample	Period	Age(Ma)	Fossil Type	$\delta^{34}S$	$\Delta^{33}S$
SF7165	Tr-13	Triassic	208.60	Brachiopd	15.7	-0.053
SF7145	Tr-37	Triassic	209.20	Brachiopd	34.3	-0.020
SF7141	Tr-53	Triassic	211.90	Conodont	18.3	0.040
SF7136	Tr-63+64	Triassic	214.70	Conodont	17.9	-0.012
SF7137	Tr-70	Triassic	220.30	Conodont	18.2	0.000
SF7152	Tr-79	Triassic	225.00	Conodont	19.6	-0.006
SF7139	Tr-85	Triassic	226.00	Brachiopd	18.8	0.005
SF7138	Tr-93	Triassic	226.90	Brachiopd	19.5	0.024
SF7149	Tr-108	Triassic	228.40	Brachiopd	19.9	-0.006
SF7144	Tr-117	Triassic	229.80	Brachiopd	16.5	-0.002
SF7153	Tr-122	Triassic	231.00	Conodont	24.0	-0.029
SF7146	Tr140	Triassic	233.70	Brachiopd	17.5	-0.028
SF7162	Tr-142	Triassic	234.10	Brachiopd	16.9	-0.054
SF7155	Tr-150	Triassic	235.20	Brachiopd	17.3	-0.004
SF7134	Tr-154	Triassic	236.20	Conodont	29.6	0.010
SF7167	Tr-159	Triassic	236.90	Conodont	36.3	0.002
SF7142	Tr-161	Triassic	237.10	Brachiopd	23.0	0.000
SF7154	Tr-168	Triassic	237.80	Brachiopd	17.8	0.003
SF7157	Tr-176	Triassic	238.00	Conodont	19.5	0.006
SF7160	Tr-177	Triassic	238.20	Conodont	32.7	0.008
SF7148	Tr-180	Triassic	238.40	Conodont	30.2	0.026
SF7156	Tr-186	Triassic	238.70	Conodont	31.4	0.006
SF7133	Tr-187	Triassic	238.80	Brachiopd	29.6	-0.003
SF7147	Tr-194	Triassic	239.00	Brachiopd	27.0	-0.006
SF7140	Tr-200	Triassic	239.30	Brachiopd	22.2	-0.029
SF7163	Tr-204	Triassic	239.50	Brachiopd	28.0	0.007
SF7166	Tr-207	Triassic	239.60	Brachiopd	25.2	0.001
SF7159	Tr-218	Triassic	240.10	Brachiopd	21.7	0.037
SF7151	Tr-253	Triassic	241.40	Conodont	20.0	-0.066

Table 5 Sulfur isotope data for Permian CAS

Lab #	Sample	Period	Age(Ma)	Fossil Type	$\delta^{34}S$	$\Delta^{33}S$
SF7117	P-2	Permian	245.00	Brachiopd	16.3	0.020
SF7122	P-13	Permian	245.70	Brachiopd	26.5	0.014
SF7129	P-23	Permian	246.90	Brachiopd	16.7	0.010
SF7132	P-28	Permian	248.40	Brachiopd	21.5	-0.065
SF7131	P-33	Permian	251.30	Brachiopd	14.9	0.006
SF7125	P-35	Permian	255.00	Brachiopd	15.9	-0.009
SF7120	P-50	Permian	256.10	Brachiopd	23.4	-0.011
SF7127	P-57	Permian	256.70	Brachiopd	11.9	-0.058
SF7113	P-60+61	Permian	258.00	Brachiopd	16.9	0.030
SF7114	P-62+65	Permian	259.00	Brachiopd	15.9	-0.002
SF7121	P-78	Permian	268.80	Brachiopd	22.2	0.003
SF7123	P-84	Permian	275.50	Brachiopd	16.4	0.015
SF7130	P-86	Permian	280.00	Brachiopd	16.9	0.008
SF7124	P-93	Permian	284.70	Brachiopd	13.7	-0.020

Table 6 Sulfur isotope data for Devonian CAS

Lab #	Sample	Period	Age(Ma)	Fossil Type	$\delta^{34}S$	$\Delta^{33}S$
SF7079	Dev07+10	Devonian	366.20	Brachiopod	19.7	-0.007
SF7108	Dev40+41	Devonian	367.70	Brachiopod	26.0	-0.004
SF7090	Dev55-58	Devonian	369.00	Brachiopod	17.8	0.002
SF7109	Dev96+97	Devonian	370.10	Brachiopod	33.0	-0.003
SF7104	Dev105	Devonian	372.00	Brachiopod	37.5	0.036
SF7094	Dev110	Devonian	373.70	Brachiopod	21.6	0.007
SF7093	ev115+116	Devonian	377.60	Brachiopod	19.3	0.014
SF7101	Dev121	Devonian	378.60	Brachiopod	22.4	0.021
SF7102	)ev130-132	Devonian	379.70	Brachiopod	21.9	0.044
SF7081	ev173+176	Devonian	380.90	Brachiopod	17.2	-0.001
SF7092	Dev183	Devonian	381.90	Brachiopod	24.5	0.034
SF7105	Dev200	Devonian	383.50	Brachiopod	19.3	-0.035
SF7106	)ev224-227	Devonian	384.50	Brachiopod	31.1	0.027
SF7101	)ev262-264	Devonian	385.70	Brachiopod	17.7	0.013
SF7080	Dev273	Devonian	385.80	Brachiopod	16.4	0.008
SF7091	ev302+303	Devonian	385.90	Brachiopod	14.0	-0.024
SF7107	)ev340-347	Devonian	386.60	Brachiopod	11.0	-0.037
SF7110	Dev360	Devonian	388.60	Brachiopod	20.4	0.026

Table 7 Sulfur isotope data for Ordovician CAS

Lab #	Sample	Period	Age(Ma)	Fossil Type	$\delta^{34}S$	$\Delta^{33}S$
SF7083	Ord-36+37	Ordovician	439.80	*Oniella*	26.2	0.017
SF7069	Ord-50+53	Ordovician	440.50	*Leptaena*	21.2	0.007
SF7070	Ord-57-60	Ordovician	443.20	*Dalmanella*	25.1	0.005
SF7077	Ord-70-73	Ordovician	447.30	*Dalmanella*	28.0	0.019
SF7097	Ord-77	Ordovician	453.60		23.3	0.002
SF7099	Ord-96-99	Ordovician	457.20	*Dalmanella*	21.4	-0.009
SF7096	Ord-104-110	Ordovician	459.90	*Mimella extensa*	32.4	0.038
SF7098	Ord-115-118	Ordovician	470.70		26.5	-0.008
SF7082	Ord-121-124	Ordovician	474.40	*uliticostella Convexa*	35.9	0.001

Table 8 Sulfur isotope data for Carboniferous CAS

Lab #	Sample	Period	Age(Ma)	Fossil Type	$\delta^{34}S$	$\Delta^{33}S$
SF7239	C-1+2+3	Carborniferous	290.00	Brachiopod	13.3	0.019
SF7242	C-5+7	Carborniferous	291.00	Brachiopod	11.7	-0.028
SF7179	C-9	Carborniferous	291.60	Brachiopod	13.2	-0.016
SF7214	C-10+11	Carborniferous	292.10	Brachiopod	12.8	0.036
SF7249	C-12+13	Carborniferous	293.30	Brachiopod	15.2	0.022
SF7268	C-23+24	Carborniferous	295.10	Brachiopod	11.0	-0.020
SF7247	C-28	Carborniferous	297.30	Brachiopod	15.8	0.066
SF7225	C-32	Carborniferous	297.70	Brachiopod	12.3	0.005
SF7226	C-35	Carborniferous	298.60	Brachiopod	11.8	-0.015
SF7234	C-38+39	Carborniferous	299.60	Brachiopod	8.4	-0.023
SF7229	C-40	Carborniferous	301.50	Brachiopod	14.0	-0.019
SF7286	C-42	Carborniferous	302.40	Brachiopod	9.8	-0.075
SF7215	C-45+47	Carborniferous	303.10	Brachiopod	12.1	0.004
SF7193	C-49	Carborniferous	303.40	Brachiopod	12.7	0.003
SF7237	C-53	Carborniferous	303.60	Brachiopod	11.0	-0.023
SF7228	C-58	Carborniferous	303.80	Brachiopod	12.3	-0.020
SF7217	C-68	Carborniferous	304.90	Brachiopod	10.9	0.000
SF7227	C-75	Carborniferous	305.40	Brachiopod	12.3	0.005
SF7216	C-89	Carborniferous	308.20	Brachiopod	14.5	0.032
SF7194	C-92	Carborniferous	308.70	Brachiopod	14.0	-0.010
SF7279	C-93	Carborniferous	308.80	Brachiopod	14.2	-0.014
SF7196	C-98	Carborniferous	308.90	Brachiopod	15.0	0.026
SF7281	C-103	Carborniferous	309.10	Brachiopod	14.4	-0.014
SF7180	C-112	Carborniferous	309.20	Brachiopod	13.7	0.015

Lab #	Sample	Period	Age(Ma)	Fossil Type	$\delta^{34}S$	$\Delta^{33}S$
SF7230	C-118	Carborniferous	310.20	Brachiopod	10.6	-0.012
SF7252	C-121	Carborniferous	310.80	Brachiopod	15.1	-0.006
SF7287	C-140	Carborniferous	313.80	Brachiopod	12.5	-0.055
SF7260	C-144	Carborniferous	314.50	Brachiopod	11.9	-0.016
SF7271	C-149	Carborniferous	315.20	Brachiopod	12.0	-0.016
SF7204	C-155	Carborniferous	316.80	Brachiopod	10.1	-0.022
SF7290	C-164	Carborniferous	317.70	Brachiopod	21.1	0.014
SF7200	C-206	Carborniferous	331.80	Brachiopod	16.6	0.014
SF7212	C-215	Carborniferous	332.70	Brachiopod	16.2	0.056
SF7245	C-221	Carborniferous	333.40	Brachiopod	15.7	-0.019
SF7272	C-230	Carborniferous	334.10	Brachiopod	12.5	-0.030
SF7258	C-234	Carborniferous	334.20	Brachiopod	17.5	-0.015
SF7177	C-235	Carborniferous	334.40	Brachiopod	14.0	-0.037
SF7288	C-238	Carborniferous	334.50	Brachiopod	18.5	-0.048
SF7259	C-242	Carborniferous	335.30	Brachiopod	14.6	-0.001
SF7218	C-243	Carborniferous	335.40	Brachiopod	15.4	0.016
SF7264	C-260	Carborniferous	336.50	Brachiopod	18.1	-0.022
SF7267	C-263	Carborniferous	336.70	Brachiopod	21.0	-0.039
SF7262	C-277+278	Carborniferous	337.50	Brachiopod	14.2	0.025
SF7176	C-280	Carborniferous	337.70	Brachiopod	13.1	-0.013
SF7266	C-291	Carborniferous	338.20	Brachiopod	18.8	-0.031
SF7238	C-292+293	Carborniferous	338.40	Brachiopod	18.3	-0.002
SF7236	C-303	Carborniferous	339.40	Brachiopod	14.1	0.009
SF7275	C-307	Carborniferous	339.70	Brachiopod	16.7	0.018
SF7235	C-311	Carborniferous	340.00	Brachiopod	14.5	0.010
SF7246	C-313+314	Carborniferous	340.20	Brachiopod	27.3	0.001
SF7173	C-318	Carborniferous	340.30	Brachiopod	19.9	0.006
SF7265	C-319	Carborniferous	340.50	Brachiopod	18.3	-0.006
SF7253	C-323	Carborniferous	340.60	Brachiopod	12.8	-0.022
SF7187	C-329	Carborniferous	341.60	Brachiopod	19.5	-0.037
SF7174	C-332	Carborniferous	341.80	Brachiopod	21.7	0.007
SF7186	C-340	Carborniferous	342.70	Brachiopod	19.6	-0.015
SF7257	C-350	Carborniferous	343.10	Brachiopod	16.8	-0.026
SF7278	C-366	Carborniferous	343.40	Brachiopod	16.3	-0.031
SF7241	C-368	Carborniferous	343.60	Brachiopod	20.3	-0.025
SF7261	C-371	Carborniferous	343.80	Brachiopod	10.0	-0.056
SF7181	C-372	Carborniferous	343.80	Brachiopod	17.4	-0.031
SF7219	C-380	Carborniferous	345.20	Brachiopod	19.5	0.012
SF7251	C-382	Carborniferous	345.30	Brachiopod	19.1	0.006
SF7254	C-389	Carborniferous	346.20	Brachiopod	22.2	-0.005
SF7244	C-390	Carborniferous	346.30	Brachiopod	16.6	-0.009
SF7289	C-391	Carborniferous	346.40	Brachiopod	21.9	-0.020
SF7171	C-393	Carborniferous	346.70	Brachiopod	17.3	-0.003
SF7183	C-395	Carborniferous	347.20	Brachiopod	21.2	0.000
SF7282	C-398	Carborniferous	348.70	Brachiopod	21.7	0.004
SF7199	C-399	Carborniferous	349.00	Brachiopod	22.4	0.004
SF7263	C-410+411	Carborniferous	350.80	Brachiopod	23.9	0.042
SF7175	C-412	Carborniferous	350.90	Brachiopod	22.2	0.051
SF7243	C-415	Carborniferous	351.50	Brachiopod	20.2	0.015
SF7256	C-416	Carborniferous	351.90	Brachiopod	18.5	0.031
SF7273	C-418	Carborniferous	351.90	Brachiopod	20.3	0.027
SF7250	C-419+420	Carborniferous	352.10	Brachiopod	20.2	0.041
SF7190	C-425	Carborniferous	353.10	Brachiopod	18.0	0.017
SF7172	C-429	Carborniferous	354.20	Brachiopod	11.8	-0.027
SF7185	C-434	Carborniferous	354.40	Brachiopod	19.3	-0.014
SF7231	C-436	Carborniferous	354.70	Brachiopod	21.2	-0.004
SF7283	C-437-440	Carborniferous	355.90	Brachiopod	21.0	0.006
SF7269	C-450	Carborniferous	357.20	Brachiopod	14.8	-0.045
SF7184	C-452	Carborniferous	359.00	Brachiopod	22.7	0.001
SF7188	C-459	Carborniferous	360.90	Brachiopod	23.8	0.031

Table 9-1 Sulfur isotope data for Carboniferous Barite

Site	Core	Depth	Age(Ma)	$\delta^{34}S$	$\Delta^{33}S$
63	7	3-4	1E-07	21.1	0.085
63	7	2-3	0.001	20.8	0.045
20		4-5	0.001	20.7	0.055
88	5	14-16	0.001	20.7	0.056
20		9-10	0.001	20.9	0.012
PC	72	798-800	0.4	20.9	0.036
574A	2-3	101-102	1.937	22.0	0.029
574A	2-3	101-102	1.937	21.9	0.036
574A	2-3	101-102	1.937	22.1	0.025
572A	8-3	53-57	4.552	21.8	0.060
577	6H-4	96-105	4.85	22.1	0.038
572A	12-3	48-52	5.4	21.8	0.029
572A	16-3	52-56	6.231	22.2	0.050
572D	7-2	42-46	7.854	22.5	0.026
575B	4-3	19-23	12.488	22.0	0.031
575B	4-3	19-23	12.488	21.9	0.047
572D	20-2	79-85	12.774	22.7	0.052
575B	4-6	141-145	12.782	22.4	0.037
575B	5-3	125-129	13	22.5	0.087
575B	5-6	70-74	13.274	22.2	0.061
575B	5-6	70-74	13.274	22.0	0.059
575B	6-5	112-116	13.717	22.1	0.057
575B	7-2	94-98	14.054	22.1	0.026
575B	9-2	96-100	14.983	21.8	0.044
575B	12-2	94-98	16.195	21.9	0.072
574C	5-4	25-29	18.132	21.8	0.039
574C	5-4	25-29	18.132	21.7	0.007
574C	5-4	25-29	18.132	21.8	0.049
574C	11-3	136-140	20.138	21.7	0.017
574C	13-4	21-25	21.079	22.5	0.000
574C	17-1	104-108	23.547	21.9	0.039
305	7-2	25-31	24.6	21.6	0.036

Table 9-2Sulfur isotope data for Cenozic Barite

Site	Core	Depth	Age(Ma)	$\delta^{34}S$	$\Delta^{33}S$
305	7-2	80-85	24.8	21.4	0.035
574C	19-2	2-6	25.679	21.6	0.074
574C	20-2	101-105	26.363	21.3	0.035
574C	22-3	17-21	28.445	21.3	0.018
574C	24-4	20-24	29.058	21.4	0.017
305	8-2	44-50	31	22.0	0.026
305	8-2	44-50	31	21.7	0.043
305	9-4	80-85	33.9	21.5	0.035
366	10-2	44-47	34.4	22.8	0.042
366	10-2	44-47	34.4	22.5	0.055
574C	33-2	77-81	34.95	22.2	0.032
366	12-2	52-56	35.2	20.5	0.174
305	9-6	71-76	35.4	21.8	0.088
305	9-6	71-76	35.4	21.7	0.097
366	14-2	50-53	35.8	23.4	0.041
366	14-2	50-53	35.8	23.1	0.047
305	10-2	30-36	36	21.8	0.052
574C	35-2	60-80	36.306	22.5	0.044
305	10-4	60-65	37.5	22.0	0.046
366	16-2	47-50	38.7	23.1	0.063
366	20-2	51-53	39.5	22.4	0.042
366	24-3	98-101	42.5	22.5	0.052
366	34-2	50-53	49.7	20.0	0.044
577	8H-4	70-80	49.7	19.3	0.044
366	38-2	50-53	50.8	18.1	0.032
305	12-2	25-31	52	17.8	0.025
577	9H-4	8-15	52.818	17.4	0.022
366	45-2	48-52	55.8	18.1	0.023
366	45-2	48-52	55.8	18.0	0.026
577	10H-6	5-13	57.2	17.6	0.025
577	11-3	94-100	59.6	18.1	0.026
577	11-6	110-116	62.2	18.7	0.082
577	12-1	61-69	62.4	19.0	0.037
577	12-6	60-70	64.9745	19.6	0.036

Reference

Amthor J. E., Grotzinger J. P., Schroder S., Bowring S. A. Ramezani J., Martin M. W. and Matter A. (2003) Extinction of Cloudina and Namacalathus at the Precambrian–Cambrian boundary in Oman. Geology 31, 431–434.

Berner R. A. (1987) Models for carbon and sulfur cycles and atmospheric oxygen: application to Paleozoic geologic history. Am. J. Sci. 287, 177–196.

Berner R. A. (2001) Modeling atmospheric O2 over Phanerozoic time. Geochim. Cosmochim. Acta 65, 685–694.

Berner R. A. (2004) A model for calcium, magnesium and sulfate in seawater over Phanerozoic time. Am. J. Sci. 304, 438–453.

Berner R. A. (2006) GEOCARBSULF: a combined model for Phanerozoic atmospheric O2 and CO2. Geochim. Cosmochim. Acta 70, 5653–5664.

Berner R. A. and Raiswell R. (1983) Burial of organic carbon and pyrite sulfur in sediments over Phanerozoic time: a new theory. Geochim. Cosmochim. Acta 47, 855–862.

Böttcher, M. E., H.-J. Brumsack and C. Duerselen (2007). The isotopic composition of modern seawater sulfate: I. Coastal waters with special regard to the North Sea. J. mar. syst. 67: 73-82

Bottrell S. H. and Newton R. J. (2006) Reconstruction of changes in global sulfur cycling from marine sulfate isotopes. Earth Sci. Rev. 75, 59–83.

Bowring S. A., Grotzinger J. P., Condon D. J., Ramezani J. and Newall M. (2007) Geochronologic constraints on the chronostratigraphic framework of the Neoproterozoic Huqf Supergroup, Sultanate of Oman. Am. J. Sci. 307, 1097–1145.

Brimblecombe, P., Hammer C., Rodhe, H., Ryaboshapko, A., Boutron, C.F. (1989) Human influence on the sulphur cycle. In: Brimblecombe, P., Lein, A.Y. (Eds.), Evolution of the Biogeochemical Sulphur Cycle SCOPE 39. John Wiley and Sons, Chichester, 77– 121.

Burdett, J.W., Arthur, M.A., Richardson, M. (1989) A Neogene seawater sulfur isotope age curve from calcareous pelagic microfossils. Earth and Planetary Science Letters 94,189–198.

Canfield D. E. (2001) Biogeochemistry of sulfur isotopes. In Stable Isotope Geochemistry, vol. 43, pp. 607–636.

Canfield D. E. (2004) The evolution of the Earth surface sulfur reservoir. Am. J. Sci. 304, 839–861.

Canfield D. E. (2005) The early history of atmospheric oxygen: Homeage to Robert M. Garrels. Annu. Rev. Earth Planet. Sci. 33, 1–36.

Canfield D. E. and Farquhar J. (2009) Animal evolution, bioturbation, and the sulfate concentration of the oceans. Proc. Natl Acad. Sci. USA 106(20), 8123–8127.

Canfield D. E. and Raiswell R. (1999) The evolution of the sulfur cycle. Am. J. Sci. 299, 697–723.

Canfield DE, Farquhar J, Zerkle AL. High isotope fractionations during sulfate reduction in a low-sulfate euxinic ocean analog. Geology 2010, 38(5), 415-418.

Canfield, D.E.; Poulton, S.W.; Narbonne, G.M. (2007). Late-Neoproterozoic deep-ocean oxygenation and the rise of animal life Science (Wash.) 315(5808): 92-95

Claypool G. E., Holser W. T., Kaplan I. R., Sakai H. and Zak I. (1980) The age curves of sulfur and oxygen isotopes in marine sulfate and their mutual interpretation. Chem. Geol. 28, 199–260.

Coplen T. B., Bo ̈hlke J. K., De Bie`vre P., Ding T., Holden N. E., Hopple J. A., Krouse H. R., Lamberty A., Peiser H. S., Re ́ve ́sz K., Rieder S. E., Rosman K. J. R., Roth E., Taylor P. D. P., Vocke J. R. and Xiao Y. K. (2002) Isotope-abundance variations of selected elements. Pure Appl. Chem. 74, 1987–2017.

Dahl, T. W., et al. A Devonian rise of atmospheric oxygen correlated to the radiations of terrestrial plants and predatory fish. PNAS 107, 17911-17915 (2010).

Danielache, S. O., Eskebjerg, C., Johnson, M. S., Ueno, Y. & Yoshida, N. (2008).High-precision spectroscopy of 32S, 33S, and 34S sulfur dioxide: Ultraviolet absorption cross sections and isotope effects. J. Geophys. Res. - Atmospheres 113.

Detmers J., Br ̈uchert V., Habicht K. S., and Kuever J. (2001) Diversity of sulfur isotope fractionations by sulfate-reducing prokaryotes. Appl. Environ. Microbiol. 67, 888–894.

Domagal-Goldman S. D., Kasting J. F., Johnston D. T. and Farquhar J. (2008) Using multiple sulfur isotopes to constrain Archean atmosphere. Earth Planet. Sci. Lett. 269, 29–40.

Farquhar J., Canfield D. E., Masterson A. J. and Johnston D. T. (2008) Sulfur and oxygen isotope study of sulfate reduction in experiments with natural populations from Fllestrand, Denmark. Geochim. Cosmochim. Acta 72, 2805–2821.

Farquhar J., Johnston D. T. and Wing B. A. (2007) Influence of network structure on sulfur isotope phase space of dissimilatory sulfate reduction: implications of conservation of mass effects on mass-dependent isotope fractionations. Geochim. Cosmochim. Acta 71, 5862–5875.

Farquhar J., Johnston D. T., Wing B. A., Habicht K. S., Canfield D. E., Airieau S. and Thiemens M. H. (2003) Multiple sulfur isotopic interpretations of biosynthetic pathways: implications for biological signatures in the sulfur isotope record. Geobiology 1, 27–36.

Farquhar, J., and Wing, B. A. (2003) Multiple sulfur isotopes and the evolution of the atmosphere. Earth and Planetary Science Letters, 213, 1-13.

Farquhar, J., Bao, H., Thiemens, M., 2000a. Atmospheric influence of Earth's earliest sulfur cycle. Science 289, 756–759.

Farquhar, J., Savarino, J., Airieau, S. & Thiemens, M. H. (2001). Observation of wavelength- sensitive mass-independent sulfur isotope effects during SO2 photolysis: Implications for the early atmosphere. J.Geophys. Res.-Planets 106, 32829-32839

Fike D. A. and Grotzinger J. P. (2008) A paired sulfate-pyrite delta S-34 approach to understanding the evolution of the Ediacaran–Cambrian sulfur cycle. Geochim. Cosmochim. Acta 72(11), 2636–2648.

Fike D.A., Grotzinger J.P., Pratt L.M., Summons R.E. (2006) Oxidation of the Ediacaran Ocean. Nature. 444, 744–747.

Gaffin S. (1987) Ridge volume dependence on seafloor generation rate and inversion using long-term sealevel change. Am. J. Sci. 287, 596–611.

Garrels R. M. and Lerman A. (1981) Phanerozoic cycles of sedimentary carbon and sulfur. Proc. Natl. Acad. Sci. USA 78, 4550–4656.

Garrels R. M. and Lerman A. (1984) Coupling of sedimentary sulfur and carbon cycles – an improved model. Am. J. Sci. 284, 989–1007.

Garrels, R. M., and Mackenzie, F. T., Evolution of Sedimentary Rocks: A Geochemical Approach (Norton, New York, 1971).

Gill, B.C., Lyons T.W., Frank, T.D. (2008) Behavior of carbonate-associated sulfate during meteoric diagenesis and implications for the sulfur isotope paleoproxy: Geochim. Cosmochim. Acta. 72, 4699-4711.

Gill, B.C., Lyons, T.W., Saltzman M.R. (2007) Parallel, high-resolution carbon and sulfur isotope records of the evolving Paleozoic marine sulfur reservoir, Palaeogeogr. Palaeoclimatol. Palaeoecol. 256, 156–173.

Goldberg T., Poulton S. W. and Strauss H. (2005) Sulphur and oxygen isotope signatures of late Neoproterozoic to early Cambrian sulphate, Yangtze Platform, China: diagenetic constraints and seawater evolution. Precamb. Res. 137, 223–241.

Goldberg.T,Shields. G, Newton.R, (2011),Analytical Constraints on the Measurement of the Sulfur Isotopic Composition and Concentration of Trace Sulfate in Phosphorites: Implications for Sulfur Isotope Studies of Carbonate and Phosphate Rocks,Geostandards and Geoanalytical Research ,(35) DOI: 10.1111/j.1751-908X.2010.00102.x

Habicht K. S., Gade M., Thamdrup B., Berg P. and Canfield D. E. (2002) Calibration of sulfate levels in the Archean Ocean. Science 298, 2372–2374.

Halas, S., Szaran, J. (2001): Improved thermal decomposition of sulfates to SO2 and mass spectrometric determinations of δ34S of IAEA-SO-5, IAEA-SO-6 and NBS-127 sulfate standards. Rapid Communications in Mass Spectrometry, 15 (17), 1618-1620.

Halevy, I, S. E. Peters and W. W. Fischer, Sulfate burial constraints on the Phanerozoic sulfur cycle, *Science*, 337, 2012.

Halevy, I., Johnston, D. T. & Schrag, D. P. (2010). Explaining the structure of the Archean 764 mass-independent sulfur isotope record. Science 329, 204-207

Harrison, A.G. & Thode, H.G. (1957).Mechanism of the bacterial reduction of sulphate from 766 isotope fractionation studies. Transactions of the Faraday Society 54, 84-92

Hayes, J. M. (2001) Fractionation of carbon and hydrogen isotopes in biosynthetic processes, in J.W. Valley, D.R. Cole eds., Stable Isotope Geochemistry: Reviews in Mineralogy & Geochemistry 43, 225-277.

Holser W. T., Schidlowski M., Machenzie F. T. and Maynard J. B. (1988) Chemical Cycles in the Evolution of Earth. Wiley Press, New York.

Holser, W.T., Maynard J.B., Cruikshank K.M. (1989) Modeling the natural cycle of sulphur through Phanerozoic time. In: Brimblecombe, P., Lein, A.Y. (Eds.), Evolution of the Global Biogeochemical Sulphur Cycle. Wiley, New York, 21–56.

Horita, J., Zimmermann, H., Holland, H.D., 2002. Chemical evolution of seawater during the Phanerozoic: implications from the record of marine evaporites. Geochim. Cosmochim. Acta. 66, 3733–3756.

Horn, R.A. (1969) Marine chemistry. The structure of water and chemistry of hydrosphere. Wiley-intrscience, New York, 568pp.

Hurtgen M.T., Pruss, S.B., Knoll, A.H., (2009) Evaluating the relationship between the carbon and sulfur cycles in the later Cambrian ocean: An example from the Portau Port Group, western Newfoundland, Canada. Earth and Planetary Science Letters, v. 281, 288-297.

Johnston D. T., Farquhar J. and Canfield D. E. (2007) Sulfur isotope insights into microbial sulfate reduction: when microbes meet models. Geochim. Cosmochim. Acta 71, 3929–3947.

Johnston D. T., Farquhar J., Habicht K. S. and Canfield D. E. (2008) Sulphur isotopes and the search for life: strategies for identifying sulphur metabolisms in the rock record and beyond. Geobiology 6, 425–435.

Johnston D. T., Farquhar J., Summons R., Shen Y., Kaufman A. J., Masterson A. L. and Canfield D. E. (2008) Late Paleo-Mesoproterozoic sulfur isotope biogeochemistry: insight from the McArthur Basin. Geochim. Cosmochim. Acta 72, 4278–4290.

Johnston D. T., Farquhar J., Wing B. A., Kaufman A., Canfield D. E. and Habicht K. S. (2005b) Multiple sulfur isotope fractionations in biological systems: a case study with sulfate reducers and sulfur disproportionators. Am. J. Sci. 305, 645–660.

Johnston D. T., Poulton S. W., Fralick P. W., Wing B. A., Canfield D. E. and Farquhar J. (2006) Evolution of the oceanic sulfur cycle at the end of the Paleoproterozoic. Geochim. Cosmochim. Acta 70, 5723–5739.

Johnston D. T., Wing B. A., Farquhar J., Kaufman A. J., Strauss H., Lyons T. W., Kah L. C. and Canfield D. E. (2005a) Active microbial sulfur disproportionation in the Mesoproterozoic. Science 310, 1477–1479.

Johnston, D.T. (2011).Multiple sulfur isotopes and the evolution of Earth's surface sulfur cycle. Earth-Science Reviews 106, 161-183

Jorgensen, B. B., (2006) Sulfur cycling and methane oxidation. In: Schulz, H.D., Zabel, M (Eds.),Marine Geochemistry. Springer, Berlin,271-310.

Jorgensen, B. B., and Kasten S. 2006 (2006) Sulfur cycling and methane oxidation, in H.D. Shultz, Z. Mattias eds., Marine Geochemistry, 271-309.

Kamber, B.S. & Whitehouse, M.J. (2007). Micro-scale sulphur isotope evidence for sulphur cycling in the late Archean shallow ocean. Geobiology 5, 5-17

Kampschulte A. and Strauss H. (2004) The sulfur isotopic evolution of Phanerozoic seawater based on the analysis of structurally substituted sulfate in carbonates. Chem. Geol. 204,255–286.

Kampschulte A., Bruckschen P. and Strauss H. (2001) The sulphur isotopic composition of trace sulphates in Carboniferous brachiopods: implications for coeval seawater, correlation with other geochemical cycles and isotope stratigraphy. Chem. Geol. 175, 149–173.

Kaufman, A.J., Johnston, D.T., Farquhar, J., Masterson, A.L., Lyons, T.W., Bates, S., Anbar, A.D., Arnold, G.L., Garvin, J. & Buick, R. (2007). Late Archean biospheric oxygenation and atmospheric evolution. Science 317, 1900-1903

Lein, A.Y., Ivanov, M.V. (1989) Contribution of endogenous sulfur to the global biogeochemical cycle in the geological past.In: Brimblecombe, P., Lein, A.Y. (Eds.), Evolution of the Global Biogeochemical Sulphur Cycle. Wiley, New York, pp. 65–76.

Li, C., Love, G.D., Lyons, T.W., Fike, D.A., Sessions, A.L., and Chu, X., 2010, A stratified redox model for the Ediacaran ocean: *Science*, v. 328, p. 80-83.

Lowenstein, T.K., Hardie, L.A., Timofeeff, M.N., Demicco, R.V. (2003) Secular variation in seawater chemistry and the origin of calcium chloride basinal brines. Geology 31, 857-860.

Lyons, J. R. (2007).Mass-independent fractionation of sulfur isotopes by isotope-selective photodissociation of SO2. Geophys. Res. Lett. 34, L22811

McCarron G. (2000) The sedimentology and chemostratigraphy of the Nafun Group, Huqf Supergroup, Oman. Ph.D. Thesis, Oxford University, p. 175.

McFadden K. A., Huang J., Chu X., Jiang G., Kaufman A. J., Zhou C., Yuan X. and Xiao S. (2008) Pulsed oxidation and biological evolution in the Ediacaran Doushantuo Formation. Proc. Natl. Acad. Sci. USA 105, 3197–3202.

Meybeck, M., (1979) Major elements contents of river waters and dissolved inputs to the oceans. 794 Revue de Ge ́ologie Dynamique et de Ge ́ographie Physique 21 (3), 215–246.

Miller, K.G., Kominz, M.A., Browning, J.V., Wright, J.D., Mountain, G.S., Katz, M.E., Sugarman, P.J., Cramer, B.S., Christie-Blick, N., and Pekar, S.F., 2005, The Phanerozoic record of global sea-level change: Science, v. 312, p. 1293-1298.

Newton, R.J., Pevitt, E.L., Wignall, P.B., Bottrell, S.H., (2004) Large shifts in the isotopic composition of seawater sulphate across the Permo-Triassic boundary in northern Italy. Earth and Planetary Science Letters 218, 331–345.

Ono S., Wing B. A., Johnston D. T., Farquhar J. and Rumble D. (2006) Mass-dependent fractionation of quadruple stable sulfur isotope system as a new tracer of sulfur biogeochemical cycles. Geochim. Cosmochim. Acta 70, 2238–2252.

Paytan, A., Kastner, M., Campbell, D., Thiemens, M.H., (1998) Sulfur isotopic composition of Cenozoic seawater sulfate. Science 282,1459–1462.

Paytan, A., Kastner, M., Campbell, D., Thiemens, M.H., (2004) Seawater sulfur isotope fluctuations in the Cretaceous. Science 304,1663–1665.

Pingitore, J., Nicholas, E., Meitzner, G., Love, K.M., (1995) Identification of sulfate in natural carbonates by X-ray absorption spectroscopy. Geochimica et Cosmochimica Acta 59, 2477–2483.

Raab, M. and Spiro, B. (1991) Sulfur isotopic variations during seawater evaporation with fractional crystallization. Chemical Geology. Isotope Geoscience Section 86, 323–333.

Railsback, L. Bruce, 1992, A geological numerical model for Paleozoic global evaporite deposition: *Journal of Geology,* v. 100, p. 261-277.

Rees, C.E., 1973. A steady-state model for sulphur isotope fractionation in bacterial reduction processes. Geochim. Cosmochim. Acta 37, 1141–1162.

Rees, C.E., Jenkins, W.J., Monster, J., 1978. The sulphur isotopic composition of ocean water sulphate. Geochim. Cosmochim. Acta. 42, 377–381.

Schidlowski, M., (1989) Evolution of the sulfur cycle in the precambrian. In: Brimblecombe, P., Lein, A.Y. (Eds.), Evolution of the Global Biogeochemical Sulphur Cycle. Wiley, New York, pp. 3–20.

Schro¨der S., Schreiber B. C., Amthor J. E. and Matter A. (2004) Stratigraphy and environmental conditions of the terminal Neoproterozoic–Cambrian period in Oman: evidence from sulphur isotopes. J. Geol. Soc. 161, 489–499.

Shields, G., Kimura, H., Yang, J., Gammon, P., (2004) Sulphur isotopic evolution of Neoproterozoic–Cambrian seawater: new francolite bound sulphate δ34S data and a critical appraisal of the existing record. Chemical Geology 204, 163–182.

Staudt, W.J., Schoonen, M.A.A., 1995. Sulfate incorporation into sedimentary carbonates. In: Vairavamurthy, M.A., Schoonen,M.A.A.Eds.., Geochemical Transformations of Sedimentary Sulfur. Am. Chem. Soc., Washington, pp. 332–345.

Strauss H. (1999) Geological evolution from isotope proxy signals – sulfur. Chem. Geol. 161, 89–101.

Strauss, H., 1997. The isotopic composition of sedimentary sulfur through time. Paleogeogr., Paleoclimat., Paleoecol. 132, 97–118.

Takano, B., (1985) Geochemical implications of sulfate in sedimentary carbonates. Chemical Geology 49, 393–403.

Thiemens M. H. (1999) Atmosphere science - Mass-independent isotope effects in planetary atmospheres and the early solar system. Science 283(5400), 341-345.

Thode H. G., Monster L. and Dunford H. B. (1961) Sulphur isotope geochemistry. Geochim. Cosmochim. Acta 25, 159–174.

Ueno, Y., Ono, S., Rumble, D. & Maruyama, S. (2008).Quadruple sulfur isotope analysis of ca.3.5 Ga Dresser Formation: New evidence for microbial sulfate reduction in the early Archean. Geochim. Cosmochim. Acta 72, 5675-5691

Veizer, J., Ala, D., Azmy, K., Bruckschen, P., Bu 833 hl, D., Bruhn, F.,Carden, G.A.F., Diener, A., Ebneth, S., Godderis, Y., (1999) 87Sr/86Sr, δ13C and δ18O evolution of Phanerozoic seawater. Chemical Geology 161, 59–88.

Wu, N., Farquhar, J., Strauss, H., Kim, S.-T., and Canfield, D. E. (2010) Evaluating the S-isotope fractionation associated with Phanerozoic pyrite burial. Geochim. Cosmochim. Acta. 74, 2053-2071

Zerkle A. L., Farquhar J., Johnston D. T., Cox R. P. and Canfield D. E. (2009) Fractionation of multiple sulfur isotopes during phototrophic oxidation of sulfide and elemental sulfur by a green sulfur bacterium. Geochim. Cosmochim. Acta 73, 291–306.

Zerkle AL, Claire MW, Domagal-Goldman SD, Farquhar J, Poulton SW. A bistable organic-rich atmosphere on the Neoarchaean Earth. Nature Geoscience 2012, 5(5), 359-363.